SUGARCANE STILLAGE TREATMENT BY MEMBRANE DISTILLATION

Omayra Beatriz Ferreiro Balbuena

Tese de Doutorado apresentada ao Programa de Pós-graduação em Engenharia Química, COPPE, da Universidade Federal do Rio de Janeiro, como parte dos requisitos necessários à obtenção do título de Doutor em Engenharia Química.

Orientadores: Cristiano Piacsek Borges
Frederico de Araujo Kronemberger

Rio de Janeiro
Janeiro de 2021

SUGARCANE STILLAGE TREATMENT BY MEMBRANE DISTILLATION

Omayra Beatriz Ferreiro Balbuena

TESE SUBMETIDA AO CORPO DOCENTE DO INSTITUTO ALBERTO LUIZ COIMBRA DE PÓS-GRADUAÇÃO E PESQUISA DE ENGENHARIA DA UNIVERSIDADE FEDERAL DO RIO DE JANEIRO COMO PARTE DOS REQUISITOS NECESSÁRIOS PARA A OBTENÇÃO DO GRAU DE DOUTOR EM CIÊNCIAS EM ENGENHARIA QUÍMICA.

Orientadores: Cristiano Piacsek Borges
Frederico de Araujo Kronemberger

Aprovada por: Prof. Cristiano Piacsek Borges
Prof. Frederico de Araujo Kronemberger
Prof. Alberto Claudio Habert
Prof. Argimiro Resende Secchi
Prof. Eduardo Rocha de Almeida Lima
Profª. Miriam Cristina Santos Amaral

RIO DE JANEIRO, RJ – BRASIL
JANEIRO DE 2021

Balbuena, Omayra Beatriz Ferreiro

Sugarcane Stillage Treatment by Membrane Distillation/ Omayra Beatriz Ferreiro Balbuena. – Rio de Janeiro: UFRJ/COPPE, 2021.

XX, 156 p.: il.; 29,7 cm.

Orientadores: Cristiano Piacsek Borges

Frederico de Araujo Kronemberger

Tese (doutorado) – UFRJ/ COPPE/ Programa de Engenharia Química, 2021.

Referências Bibliográficas: p. 135-156.

1. Membrane distillation. 2. Sugarcane Stillage. 3. Wastewater Treatment. I. Borges, Cristiano Piacsek *et al*. II. Universidade Federal do Rio de Janeiro, COPPE, Programa de Engenharia Química. III. Título.

À Deus, aos meus pais, ao meu companheiro de vida

Agradecimentos

Aos meus orientadores Cristiano e Frederico por todos os ensinamentos passados ao longo destes anos, por todo o acompanhamento, paciência e atenção. Muito grata pelas sugestões, correções e palavras que só contribuíram a crescer tanto profissional como pessoalmente.

Ao PAM, a todos e cada um dos integrantes deste laboratório onde sempre me senti bem acolhida em especial aos meus flamenguistas favoritos Cátia e Bob, ao Marcos, à Alana e à sala 22.

Aos professores e funcionários do PEQ/COPPE.

Aos responsáveis pelo LabPol/PEQ/COPPE por me permitirem o uso do espectrofotômetro para as determinações de DQO. À Prof[a]. Fabiana da Fonseca Araújo pelas inúmeras vezes que foi necessário o uso dos equipamentos do LabTare/EQ/UFRJ para as caracterizações do vinhoto. Ao Prof. Paulo Laranjeira pelas correções e sugestões durante os seminários de acompanhamento e por ter me permitido realizar as determinações de viscosidade do vinhoto no LTFD/PEQ/COPPE. Aos responsáveis do GRIFIT/PEQ/COPPE pelas determinações de tensão superficial. Ao Fábio Diniz, Rui Castro e Prof[a]. Denise Freire do LABIM/IQ/UFRJ pela ajuda com as análises de HPLC.

Ao Paulo Yoshida, Francisco Oliveira, José Ieda Neto, Paula Figueiredo e a USJ Açúcar e Álcool S.A. Unidade São João – Araras - SP pelas amostras de vinhoto industrial.

À Maria Rosa e o Bruno Valim pelo companheirismo.

À Karla Licona, uma grande amiga quem me apresentou o PAM e quem me acompanha sempre desde os meus primeiros anos no Brasil.

Ao meu companheiro de vida, Bernardo, pela paciência ao longo de todos estes anos, pelo seu companheirismo, apoio incondicional e pelo seu amor.

A toda minha família, em especial aos meus pais Omar e Blanca, por sempre darem o seu apoio e a oportunidade de cumprir meus sonhos, por sempre me acompanharem na distância.

Às minhas irmãs Olivia e Ornella por sempre estarem presentes e por toda a sua ajuda.

À minha família brasileira Braga-Ferreira por seu carinho e cuidado todos estes anos.

Aos meus amigos do Brasil e do Paraguai, aos que sempre estão, aos que já não estão e aos que sempre estarão no meu coração.

A todos os que fizeram possível direta ou indiretamente este trabalho, muito obrigada!

¡Muchas gracias!

Aguije!

Resumo da Tese apresentada à COPPE/UFRJ como parte dos requisitos necessários para a obtenção do grau de Doutor em Ciências (D.Sc.)

DESTILAÇÃO POR MEMBRANAS PARA O TRATAMENTO DE VINHOTO

Omayra Beatriz Ferreiro Balbuena

Janeiro/2021

Orientadores: Cristiano Piacsek Borges
Frederico de Araujo Kronemberger

Programa: Engenharia Química

Este trabalho apresenta o uso da destilação por membranas para o tratamento de vinhoto. O vinhoto é o principal efluente líquido da indústria do etanol. Este efluente sai da coluna de destilação a temperaturas entre 70-90 ºC, onde para cada litro de etanol são produzidos de 12 a 20 litros de vinhoto. Desta forma, novas alternativas de tratamento são necessárias para diminuir o impacto da produção de etanol. A destilação por membranas é um processo de separação por membranas cuja força motriz é dada pela diferença de pressão de vapor entre os dois lados da membrana. Assim, este processo implica a transferência de calor e massa simultâneas. A sua principal limitação é o requerimento energético necessário para aquecer a corrente a ser tratada. Neste trabalho, foram realizados testes de laboratório utilizando uma solução sintética de vinhoto e vinhoto industrial. Um modelo matemático foi desenvolvido para simular o processo de destilação por membranas para o tratamento de uma solução multicomponente com as características do vinhoto. O modelo foi validado com os resultados experimentais. Uma análise de viabilidade técnica e econômica mostrou que esta tecnologia pode ser integrada ao processo de produção de etanol e utilizada para o tratamento do vinhoto a um custo estimado de 1.1 $\$/m^3$ de água recuperada.

Abstract of Thesis presented to COPPE/UFRJ as a partial fulfillment of the requirements for the degree of Doctor of Science (D.Sc.)

SUGARCANE STILLAGE TREATMENT BY MEMBRANE DISTILLATION

Omayra Beatriz Ferreiro Balbuena

January/2021

Advisors: Cristiano Piacsek Borges
Frederico de Araujo Kronemberger

Department: Chemical Engineering

This work presents the sugarcane stillage treatment by membrane distillation. Stillage is the main liquid wastewater of ethanol production. This wastewater leaves the distillation column at temperatures between 70-90 ºC and, for each liter of ethanol, 12-20 liters of stillage are obtained. In this way, new treatment alternatives are necessary in order to reduce the ethanol production impact. Membrane distillation is a membrane separation process in which the vapor pressure difference is the driving force of the process. This process implies a simultaneously transfer of heat and mass. The main limitation of this technology is the energy requirement for heating the stream to be treated. In this work, experimental results were performed using a synthetic stillage solution as well as industrial stillage. Besides, a mathematical model was developed to simulate the membrane distillation process for a multicomponent solution treatment which has the stillage characteristics. The model was validated with the experimental data. An analysis of technical and economic feasibility showed that this technology is suitable to be integrated to the ethanol production plant and to be used for the stillage treatment at a cost of $ 1.1 per m^3 of recovered water.

Contents

List of figures

List of tables

List of abbreviations

AD: anaerobic digestion
AGMD: air gap membrane distillation
ANN: artificial neural networks
BOD: biochemical oxygen demand
CFD: computational fluid dynamics
CGMD: conductive gap membrane distillation
COD: chemical oxygen demand
CPC: concentration polarization coefficient
DCMD: direct contact membrane distillation
DOE: design of experiments
DDGS: distilled dried grains solubles
DW: distilled water
EMSO: Environment for Modelling, Simulation and Optimization
EOS: equations of state
FO: forward osmosis
FS: flat sheet
GOR: gained output ratio
HF: hollow fiber
LEP: liquid entry pressure
MD: membrane distillation
MDC: Membrane distillation-crystallization
MED: multi-effect distillation
MF: microfiltration
MSF: multi-stage flash distillation
MSP: membrane separation processes
NF: nanofiltration
O&M: operational and maintenance
OCFEM: Orthogonal collocation finite element methods
OD: osmotic distillation
PEDCMD: Pressure-Enhanced Direct Contact Membrane Distillation
PGMD: permeate gap membrane distillation
PP: polypropylene
PR: Peng-Robinson
PRO: pressure-retarded osmosis
PSD: Pore size distribution
PTFE: polytetrafluoroethylene
PVDF: polyvinylidenefluoride
REC: permeate recuperation
RID: refractive index detector
RO: reverse osmosis
RR: recycle ration

SEEC: specific electric energy consumption
SGMD: sweep gas membrane distillation
SRK: Soave-Redlich-Kwong
STEC: specific thermal energy consumption
SW: spiral wound
TC: ton of processed cane
TDS: total dissolved solids
TOC: total organic carbon
TPC: temperature polarization coefficient
TS: total solids
TVS: total volatile solids
UF: ultrafiltration
UV: ultraviolet
VEDCMD: Vaccum-Enhanced Direct Contact Membrane Distillation
VLE: vapor liquid equilibrium
VMD: vacuum membrane distillation

Nomenclature

A: membrane area
c: concentration
C: concentration
$C_{p,i}$: specific heat
d_i: diameter
D_{ij}: binary mass diffusivity
h: heat transfer coefficient
H_R: maximum recoverable energy
H_i: enthalpy
J: diffusive flux
K_i: partition coefficient
k: mass transfer coefficient
ℓ: film thickness
L: module length
M_i: mass molar
m: mass
$\dot{m}_i$: mass flow rate
N_{fibers}: number of tubes in the module
N_i: permeate flux
P_i: pressure
Q_i: flow rate of i stream
q: heat flux
r. radius
Re: Reynolds number
T_i^j: temperature
t: time
v_{ij}: velocity (i direction and j side)
W_i: pump power
x_i: molar fraction of i in liquid phase
y_i: molar fraction of i in gas phase

Greek letter

γ_i: activity coefficient
γ_i: liquid surface tension
δ_i: thickness
δ_{ij}: Kronecker's delta
ΔH: latent heat of vaporization
ΔP: pressure drop
ε: pump efficiency

ϵ: membrane porosity
K: geometric factor determined by pore structure
θ: liquid/solid contact angle.
η: dimensionless radial coordinate
η_{DCMD}: thermal efficiency in the DCMD module
κ_i: thermal conductivity
μ: viscosity
ν_i: determinacy coefficient
ρ: density
τ: membrane tortuosity
ϕ_i^j: fugacity coefficient
Φ: packing density

Subscript

A: volatile
a: lumen side
ax: axial
B: non-volatile
b: shell side
c: critical
cond: conduction
conv: convective
f: feed
fs: free surface
HX: heat exchanger
g: gas
in: inlet property
l: internal (lumen side)
L: liquid
MD: membrane distillation
M.T.: mass transfer
m: membrane
max: maximum
mod: module
out: outlet property
p: permeate
P: pore
R: reduced property
r: radial direction
S: solid
s: external (shell side)
t: total

v: vapor
w: water
z: axial direction

Superscript

b: bulk
c: concentration
L: liquid
m: membrane
v: vapor
t: thermal

Chapter 1

Introduction

1.1. Contextualization and motivation

Stillage (also named vinasse or spentwash) is the main liquid wastewater in ethanol production industry and it is formed in the bottom of the distillation column [1]. Ethanol from sugarcane is considered the biofuel with the smallest carbon footprint [2]. Nowadays, Brazil is the second largest producer of bioethanol in the world and sugarcane is the main feedstock used [3,4]. Besides, in this country, bioethanol is used in cars directly as a fuel or as an additive to gasoline [2,5].

Stillage is rich in nutrients such as potassium, sulfur, nitrogen and phosphorus [1,6] and it characterizes by an high content of total solids (27,000 mg/L). It also presents high content of organic matter, which expressed as chemical oxygen demand (COD) takes values around 33,000 mg/L [7]. Sugars, traces of volatile organic components and alcohols are the responsible for this organic content [1,8]. The low pH is attributed to the organic acids and the sulfuric acid added in the fermentation vats [9,10].

Stillage can be used as fertilizer for it contains the soil fertilizing elements requires for plants. Besides, the organic matter allows to affect the microbial community and other properties of the soil [11]. For this reason, stillage, both dilute or concentrated, is widely used in Brazil as fertilizer by spreading over agricultural fields [8,12]. However, some authors refer that the long-term consequences of such application are not well established [8,12–16]. Due to its characteristic is recommended the stillage treatment before its use as fertilizer in order to reduce the environmental impact of this practice [7].

In this way, several treatments have been suggested for stillage disposal. Physicochemical, biological and membrane processes have been studied [17–20]. In the literature it is shown that membrane separation processes (MSP) as microfiltration (MF), ultrafiltration (UF), nanofiltration (NF) and reverse osmosis (RO) can be used for stillage

treatment despite some technical limitations [11,17,21–24]. These membrane processes were proposed to be used alone or combined with other processes as biological treatments. Among these last, anaerobic treatments are the most used due to the enabling of producing valuable product, such as biogas [11]. This has been widely studied by many authors as an economically viable alternative for reducing the organic content of stillage [9,11,17,25–27]. By the other hand, concentration has been proposed as an alternative for stillage disposal. Thermal concentration by evaporation [24] and concentration by reverse osmosis (RO) [16] are the technologies that have been used to concentrate stillage. Concentration allows water to be recuperated while reducing the volume of stillage to be disposed. The concentrated stillage can also be used for fertirrigation allowing to reduce the transportation cost associated.

Membrane distillation (MD) is a membrane separation process in which the vapor pressure difference is the driving force of the process [28]. There are four membrane distillation configurations commonly found in the literature; namely: vacuum membrane distillation (VMD), sweep gas membrane distillation (SGMD), air gap membrane distillation (AGMD) and direct contact membrane distillation (DCMD). Among these, DCMD has stood out when the solution to be treated has a high water content and for the simplicity of operation [29]. In this configuration, a solution to be treated is heated and placed in direct contact with one side of the membrane while the other side is in contact with a cold solution in which the permeate condensates. Thus, a temperature difference is created across the membrane, generating a vapor pressure difference, permitting the mass transfer process. The hydrophobic microporous membrane used in this process allows establishing a liquid-gas interface in the entry of the pores in both sides of the membrane. The volatile compounds present in the feed stream evaporates in this interface at the feed side and then permeates through the membrane, condensing in the liquid-gas interface formed at the permeate side. In this way, DCMD is characterized for concentrating non-volatile compounds, while volatile compounds are collected in the permeate side [30–33].

DCMD is a technology whose market has been growing in the recent years, mainly for seawater desalination. DCMD has an energy consumption as large as evaporation processes [29,34]. Nonetheless, the required temperatures are lower than the boiling temperature. For this reason, the use of waste heat or alternative energy sources has been extensively proposed to reduce the overall energy requirements [35–37]. The thermal

energy needed in DCMD is used for heating the feed solution. Therefore, if the solution to be treated is a stream with a relatively high temperature (higher than 50 ºC), the DCMD process can be expected to be suitable for its treatment without any additional heat source. Stillage leaves the distillation column at temperatures between 70-90ºC. Therefore, in order to perform its concentration by DCMD, it is expected that no additional heat sources should be needed for starting the process.

1.2. Objectives

The main objective of this thesis is to investigate the membrane distillation process to treat sugarcane stillage and its integration with the ethanol plant industry looking for the reduction of energy requirement. The specific objectives are:

- Assess the MD permeate flux studying the process variables such as temperature, concentration and flow rate, as well as the partial recycling of distillated and concentrated streams.

- Evaluate the removal efficiency of volatile and non-volatile components and other parameters as the chemical oxygen demand and the ionic conductivity from the treated sugarcane stillage.

- Investigate the fouling and wettability phenomena and the procedures to recover the membrane transport properties.

- Develop a mathematical model that allows simulation of the sugarcane stillage treatment process and validate this model with experimental results.

- Evaluate the energetic feasibility to integrate the MD process within the ethanol industry.

- Perform a preliminary economical study in order to determine the stillage treatment cost by direct contact membrane distillation.

1.3. Justification and relevance

As it was mentioned, Brazil is the second largest producer of bioethanol in the world and sugarcane is the main feedstock used. In the sugarcane processing, it is generated from 8 to 20 L of stillage per liter of produced ethanol, depending on several process factors [1,6].

Effluents conventional treatments such as biological and physicochemical have been used to treat stillage, however, most of the time the stillage stream has to be cooled before the treatment. Nevertheless, it is not always possible to reach the permissible levels for discharge.

MD is a thermally driven process where the driving force is given by vapor pressure difference; due to the exponential dependence of vapor pressure with the temperature, the feed has to be heated to induce the migration of water vapor from the feed side to the permeate one. MD presents high thermal energy consumption, since the feed stream needs to be heated and this has limited the commercial use of this technology.

In the last crop – 2018/2019 –, $33.14 \cdot 10^6\ m^3$ of ethanol were produced in Brazil [2,4,38], and it is estimated that in 2030, a volume of $540 \cdot 10^6\ m^3$ of stillage will be produced, considering an ethanol:stillage volume ratio of 1:12 [39]. Due to the characteristics of the stillage and the large quantities produced, it is mandatory its treatment making important the study of new technologies for its treatment and disposal.

In this way, the stillage treatment using membrane distillation becomes advantageous, since stillage leaves the distillation column at temperatures between 70 and 90ºC. Thereby, no additional source of energy would be required. So, it would be possible to perform the stillage concentration by DCMD and, in a subsequent step, to incinerate the concentrated stillage as biofuel in the boiler of the sugar and ethanol plant. It is estimated that it is possible to obtain 65.2 kg of steam (480ºC/65 bar) per ton of sugarcane processed when the concentrated stillage is incinerated [18].

In this thesis, the use of direct contact membrane distillation process for the sugarcane stillage treatment was proposed. Process variables were studied to assess the use of membrane distillation process for this purpose. Firstly, the efficiency of the process using a synthetic sugarcane stillage was evaluated. Subsequently, industrial stillage was

treated under the conditions previously determined. In parallel, a mathematical model was developed and validated for the sugarcane treatment using membrane distillation. This allowed to evaluate the energetic feasibility of this process and the possibility of energy integration within the bioethanol industry. Finally, a preliminary economical study was performed in order to determine the stillage treatment cost using this technology.

1.4. Scientific and technological contribution

The main scientific contribution of this Thesis is related to the study of the DCMD process performance when a complex solution is treated. In this regard, the use of the membrane distillation process for sugarcane stillage treatment has not been reported in the literature. The treatment of multicomponent solutions (containing volatile and non-volatile components) using membrane distillation is also scarce. The novelty of this work is the study of the operational parameters, the permeate flux and the specific thermal energy consumption during the sugarcane stillage treatment by direct contact membrane distillation by both experimental and computational approaches. Membrane distillation is a thermally driven membrane process in which simultaneous heat and mass transfer takes place. To simulate this process, a mathematical model was developed using the energy equation for modeling the heat transfer and the Stefan-Maxwell approach to describe the mass transfer of a complex mixture.

In this work, it is shown that the permeate stream obtained in the sugarcane stillage concentration by membrane distillation can be reused as process water and the concentrate stream can be used in the fertirrigation or as biofuel in the boiler. On this matter, it can be considered that the concentrated stillage incineration could be exploited to sustain the thermal requirements of the DCMD process, allowing to reach high concentrations due to the surplus steam obtained.

Finally, this work also presents a preliminary economic study demonstrating the feasibility of the process. In this way, the technological contribution is related to the fact that these results serve as the basis for the industrial scale-up of the process for this application.

Regarding the contributions to the scientific literature, this works resulted in a paper published in the *Waste and Biomass Valorization Journal*, title *Sugarcane Stillage Treatment Using Direct Contact Membrane Distillation* (doi: 10.1007/s12649-020-01303-y). A paper related to the simulation of the membrane distillation process for desalination was submitted in the *Brazilian Journal of Chemical Engineering.* Finally, a paper is being prepared in order to be submitted. This last will include the multicomponent model developed in this work and the simulation results.

1.5. Text organization

This work is organized in six chapters. The first chapter presents an introduction, the objectives, the justification and relevance of this work and its scientific and technological contribution. The second one presents a literature review referring to the stillage, its characteristics and the methods used for its treatment. The state of the art of membrane distillation is also presented in this chapter.

In the third chapter the methods and materials used are described in order to get acquainted about membrane distillation technology. The methodology applied to develop a mathematical model and simulation of DCMD process is also described in this chapter. In the fourth one, the experimental and modeling results obtained are presented and discussed. Conclusions are presented in the fifth chapter. Finally, in the sixth chapter, the references and bibliography are presented.

Chapter 2

Literature Review

2.1. Sugarcane stillage

Sugarcane was the first agriculture activity developed in Brazil, after arrival of the Portuguese in the year 1500. Brazilian sugarcane industry has evolved from a single product industry (sugar) to a plant of multiple products that includes sugar, ethanol and electricity [40]. Nowadays, Brazil is the second largest producer of bioethanol in the world and sugarcane is the main feedstock used. Ethanol production rises from 27 million of m^3 in 2016/2017 to more than 35.5 million of m^3 in 2019/2020 [41].

Ethanol is blended in more than 98% of US gasoline today [42]. In Brazil, ethanol is used in cars as an octane enhancer and oxygenated additive to gasoline in dedicated hydrated ethanol engines or in flex-fuel vehicles [5].

First-generation bioethanol is produced from sugar-based feedstocks mainly sugarcane, sugar beet and sweet sorghum or starch-based feedstocks, such as wheat, corn and cassava. Second-generation bioethanol is produced from lignocellulosic feedstock, such as wheat straw. Sugar-based feedstocks are preferred because the easier conversion of sucrose into ethanol. Starchy materials and lignocellulosic biomass required a previous hydrolysis for ethanol production [43].

In Brazil, the most widely used feedstock is sugarcane while U.S.A. uses corn as main feedstock to produce ethanol [42]. Sugarcane crops reach almost 642,677 million of ton in the 2019/2020 crop. In the same crop, sugar production reaches 29,606 million of ton and total ethanol reaches 35,595 million of m^3. Figure 1 shows the growth in Brazil of the production of sugarcane and ethanol and sugar production. In the last years, there has been an increase in the demand for ethanol in the Brazilian domestic market which has limited sugar production to prioritize biofuel production. This is due to the increase in oil prices, which has made hydrated ethanol gain competitiveness in the market, making the mills choose to produce ethanol over sugar. It was reported that Brazil

exported 1.82 billion liters of ethanol in the 2018/2019 crop, which implies a 26% growth compared to the volume exported in the previous crop [38]. However, for the 2020/2021 crop it is estimated a decrement of 18.1% in the ethanol production from sugarcane while an increment of 32% it is expected for sugar production. This is due to the impact on the sale and on the price of ethanol due to the pandemic [44].

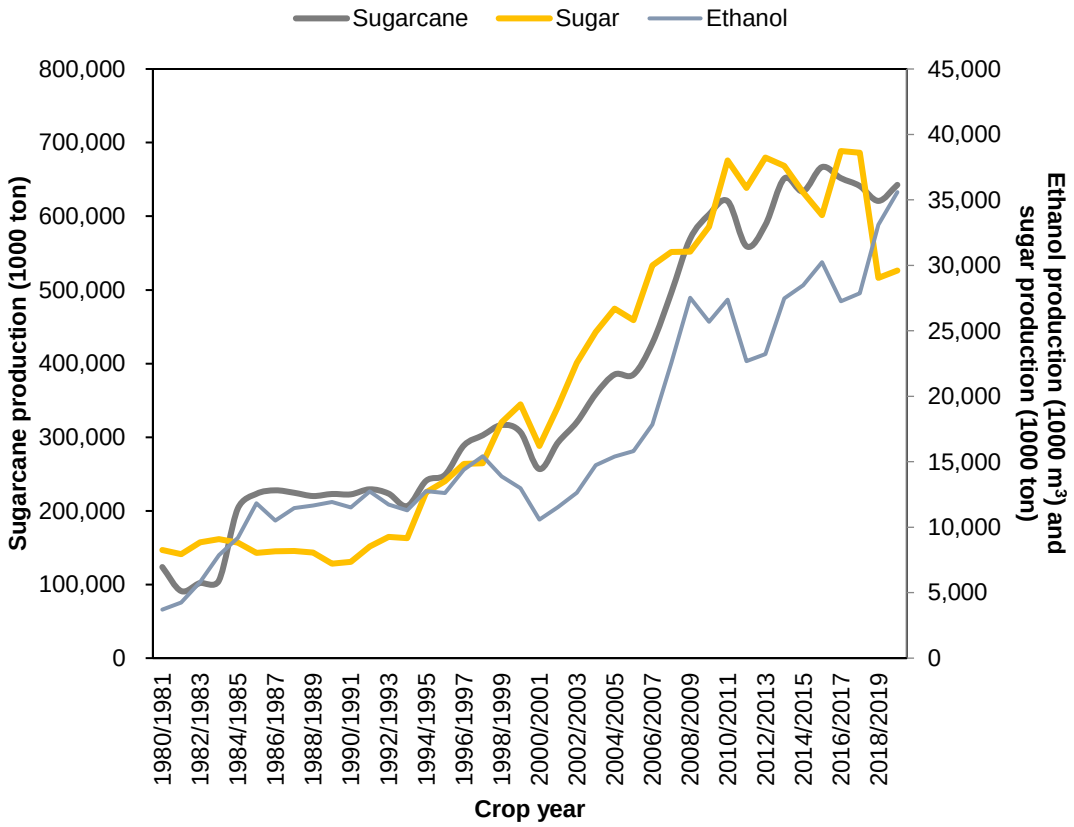

Figure 1. Ethanol, sugar and sugarcane production in Brazil since 1980/1981 crop [41].

Sugar and ethanol production (Figure 2) can be separated into five control volumes: extraction system, juice treatment, sugar production, ethanol production and cogeneration system [45]. Sugarcane is composed mainly by fiber and juice, in which sucrose is dissolved. The objective of the first step is to recover as much juice as possible, producing raw juice and bagasse. This bagasse is used in the boilers. Raw juice from extraction system is treated in order to remove sugar impurities, using chemicals, as to improve the quality of the final products. Juice is then left in a decanter to rest. Clarified juice is concentrated by removing water. In equipment called pans, by water evaporation, the syrup (concentrated juice) becomes a mixture of crystal spread in a sugary solution, which is called the cooked paste. In a centrifuge, sucrose crystals are obtained from the

sugar solution. The sugar solution remaining is called end syrup or molasses and it is sent to ethanol production [40].

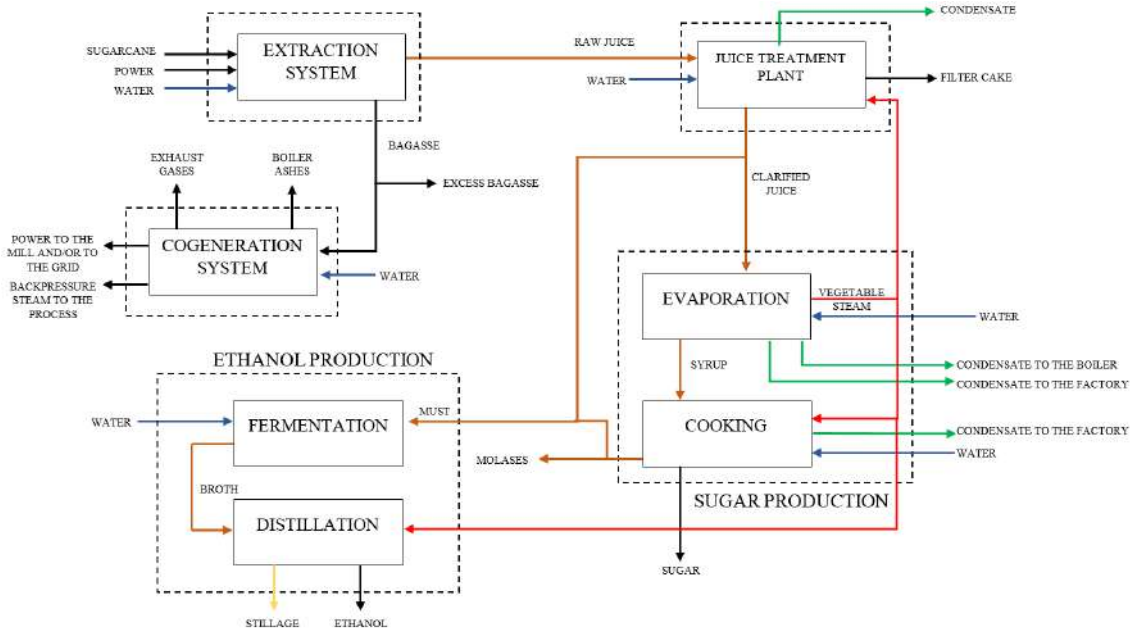

Figure 2. Sugar and ethanol production processes. Adapted from De Oliveira, 2013 [40].

Both sugarcane juice and molasses (or a mixture of both) can be used in ethanol production depending on the processing unit. Units in which ethanol is produced from sugarcane juice are called autonomous distilleries, whereas in annexed plants, a fraction of the sugarcane juice is used for sugar production and the remaining fraction is mixed with the molasses and used for ethanol production [1].

Steam-based systems are employed in Brazilian mills [40]. Bagasse generated in the extraction system is burned in combined heat and power systems to produce all thermal and electric energy required for the production process. This energy is usually used in processes that require steam at low pressure as evaporation and ethanol distillation [1]. Some mills already use steam with higher parameters to generate an excess of electricity that is sold to the grid, mainly during off season periods when the operation of the mills is stopped [1,40].

Part of the clarified juice is mixed with molasses from the sugar production. This is called must and it is used in fermentation vats where sugars are transformed into ethanol using yeast, under anaerobic conditions. After fermentation, the mixture is decanted or

centrifugated and the separated wine is sent to a distillation column while the yeast milk is returned to the process [40].

During the distillation, ethanol is separated from other components and leaves the head of the column as an azeotropic mixture with water. This processing step is very energy intensive. Subsequently, part of the ethanol-water mixture is dehydrated to obtain the anhydrous ethanol. The residue obtained at the bottom of the distillation column is called stillage [46].

Stillage represents the main liquid wastewater in ethanol production process. Sugarcane process generates from 8 to 20 L of stillage per liter of produced ethanol, depending on the type of feedstock and the level of technology used in the process [1,6]. Sugar mills with annexed alcohol distilleries generally release an average of 156 L of stillage and 250 kg of bagasse per 1,000 kg of cane, generating 12 L of ethanol and 94 kg of sugar [47].

Brazil is the largest sugar exported in the world. If Brazil will maintain the same market share in the domestic market and export to sugar and ethanol, the trend is that bioethanol production increases in the next years. Therefore, stillage management and treatment processes will have to be continuously improved and new technologies are mandatory.

2.1.1 Characteristics

Stillage can be classified according to the components in the preparation of the must, that is, clarified juice, molasses or a mixture of both [16]. Its composition can vary depending on several factors: variety of cane, agroclimatic conditions of the region, sugar manufacturing process and handling and storage [6,8]. Among the factors related to manufacturing process that can affect the composition of the stillage, it can be pointed out: the treatment of the clarified juice to reach a certain sugar concentration; the injection of indirect vapor into distillation and rectification columns, which reduce volume and concentrate its physicochemical properties; the production of ethanol hydrated or anhydrous; the products used on the fermentation, the treatment of yeast (nutrients, phosphoric acid), the components used for disinfection and the use of antifoam [16].

Even so, stillage presents a dark brown color; acidic nature (pH 4-5) and a temperature between 70 and 90ºC. Its recalcitrant nature is due to presence of phenols (tannic and humic acids) from the feedstock and melanoidins[1] responsible for the dark brown color [15,48,49]. The other recalcitrant compounds present in the waste are caramels from overheated sugars, anthocyanins, different xenobiotic compounds and furfurals from acid hydrolysis [15,49]. Stillage has a high solid concentration (approximately 2.5%) [50].

Table 1 summarizes the characteristics of stillage from cane juice and molasses. As can be seen stillage is rich in nutrients such as potassium, sulfur, nitrogen and phosphorus [1,6]. It presents high content of organic matter, high levels of biological oxygen demand (BOD), chemical oxygen demand (COD) and COD/BOD ratio neat two [8].

Table 1. Typical characteristics of sugarcane stillage. Adapted from Wilkie *et al.* (2000) [51].

Feedstock		Stillage yield L/L ethanol	COD (g/L)	BOD (g/L)	N (total, g/L)	P (total, g/L)	K (g/L)	S (total, as SO_4^2, g/L)	pH
Cane juice	Average	16.3	30.4	16.7	0.628	0.130	1.952	1.356	4.04
	std dev	5.3	8.2	3.4	0.316	0.110	1.151	1.396	0.49
	n	2	6	5	6	6	5	5	7
Cane molasses	Average	14.0	84.9	39.0	1.229	0.187	5.124	3.478	4.46
	std dev	3.3	30.6	10.8	0.639	0.350	3.102	2.517	0.35
	n	7	22	19	20	17	12	16	25

std dev = standard deviation; *n* = number of literature values used

The main organic compounds present in sugarcane stillage consists of organic acids (that provide low pH), mainly lactate and acetate as well as alcohols, mainly glycerol and ethanol and a minor amount of carbohydrates [1,8].

[1] Melanoidins are low and high molecular weight polymer formed as one of the final products of Maillard amino carbonyl reaction, which is a non-enzymatic browning reaction resulting from the reaction of reducing sugars and amino compounds [8,15]

Recently, in Brazil, seasonal characterizations were performed in order to show the variability of the composition in a crop [7,52]. It was reported that sugarcane crop cultivation and the ethanol production rather than the weather are the factors with higher influence in the chemical composition of stillage. Table 2 shows the typical characteristics of Brazilian sugarcane stillage.

Table 2. Characteristics of Brazilian sugarcane stillage from Gouvêa de Godoi *et al.* (2019) [7].

Characteristics	Value
pH	4.72 ± 0.67
Ionic conductivity	14,150 ± 2000 $\mu S/cm$
Potassium	1,542 to 3,961 mg/L
Chloride	209 to 3,550 mg/L
Magnesium	343 to 669 mg/L
Calcium	292 to 641 mg/L
Sodium	27 to 57 mg/L
Hardness (expressed as $CaCO_3$)	3,400 mg/L
Total solids	27,000 mg/L
Total suspended solids	5,000 mg/L
COD	33,000 ± 4000 mg/L
BOD_5	15,000 ± 4000 mg/L
Lactic acid	0.61 – 6.45 g/L
Methanol	0.34 – 4.55 g/L
Glycerol	0.30 – 5.44 g/L
Acetic acid	0.06 – 3.80 g/L
Aconitic acid	0.21 – 3.79 g/L
Succinic acid	0.09 – 3.44 g/L
Propionic acid	0.04 – 2.55 g/L
Citric acid	< 0.58 g/L
Ethanol	< 0.45 g/L
Sucrose	270 to 1,960 mg/L
Glucose	640 mg/L
Fructose	770 mg/L

Fuess *et al.* (2018) also found most of these components in their work [52]. Among the organic components, in addition to those presented in Table 2, they reported malic acid, iso-butyric and butyric acid in concentrations similar of those found for lactic acid. Besides a high fraction of non-identified components was reported.

2.1.2 Treatments

In Brazil, production costs of bioethanol from sugarcane have been declined continuously over the last three decades [53]. The largest cost with fuel ethanol production remains being feedstock consumption that constitutes more than 70% of the final ethanol price for the case of molasses [43,54].

Industrial costs mainly decreased because of the increasing scales of the ethanol plants. The second largest cost in ethanol production is energy consumption, especially with ethanol distillation and stillage treatment (particularly when is treated by multievaporation process) [54]. By data obtained from simulation, Lassman *et al.* (2014) [46] showed that distillation section accounts for 60% of the overall energy demand. It is expected that an alternative to offset the costs of ethanol production is to obtain valuable co-products from stillage, for example. On this matter, the production of alcohols, organic acids (mainly, lactic acid), polymers, enzymes, among other molecules, has already been studied using stillage as a medium due to its nutrient content [11].

In addition, distillery wastewater treatment is mandatory because of pollution problems, and has been the most significant and challenging matter in the industrial production of ethanol [55], added to the fact that worldwide environment regulatory authorities are more and more stringent in setting norms for discharge of wastewaters from industries, driving to improve the existing treatment or explore alternative methods of effluent management [56]. Nevertheless, it is first necessary to adopt some actions to reduce the production of stillage.

The stillage may be used as fertilizer without treatment after separation of the suspended solids or otherwise be treated in order to reduce its volume (by thermal or membrane concentration) or the organic load of it.

In order to decrease the stillage temperature, it is usually re-used to heat the must from 65º to 95ºC, reducing the energy requirement in the distillery, as well as its own temperature [50]. The stillage temperature can also be reduced by means of cooling towers up to at least 45ºC [16].

Several stillage managements have been reported at the literature that include biological and physicochemical treatments, thermal concentration, and membrane concentration and fertirrigation. Each treatment has advantages and disadvantages, and its characteristics will be discussed below. Currently, anaerobic treatment and fertirrigation are the main industrial stillage management [11].

2.1.1.1.Biological treatments

Biological treatments are widely studied for several wastewater. Anaerobic digestion (AD) is accepted as the first treatment step in distilleries and it is considered to be the most developed and economically process for stillage treatment due mainly to the fact that allows to produce biogas [11,49].

Anaerobic digestion can be used to reduce the organic matter content, by converting more than 50% of the COD to biogas, while maintain the inorganic nutrient content [1,49]. Besides, it is efficient on BOD removal. Digested stillage still contains considerable plant nutrients in terms of potassium, sulfur, nitrogen and phosphorus and large amount of micronutrients like Ca, S, Cu, Mn and Zn [15], as well as recalcitrant compounds included micro-colloidal colored compounds and protein-like substances [57]. This precludes that to be released in rivers. Fertirrigation could be a destination for the digested stillage [16], but, in this case, it has low amount of organic matter for soil treatment [1,16].

Anaerobic digestion can be carried out in mesophilic or thermophilic conditions. The last one may be economically more advantageous because stillage leaves the distillation process at a temperature of approximately 90ºC and thus, cooling to 55ºC may occur naturally. In contrast, the former forced cooling to temperatures lower than 40ºC is required [1].

Membrane separation processes also have been proposed as pretreatment of biological treatment, allowed the reduction of inhibiting substances and consequently

improved the efficiency of the treatment [58]. Further stages of treatment including ultrafiltration (UF) or centrifugation, followed by oxidation with ozone or evaporation have been proposed in order to save water, minimize the waste produced and reduce the impact on the environment [48]. Aerobic treatment has also been used as post-anaerobic treatment, however, this practice requires large land area what has limited its application [59].

Nevertheless, the main advantage of AD treatment is the biogas production and the organic matter reduction. It is estimated that 10-26.4 m^3 of biogas containing 60% of methane can be produced from the digestion of 1 m^3 of stillage [27]. This implies 5,500 kcal per m^3 of methane, which is almost 91 kWh per m^3 of stillage [60]. However, stillage needs to be cooled before AD treatment. Besides, this treatment implies long retention periods, and its efficiency depends on the feed characteristics. The high content of potassium, the presence of heavy metals and sulfate, and the melanoidins (which are not degraded by AD) could also represent a big challenge for the AD treatment [9]. Finally, digested stillage needs of post-treatments as an aerobic or a physicochemical one.

2.1.1.2.Physicochemical treatments

Physicochemical treatments are characterized by being effectives in color and COD removal. However, these methods used excess of chemicals, generating sludge that need to be disposal, high operational costs and sensitivity to variable water input [15].

Conventional treatment of wastewaters by coagulation with alum presents difficulties with sludge treatment or discharge. Souza *et al.* (2013) [61] used a natural coagulant to treat stillage for color and turbidity removal and COD reduction, although high coagulant concentration was required to obtain significant removals. Coagulation coupled with photocatalysis degradation allowed to reduce absorbance, COD and toxicity of stillage [62]. However, intermediate compounds could be formed and be more toxic in some concentrations, thus a longer irradiation period is required for their complete mineralization.

Zayas *et al.* (2007) investigated coagulation/flocculation with $FeCl_3$ as post-treatment of biologically treated stillage. Then, an electrochemical oxidation was performed by potentiostatic electrolysis with a Ti/RuPb(40%)O_x anode and

Ti/PtPd(10%)O_x cathode. Advanced oxidative processes by ozonization, O_3/UV or O_3/UV/TiO_2 have been also proposed as pretreatment, as well as post-treatment stages of a biological treatment [63,64].

2.1.1.3.Thermal and membrane concentration

Stillage concentration aims mainly to reduce its volume for use in the fertirrigation avoiding the excessive transport of water and allowing its use in more distant cane plantations where the fertirrigation is not feasible. Two technologies are widely used to concentrate stillage: the thermal concentration by evaporation [24] and the membrane concentration by reverse osmosis [16].

The stillage is transferred through a high-performance centrifuge, where the wet cake containing about 30% total solids (TS) is decanted. The remaining stillage, which has a total dissolved solids (TDS) concentration range of 5-10% is transferred to the concentration unit to achieve a final TDS concentration to about 28-65%, depending on the type of raw material being processed, the efficiency achieved by mechanical separation and the fermentation process. The wet cake are dried for mixing with other recycled dry material producing distilled dried grains solubles (DDGS), which is a co-product for animal feed [14,54,65].

Temperatures within the evaporator largely influence concentrate quality and fouling behavior. Temperatures of 50º to 105ºC are used. Two types of evaporator are usually used, the falling film and the forced circulation evaporators. The selection would depend on process requirements, such as concentration ration, evaporation rate, type of heating or heat recovery system, and mainly, of the viscosity and fouling characteristics of the stillage. Stillage with high content of calcium sulfates are concentrated in forced circulation evaporators due to their tendency to scale or foul [65]. In multi-evaporators process, frequent cleaning is essential to prevent scaling, which reduces the efficiency of the system [66].

Stillage concentration in multi-effect evaporator by turbulent mist is currently one of the technology most widely used in Brazil [16]. This system utilizes the principle of descending turbulent mist and it is attached to the distillation column. It enables ten times in volume reduction and the produce concentrated stillage simultaneously to alcohol

production without additional steam consumption. It also allows the usage of the condensed low-pressure steam [67].

This technology was able to replace the multiple effect evaporators falling film from Dedini-Vogelbush due to higher energetic efficiency and less operational problems related to fouling. Nevertheless, both technologies require stainless steel equipment and large amount of energy. For instance, a five-effects equipment uses around of 0.2 kg of steam per liter of stillage to concentrate from 2 to 20º Brix, which is equivalent to almost 60% of the steam needed for hydrated ethanol distillation. The used of thermal concentration for stillage fertirrigation will depend on the process cost compared to the transportation cost for use in the field [16].

Evaporation can inactive microorganisms by heat and pressure shock. The collected distillate is free from the microorganism and solid matter [48]. The condensate represents a large volume which could be reused as dilution water in the fermentation step [8,56]. However, this stream contain volatile organic compounds including ethanol, acetic acid and formaldehyde which are inhibitors of fermentation process, which prevents 100% water recycling [51]. Also, it cannot be discharged without previous treatment because of its high organic compounds content [56].

Nandy *et al.* (2002) [66] proposed a combined process of AD with subsequent concentration through multiple effect evaporation and utilization of concentrated effluent for biocomposting of pressmud for production of biomanure which contributes to the elimination of effluent discharges. Cortes-Rodríguez *et al.* (2018) [68] performed an energy analysis of a system that integrate the juice evaporation and the stillage concentration using multiple-effect evaporator systems. It was determined that using a two-effect in the juice evaporation and a three-effect for the stillage concentration is possible to obtain per ton of cane 345 kg and 91 kWh of steam and electricity surplus for sale, respectively. Recently, Fukushima *et al*. (2019) proposed an integration of the stillage concentration with the incineration of the concentrated stillage. Without heat integration, incineration is needed for producing more steam to overcome the energy demand of the stillage concentration process. For taking advantage of the concentrated stillage as biofuel it is necessary to concentrate until 65 °Brix. By the other hand, the heat integration allows to reduce the steam consumption. The authors also showed that with an appropriate integrated system is possible to achieve 65° Brix due to the steam obtained

from the stillage incineration. The potassium-rich ash produced by combustion of stillage is another method that allow stillage disposal and can be used for land application [8].

Membrane separation processes (MSP) are promising techniques and are often used because of their high removal efficiency, optimal costs, and simple operation, besides of offering a possibility to improve the quality of treated water to meet the environmental standards or recycled into the process. Some authors reported 70-80% of water reuse [69,70]. The retentate stream can be used as an addition to fertilizers or feed for biogas production, with additional advantage of presence of dead yeast cells and yeast metabolites, which also have high nutritive value [56].

Various combinations of membrane processes may result in higher efficiency of stillage purification. Microfiltration (MF) and ultrafiltration (UF) membranes operates at lower pressure, but with low efficiency to remove COD and other soluble solutes [56], being used as pre-treatment of reverse osmosis (RO) or nanofiltration (NF). These processes appear to be the most promising methods for stillage purification with ability to produce high-quality water [56]. RO processes are the most effective with higher percentage of COD and other solutes removal, but needs higher operating pressures, which affect costs of the process. The RO membrane technology was widely used in Indian distilleries, reporting 50 to 80% of water recovery as permeate even for stillage with high dissolved solids (35,000 to 55,000 mg/L) [16,71]. While energy consumption is less than for evaporation, membrane fouling is problematic. Fouling leads to permeate flux decline, loss of product quality and shortening membranes lifetime. The understanding of fouling formation on the membrane surface is complicated since the stillage is a mixture of many different components with very variable sizes and shapes [56]. Another disadvantage is the permeation of low molecular weight organics still through the membranes, reducing the water recycle potential in the ethanol production process [51].

While by thermal concentration is possible to reach TDS of at least 20%, membrane separation allows to achieve only 12% of TDS. Besides, for performing the concentration by MSP is 7-9 kJ per kg of water recovered compared to the 1300 kJ per kg of water recovered needed for evaporation [11]. Nevertheless, these technologies can be used in combination, reducing the equipment size for the evaporation stage [16].

Peiter *et al.* (2019) [17] studied the combination of the AD followed by a concentration technology such as evaporation, reverse osmosis or forward osmosis. Among these, the combination of AD and RO showed the higher resource conversion efficiency. The authors showed that recovering 70% of water from 491.76 m^3/h of stillage allowed to reduce the external water requirement by 66%. Besides, 28% of additional electricity were generated from the biogas production.

RO is also widely used as a post-treatment stage in order to eliminate the inhibitory solutes present in the condensates from the stillage concentration by evaporation. This allows to recycle the water reducing its consumption in the ethanol production plant [11].

2.1.1.4.Fertirrigation

Until the 1960s in Brazil a large proportion of the stillage was thrown directly into the waterways causing serious problems of surface water contamination. The technical solution found at that time was the disposal of this residue in the called sacrificial areas (due to the cane plantation area was sacrificed for disposal and infiltration of stillage). This procedure was regulated by the environmental agencies, since there was, and still is, no economical solution by using conventional treatment to release in rivers.

Nowadays, in Brazil, stillage is mainly used as a fertilizer due to its high nitrogen, phosphorus and organic matter [8]. Both dilute and concentrate stillage can be spread on agriculture fields or used as organic fertilizer [12]. Agricola application of stillage presents environmental and economic advantages; however, it is still restricted to the nearest areas by the cost-beneficial ratio. Whereas its utilization is rational and in appropriate dosages, soil application has economic benefits by the partial or total substitution of mineral fertilization, improving the physicochemical characteristics of the soil and agricultural productivity [16].

Fertirrigation system of cane crop with stillage must include the transport and its distribution in the fields. Transportation is done by road transport, by tank trucks or by pipeline transportation [16]. Thus, fertirrigation is subjected to land availability in the vicinity of the distillery, mainly due to transportation costs [8,16]. An economic distance for stillage application is around 38 km, but it could vary with the cost of the conventional fertilizer, the concentration of stillage and the transport system in the plant [16].

However, this practice has been controversial due to the inadequate or indiscriminate disposition of sugarcane stillage in soils or water bodies. Stillage has a high pollution potential due to high COD, total nitrogen and total phosphate content of the effluent that may result in eutrophication of natural water bodies. The highly-colored components of the stillage reduce sunlight penetration in rivers, lakes or lagoons which in turn decrease both photosynthetic activity and dissolver oxygen concentration affecting aquatic life [8,15]. Besides, due to high strength molasses-based stillage, the odor, putrefaction, attraction of insects, the possibility of soil salinization, leaching of metals, such as manganese (inhibiting seed germination) and sulfate and groundwater contamination need to be considered [1,8,12,15]. Fuess *et al*. (2018) [52] reported that the potassium content in the stillage is higher than the concentrations require in most of the crops with a high risk of soil salinization. Another alternative proposed by the authors, it is applied biodigested stillage, however, there also is a high potential of soil solidification due to the high doses of Na-based alkalizing compounds, which concentrations could be even more than 200-fold than in raw stillage.

The effects of the application of the stillage on the soil depend on various factors, such as the quantity applied in the soil, soil type and chemical composition, crop type and the economic conditions involved in this process. Dosages should be determined based on the characteristics of each soil to avoid salinization or imbalance of nutrients, that can be leached into ground water [14,16].

In Brazil, the technical standard P4.231 establishes the criteria and procedures for agricultural soil application of stillage, in which the dosage is given according the potassium content, nutrient with the highest concentration in the stillage [72]. It is considered the root development of the cane (saturated layer with potassium) and the needs of the plant in terms of this element [16].

However, this regulation only estimates the impacts cause by stillage on soil, water and groundwater, prescribing stillage application according to its potassium content but neglecting organic matter content and atmospheric impacts due to air emissions [1].

Fertirrigation represents a hazard to surface water quality when nutrients and organic matter reach the waters through diffuse pathways or accidentally through direct pathways

from stillage storage and transportation facilities. Stillage wash-off and infiltration (wash-out) has been discussed as a source of surface water pollution [47].

Prado *et al.* (2016) found elevated concentrations of lactic, butyric, citric, tartaric, succinic, formic, and acetic acids up to 1 m of depth after 29 days of stillage application. After 63 days, no traces of those acids were found in the soil. However, there was a rise in nitrate and decline in chloride and sulfate content. However, it is expected that none underground water contamination, nor rivers with stillage application at a dosage of 450 m^3/ha for latosoils. The authors reported that reservations are placed for more permeable soils and shallower underground water.

The impact of stillage fertirrigation in sugarcane plantations on water quality of the Ipojuca River in Brazil, is demonstrated by time-dependent changes in O_2 concentrations. Downstream of the factory, organic pollution load (BOD up to 100 mg/L) is mainly originating from sugarcane planting and processing activities. Organic concentration increases in the river due to wash-off and washout during rainy periods were partially compensated by dilution effects due to increased flow rates (e.g., for phosphorous, BOD, COD). Because of the high potassium content of stillage, higher concentration of this element in surface waters indicate a washout from stillage fertirrigated soils [47].

After six years of stillage application, an assessment found enrichment of ions in groundwater at Valle del Cauca in Colombia (Na^+ and K^+) and determined that was probably due to a combination of factors: stillage dilution produced by water input and hydro-chemical processes along with nutrient removal produced by sugarcane uptake. This fact may make the aquifer vulnerable to contamination [73].

Moraes *et al.* (2014) [13] concluded that fertirrigation with biodigested stillage could reduce environmental impacts due to the decrease of global warming potential impacts and pollutant loads, which were comparable (in terms of organic matter) to the populations of some cities for a single sugarcane processing plant.

It is worth to mention that currently a single technology is insufficient to reach the allowed effluent discard limits [9,19]. Brazilian ethanol is considered one of the most efficient biofuels in terms of energy balance and it is expected high cost reductions and possible high oil prices making that the efforts made for this reduction will continue reaping benefits [53].

On this matter, it is important the study of treatment combinations, new technologies or integration processes for an adequate disposal of stillage in order to reduce its impact as well as to contribute to the reduction of the production cost.

2.2. Membrane Distillation

In the last years there was a rapid development of membrane technologies due to a scenario of water scarcity and new stricter environmental regulations in water and wastewater treatment. Thus, membrane distillation (MD) is shown as an advantageous alternative for these applications since it can operate with high feed solute concentration maintaining elevate recovery degree of high-quality water [28].

MD is a thermally driven membrane separation process, in which a microporous hydrophobic membrane separates the feed and the permeate sides. The temperature difference across both sides induces a vapor pressure difference that it is the driving force of the process [28,30,31]. This technology has been intensively investigated as it is reflected in the number of publications in recent years (Figure 3).

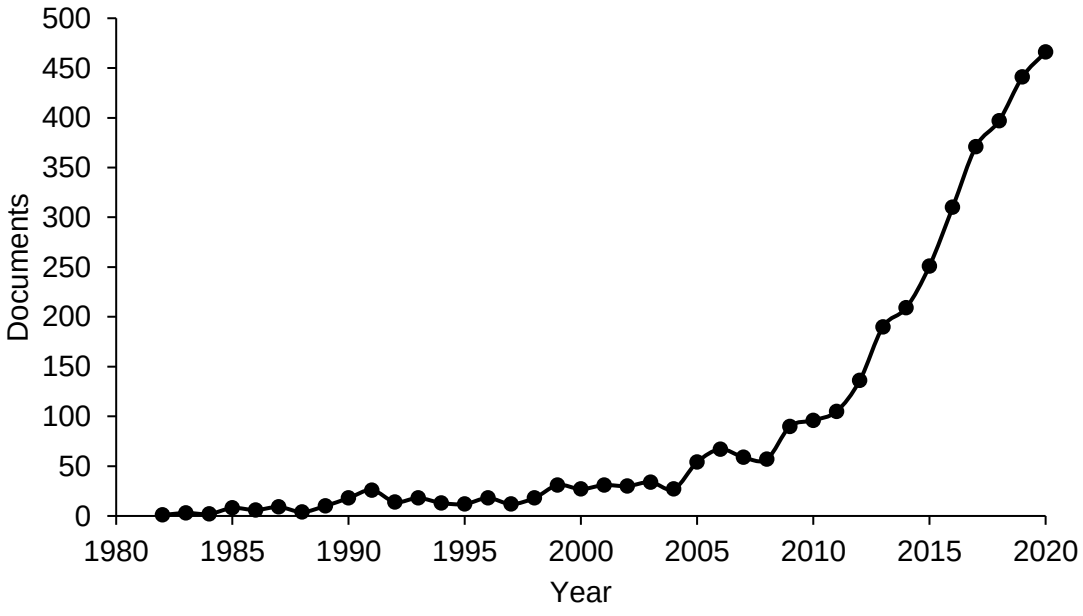

Figure 3. Documents in Membrane Distillation by year. TITLE-ABS-KEY: "Membrane Distillation"

MD operates at lower temperatures than conventional distillation, usually below the liquid boiling point. This allows to use low-grade heat such as waste heat or alternative energy sources (solar or geothermal energy) [35,37,74–76]. Furthermore, the hydrostatic pressure is lower than used in pressure-driven membrane process like reverse osmosis (RO). Therefore, membrane, modules and connections can be made using less expensive material, as plastics, reducing corrosion problems [28,30,31].

MD separation is based on the principle of vapor-liquid equilibrium and the membrane does not affect the separation selectivity [28,30,77,78]. Besides, MD can operate with high feed solute concentration or even near saturated solution, being less sensible to feed variations. In this way, MD has a potential to mitigate the environmental problem associated with the concentrated salt solution from RO or other high solute concentration solutions, approaching to the zero liquid discharge [31,79–82].

Since water is transported in the vapor phase through the membrane pores by vapor pressure difference, there is no advection solute flux and it is considered that MD is less prone to fouling phenomenon [28,30].

Nevertheless, despite the average pore size in MD membranes being significantly higher than the diameter of a liquid water molecule, liquid solution is prevented to enter in the membrane pores due to its hydrophobic nature and because of the high surface tension of water. This provokes the formation of a convex meniscus in the membrane pore which restricts pore wetting [30]. Still, pore wetting phenomenon must be avoided by operating with transmembrane pressure difference lower than the liquid entry pressure (LEP) as it will be further discussed in this text [31].

Besides the growing interest in MD, there is a lack of commercially available membranes fabricated specially for this application. The transport process could be complex, and it is usual to observe water flux decay due to concentration and temperature polarization effects. High energy consumption is also expected, since feed solution has to be continuously heated, and the module configuration is essential for a good process efficiency. Low permeate flux compared to other separation techniques has hindered a more intensive use of this technology and still there are uncertainties about economic cost for each MD application [31,83].

2.2.1. Configurations

Depending on how vapor condensation is provided, four different configurations of MD are currently known: Direct Contact Membrane Distillation (DCMD); Air Gap Membrane Distillation (AGMD); Vacuum Membrane Distillation (VMD) and Sweep Gas Membrane Distillation (SGMD).

DCMD is the most used since it is the simplest MD configuration. It is considered more suitable for aqueous solutions [83]. In this case, both the hot liquid and cold liquid are kept in contact with the membrane [32]. DCMD is carried out through the evaporation of the volatile components in the feed side at the liquid/vapor interface, followed by the transport of these molecules through the non-wet membrane pores and condensation of the vapor molecules in the permeate side [31]. When volatile solutes are contained in the feed solution, they will also permeate through the membrane [30]. The main drawback of this design is the heat lost by conduction [28].

In AGMD, only the feed solution is in direct contact with the membrane surface. At the permeate side, a stagnant air layer exists between the membrane and the condensation surface. The vapor permeates through the membrane pores and the air gap until it reaches the cold surface where condensation takes place. In this configuration the heat loss by conduction is reduced, however an additional resistance to mass transfer is created by the air gap [28]. This configuration is useful to remove trace volatile components from aqueous solution because permeate fluids are not in direct contact with the membrane surface [83].

In VMD configuration, vacuum or low pressure is applied on the permeate side. Volatile components evaporate from the feed side at the liquid/vapor interface and then permeate through the membrane pores. The vapor is condensed outside the module. The driving force is given by the partial pressure gradient and the thermal gradient between the two sides [78,84]. The heat loss by conduction is negligible in VMD and this constitutes a great advantage [28]. VMD is appropriate for the removal of volatile organic components from aqueous solutions [83].

In SGMD, a gas sweeps the permeate side carrying the vapor to an external condenser. The feed solution is kept in the feed at higher temperature than the gas. This

configuration combines relatively low conductive heat loss through the membrane due to the low thermal conductivity of gaseous phase and a reduced mass transfer resistance due the gas circulation velocity. Consequently, the permeate flux can be expected to be higher than those observed in AGMD. Nevertheless, the energy loss by membrane conduction is in same order of magnitude for both processes [28,85–87]. The main disadvantage of SGMD configuration is that a small volume of permeate diffuses in a large sweep gas volume, requiring a large condenser [28].

VMD as well SGMD configurations need an external condenser unlike DCMD, where the condensation step is carried out inside the membrane module leading, in this way, to a simpler operation mode. This makes DCMD the configuration most widely used, in spite of the fact that the heat loss by conduction through the membrane matrix is higher than other MD configurations [83].

New configurations or modified design of the existent ones were proposed to increase the MD performance. Permeate gap membrane distillation (PGMD) is one of them. This configuration is a modification of the AGMD, in which the air gap is replaced by the produced permeate. It was reported that this gap allows to enhance the internal heat recovery. Besides, it is considered that the sensible heat loss is lesser than in the DCMD but higher than AGMD configuration [88,89]. The water gap width showed to have less influence in the permeate flux than in the AGMD configuration [90].

Francis *et al.* (2013) [91] found an increment of 820% in the permeate flux using water instead of air. The authors also tested other materials such as sand, and the configuration was called material gap membrane distillation. In the conductive gap membrane distillation configuration (CGMD), the gap is filled with a high thermal conductivity material in order to reduce the thermal resistance along the transfer direction. The thermal conductance could be improved using fins on the condensation surface or conductive spacer, even increment the gap width [92].

2.2.2. Operating parameters

Temperature is the most important operating parameter. Vapor pressure, which is the driving force of MD process, has an exponential relation with temperature as described by the Antoine equation. Therefore, the permeate water flux is enhanced when increasing

the feed temperature [93–95]. In general, higher feed temperature also has a positive effect on water diffusion coefficient in the vapor phase, contributing to the increase in the permeate flux [93]. On the other hand, an increase in permeate temperature reduces the driving force for water permeation and consequently, the permeate flux. However, it has been demonstrated that it is more convenient and economical to increase the feed temperature rather than to decrease the permeate temperature in order to obtain higher fluxes in MD [96].

Specially for DCMD. the permeate flux increases with the flow rate of both feed and permeate streams. It is expected that higher flow velocities increase the heat and mass transfer in both sides of the membrane module, reducing the thermal and mass boundary layer approaching the membrane surface to the corresponding temperature and concentration in the bulk phase, respectively, increasing the driving force and the permeate flux. [77,83]. The temperature and concentration polarization effects, mainly for feed side are reduced, similarly for the permeate side in the case of presence of volatile components [28,83,97].

The influence of feed concentration on the MD flux relies significantly on the nature of the feed aqueous solutions. For the aqueous solution containing volatile solutes, the permeate flux increases with the its concentration in the solution [77]. Otherwise, for aqueous solution containing non-volatile solute, the flux decreases with the solute feed concentration due to reduction in water vapor pressure [98,99].

Schofield *et al.* (1990) [100] reported that the presence of solute in the feed also alters the density and viscosity that influence on the heat and mass transfer. However, the preponderant effect on permeate flux will depend on the solute, since vapor pressure reduction may be the major cause of flux reduction for single salts, while viscosity may have a greater effect in the case of high molecular mass solutes [101].

2.2.3. Membrane characteristics

The membrane itself acts only as a barrier to hold the liquid/vapor interfaces at the entrance of the pores and it is not necessary to be selective as required in other membrane processes [83].

MD membranes must not be wetted, and only vapor and non-condensable gases must be present within its pores, thus, to avoid pore wetting, the membrane material has to be hydrophobic. The average pore size must be small and with a narrow distribution, often between 10 nm and 1 μm. Membrane used in MD should have the following general characteristics: low resistance to mass transfer; high porosity; high liquid entry pressure to maintain the membrane pores dry; low surface energy and low thermal conductivity to reduce heat loss across the membrane. In addition, the membrane should have good thermal stability and high resistance to chemicals, such as acids and bases as well as long-term stability [28,30,83,84,102,103]. Hydrophobic microporous membranes made from polytetrafluoroethylene (PTFE), polypropylene (PP) or polyvinylidenefluoride (PVDF) are mainly used to in MD [28,83,102]. Ullah *et al.* (2018) concluded that the selection of suitable membrane materials and the membrane properties are quite important for a good MD performance.

2.2.3.1.Membrane thickness

In MD, as in other membrane separation processes, the permeate flux is inversely proportional to the membrane thickness and it plays a significant role in dictating the resistance to mass transfer. High permeability is reached using membrane as thin as possible, by contrast to achieve better heat efficiency the membrane should be as thick as possible due to the fact in MD heat loss by conduction takes place through the membrane matrix [83,104]. Some authors [104,105] reported that the optimum thickness is between 30 and 60 μm. The thickness of the membrane is also related to its mechanical integrity [84,104]. Nevertheless, in MD membrane the mechanical properties are less important when compared with other membrane separation process.

2.2.3.2.Membrane porosity

The global MD membrane porosity lies between 30 and 85%. Higher porosity provides greater surface area for evaporation in MD, consequently higher permeate fluxes are reached [83,84,106]. Ullah *et al*. (2018) [103] suggested a membrane porosity larger than 75%. However, membrane porosity shows typical trade-off with mechanical properties. Figoli *et al.* (2014) [107] showed that fibers with higher porosity present reduced Young's Modulus.

Other aspect to be considered is the coupling of mass and heat transfer, when the mass transport is favored it is also expected higher heat transport. Therefore, a compromise should be made between the mass and heat transfer, by properly adjusting the membrane porosity [106].

2.2.3.3.Membrane pore size

MD pores sizes ranging from 100 nm to 1 μm and it is admitted that the MD flux increases with the increase of the pore size. In contrast, large pores increase the risk of membrane wetting due to the lower liquid entry pressure (LEP) [84]. A pore diameter of 0.3 μm was suggested to be optimum since allows to maintain a liquid entry pressure of 2.5 bar [103]. Therefore, there must be a balance between the permeate flux maximization and the pore wetting minimization. Choosing an appropriate pore size and pore size distribution, this could be controlled [81,83,106].

LEP of porous membranes could be described by Laplace (Cantor) equation (Eq. 1) [81,83,102]:

$$LEP > \Delta P = P_L - P_v = -\frac{4\mathrm{K}\gamma_L cos\theta}{d_{max}} \quad (1)$$

where K is a geometric factor determined by pore structure, $\gamma_L$the liquid surface tension, d_{max} is the maximum pore diameter and θ is the liquid/solid contact angle.

To avoid membrane pore wetting, the hydrostatic pressure must be lower than the LEP. However, pore wetting can occur as result of solute adsorption or solute precipitation at the membrane surface. These could change the membrane properties favoring the pore wetting [104].

2.2.3.4.Pore size distribution (PSD)

The pore size distribution should be as narrow as possible [106]. The membranes employed in MD do not always meet this requirement exhibiting more than one transport mechanism simultaneously [83,84,104].

2.2.3.5.Pore tortuosity

MD flux is inversely proportional to transport length path through the membrane. Tortuosity factor measures the deviation of the pore structure from straight cylindrical pores normal to the surface [83,106]. Due to the difficulties in measuring the real value of membrane tortuosity for microporous membrane, it is frequently assumed being 2 or is estimated using expressions that relate it to the membrane porosity [106]. It has been reported that tortuosity factor values should be between 1.1 and 1.2 [103]

Srisurichan *et al*. (2006) [108] employed a correlation proposed by Mackie and Meares (1955) to estimate the tortuosity of the membrane in DCMD (Eq. 2).

$$\tau = \frac{(2-\epsilon)^2}{\epsilon} \tag{2}$$

Some authors have estimated the membrane tortuosity using a method based on the theoretical model random clustered polymer structures (Eq. 3) [96,104].

$$\tau = \frac{1}{\epsilon} \tag{3}$$

2.2.3.6. Thermal conductivity

The thermal conductivity of the membrane is a combination of the polymer in the membrane matrix and the gaseous phase in the membrane pores [109]. Thermal conductivity of the most used materials used in MD membranes is resumed in Table 3 [106]. Thermal conductivity in the range of 0.06 $W/m \cdot K$ was indicated as an appropiate value [103].

Table 3. Thermal conductivity of polymers.

Material	Thermal conductivity ($W/m \cdot K$)	Temperature (K)
PVDF	0.17-0.19	296
	0.21	348
PP	0.11-0.16	296
	0.20	348

PTFE	0.25-0.27	296
	0.29	348

2.2.3.7.Membrane surface chemistry

A hydrophobic surface is requisite for MD process. Highly hydrophobic material can prevent water from wetting the membrane pores [104]. Fluropolymers have been used by their high thermal stability, mechanical strength and low surface energy [110]. PP, PTFE and PVDF are the most used in MD by their good thermal and chemical resistance and their hydrophobicity. PTFE has the lowest surface energy (i.e. most hydrophobicity), however PVDF is the most used because of its easy processability [104].

MD membrane also must have chemical resistance to the feed solutions. If the membrane has to be cleaned frequently, resistance to acid and base components is also necessary. Several surface modification techniques have been used to protect the surface membrane (facing hot solution) by increasing its hydrophobicity [83,106]. Membrane modification methods include surface grafting, coating, blending and filling [110].

2.2.3.8.Membrane fouling

One of the main challenges associated with MD is its fouling effect. Membrane fouling is the accumulation of unwanted materials on the surface or inside the pores of a membrane that results to a detrimental effect on the overall MD performance [111]. Another effect of these foulants is the tendency to modify membrane surface properties resulting in a decrement of the net hydrophobicity and changes in the pore structure, which facilities pores wetting and causes a reduction of permeate quality [30,112,113]. Scaling may create a hydrodynamically stagnant or slow moving layer of water at the surface of the membrane which can increase the effects of temperature and concentration polarization [113].

The main factors that affect fouling are: foulant characteristics (concentration, molecular size, solubility, diffusivity, hydrophobicity, charge, etc.); membrane properties (surface roughness, pore size, surface charge, etc.); operational conditions (flow rate, temperature); and feed characteristics (nature, pH, presence of organic/inorganic matters, dissolved gases) [30,111–113].

Solubility and crystal formation of individual salts depend strongly on the temperature. For this reason, temperature has an important influence on scaling and fouling of MD membranes. Besides, temperature can have significant effect on biofouling due to microorganism' lack of tolerance for high temperature and also because of thermal effects on organic compounds [113].

The flux decline occasioned by fouling causes an increment in the power consumption, in the membrane area requirement and change the hydrophobicity of the membrane decreasing its lifespan [114]. Scaling and membrane wetting leads to the permeate flux decline as result of three processes: suppressing the driving force for the transport of water vapor, narrowing the liquid-vapor interface and blocking the diffusion pathway of water vapor [115].

Several types of fouling or scaling has been reported in the literature. Substance such as $CaSO_4$ and $CaCO_3$, known as scalants, may gradually deposit on the membrane surface or within its pores reducing the permeate flux with time [30,33,83,111,112]. The layers deposited on the membrane surface can be porous or homogenous (non-porous). In the former case, a decline of the permeate flux mainly results from an increase of the thermal resistance. The formation of homogeneous fouling layer interferes in the mass transportation [112].

Other foulants reported are particulates and colloidal, organic compounds and biological matter (biofouling) which can also cause flux decline. Organic fouling is mainly associated with the adsorption/deposition of dissolved and colloidal organic matter on the membrane surface. Biological fouling is caused mainly by microorganism such as bacteria and fungi, sludge, algae, yeast, etc. [30,111,112]. In most of cases, a combination of different fouling materials and mechanisms take place in MD process which makes dealing with this phenomenon more complicated.

Feed treatment and periodical membrane cleaning are techniques that allows to minimize and control membrane fouling [31]. Coagulation/precipitation, media filtration, sonication, boiling, thermal softening, membrane filtration, pH changes and chlorination are some pretreatments that were effective for fouling minimize [111,113].

2.2.3.9.Membrane wetting

Membrane wetting takes place due to the intermolecular interaction between the solid membrane surface and the gas, liquid or solid in contact with. Membrane pores wetting also can occur and, in this case, could be partial or complete wetting. In the former, the liquid penetrates the pores of the membrane which causes a flux decrement because the blockage of the pore. While when a complete wetting occurs, there is a sudden increment in the permeate flux as well as a decrement in the permeate quality because of the passage of the salts dissolved in the liquid [116,117].

As it was mentioned, the membrane hydrophobicity is very important to avoid the liquid entry in the pores. Besides, LEP is a parameter that allows to determine the membrane resistance to the wetting.

Pore wetting could be due to: the use of transmembrane pressure higher than LEP; the capillary condensation due to loss of temperature gradient; the scale deposition and the organic fouling; the presence of surfactant or other low surface tension components; or the membrane degradation as result of the long-term operation [116,118].

After the membrane wetting, to recover the initial membrane characteristics is proposed a backwashing using a nonaqueous solution that wetted the membrane. Then, the solution is evaporated from the membrane by drying in an oven. Another, alternative it is performed a backwashing by pressurized air. This allows to come out the foulant and the water present in the pores of the membrane [117]. Rinsing followed by drying is also reported however in general it is inefficient due to the hydrophilic groups present on the membrane surface [118].

Table 4 presents the permeate flux in different membrane configurations found in the literature. The membrane characteristics and operational parameters are also presented. As aforementioned, PTFE, PP and PVDF are the main material used for this application.

The DCMD process is preferred for testing NaCl solution, brine, and seawater. For DCMD, permeate fluxes between 2.8 and 195 kg/m^2h are reported depending on the membrane characteristics as well as the operational parameters. For example, a permeate flux of 195 kg/m^2h was possible to achieve operating with a hydrostatic pressure of 3 atm and feed temperatures of 128 °C [119]. VMD is also widely used for NaCl treatment and for volatile separation. In general, for VMD the permeate fluxes are higher than for DCMD because of the higher thermal efficiency of the former due to the lower heat loss by conduction across the membrane [120,121].

Rao *et al*. (2015) [121] proposed a vaccum-enhanced (VEDCMD) and pressure-enhanced (PEDCMD) direct-contact MD. In the former, vacuum is applied on the permeate side and the later a hydraulic pressure is applied on the feed side. VEDCMD showed a higher permeate flux due to the lesser compaction and lower air pressure inside the membrane pores.

AGMD and SGMD configurations are often studied for different applications. The PGMD configuration which is a modified configuration of the AGMD is also found in presented in Table 4.

Table 4. Operational parameters and permeate flux in different membrane configurations.

Membrane Configuration	DCMD	DCMD	DCMD	DCMD	DCMD	DCMD	DCMD
Membrane Characteristics	PTFE – FS $r_P = 0.1\ \mu m; \epsilon = 0.72;\ \delta_m = 130\ \mu m$	PTFE – FS $r_P = 0.22\ \mu m;\ \delta_m = 175\ \mu m$	PVDF – FS $r_P = 0.22\ \mu m;\ \delta_m = 125\ \mu m; \epsilon = 62\%$	PP – FS $r_P = 0.064\ \mu m;\ \delta_m = 25\ \mu m; \epsilon = 55\%$	PTFE – FS $r_P = 0.22\ \mu m;\ \delta_m = 160\ \mu m$	PTFE – HF $r_P = 0.24\ \mu m; \epsilon = 0.5;\ \delta_m = 205\ \mu m;\ O.D = 1.94\ mm$	PTFE – FS $r_P = 0.3\ \mu m; \epsilon = 0.65;\ \delta_m = 24\ \mu m$
Operational parameters	NaCl solution 3.5 wt%, $T_f = 45°C; T_p = 25°C; v_f = 0.02\ m/s$	$T_f = 70°C;$ $T_p = 30°C;$ $Q_f = 1.5 L/min$	Seawater Boron 5.37 mg/L $T_f = 59°C; T_p = 20°C; Q_f = Q_p = 20\ L/h; pH = 7.84$	$\Delta T = 50°C;$ $Re_f = 3657;$ $Re_p = 419$	NaCl solution 3.5wt% $T_f = 60°C; T_p = 20°C; Q_f = 1.6 L/min$	NaCl solution 1wt% $T_f = 118°C; T_p = 30°C; P = 2-3\ atm$ Feed by the shell	NaCl solution 1wt% $T_f = 128°C; T_p = 25-30°C; Q_f = 500\ \frac{mL}{min}; P = 3\ atm$
Permeate flux, $\frac{kg}{m^2 h}$	≈ 2.8	≈ 29 (Brine from MSF)	≈ 26 (Seawater)	≈ 2.53 (NaCl – 0.118 mM)	≈ 3.40 (Brackish water)	≈ 2.40 (Seawater)	≈ 25.6	≈ 115	≈ 195
Reference	[126]	[114]	[125]	[124]	[123]	[122]	[119]		

Table 4. Operational parameters and permeate flux in different membrane configurations (continued).

Membrane Configuration	VMD	VMD	VMD	VMD	DCMD	DCMD	PEDCMD	VEDCMD
Membrane Characteristics	PVDF – FS $r_P = 0.2\ \mu m; \frac{\epsilon}{\tau\delta} = 14000 - 17000\ m^{-1}$	PTFE – FS $r_P = 0.22\ \mu m; \epsilon = 0.70;\ \delta_m = 0.175\ \mu m$	PP - HF $r_P = 0.2\ \mu m, \epsilon = 0.60, O.D. = 0.5\ mm, I.D. = 0.25 mm$	PVDF – FS $r_P = 0.49\ \mu m;$ $\delta_m = 82\ \mu m; \epsilon = 78\%$		PTFE – FS $\delta_m = 67\ \mu m; \epsilon = 80\%$		
Operational parameters	NaCl solution 2wt% $T_f = 90°C; P = 14.5\ kPa; Q_f$ $1.8\ L/min$	NaCl solution 10 g/L + 2000 ppb $NaAsO_2$ $T_f = 40°C; P = 5\ kPa; Re = 3400$	NH_4OH $218\ ppm +$ $NaCl\ 500\ ppm$ $T_f = 50.4°C; P = 100 - 400Pa; Q_f = 200\frac{mL}{min}$	NaCl 35g/L $T_f = 85°C; Q_f = \frac{54L}{h}; P = 70kPa$	NaCl 35g/L $T_f = 85°C; T_p = 25°C; Q_f = Q_p = 54L/h$	NaCl 35 g/L $T_f = 40°C; Q_f = 1\frac{L}{min}$ Feed/distillate pressure (kPa)		
						20/20 ($\Delta P = 0kPa$)	100/20 ($\Delta P = 80kPa$)	20/-60 ($\Delta P = 80kPa$)
Permeate flux $\frac{kg}{m^2h}$	≈ 62.51	≈ 5.05	≈ 1.00	≈ 38.95	≈ 32.00	≈ 12.1	≈ 13.1	≈ 20.8
Reference	[129]	[128]	[127]	[120]			[121]	

Table 4. Operational parameters and permeate flux in different membrane configurations (continued).

Membrane Configuration	VMD	AGMD	AGMD			SGMD	SGMD	SGMD
Membrane Characteristics	PTFE – FS $r_P = 0.23\ \mu m; \frac{\epsilon}{\tau\delta_m} = 916.2\ m^{-1}$	TIPS-iPP – HF $r_P = 0.2\ \mu m; \epsilon = 0.68;\ \delta_a = 0.5\ mm$	PTFE – FS $\delta_m = 175\ \mu m$			PTFE – FS $r_P = 0.2\ \mu m$	PVDF – HF $r_P = 0.1\ \mu m; \epsilon = 0.55; L = 0.127\ m; d_i = 230\ \mu m; d_o = 330\ \mu m$	PTFE – FS $r_P = 0.45\ \mu m; \epsilon = 0.7; \delta_m = 100 - 200\ \mu m$
			TF200 $r_P = 0.2\ \mu m$	TF450 $r_P = 0.45\ \mu m$	TF1000 $r_P = 1.0\ \mu m$			
Operational parameters	Ammonia solution 0.89 M $T_f = 50°C; P = 8.3\ kPa; v_f = 0.15\ m/s$	NaCl solution 30g/L $T_f = 90°C; T_p = 20°C; Q_f = 10\frac{L}{h}$	Produced water $T_f = 50°C; T_p = 10°C; Q_f = 1.89\frac{L}{min}$			Ethanol 5wt% (aqueous solution) $T_f = 55°C; T_f = 25ºC;\ Q_g = 4.65NL/min; Q_f = 600mL/min$	Brine $T_f = 72°C; v_g = 0.54m/s; v_f = 0.02m/s$	Ammonia solution 100 mg/L, pH = 11.5 $T_f = 75°C; Q_g = 5\ L/min; Q_f = 0.25\ L/min$
Permeate flux $\frac{kg}{m^2h}$	≈ 10.71 (average separation factor ≈ 3.63)	≈ 3.58	≈ 8.50	≈ 10.13	≈ 10.44	≈ 2.5	≈ 1.19 $[mol/m^2min]$	≈ 14.84
Reference	[133]	[132]	[93]			[131]	[86]	[130]

Table 4. Operational parameters and permeate flux in different membrane configurations (continued).

Membrane Configuration	PGMD	AGMD	AGMD	DCMD		PGMD	
Membrane Characteristics	PTFE – SW $A = 10\ m^2; \delta = 70\mu m;\ r_p = 0.2\ \mu m, \epsilon = 80\%;\ \delta_p = 1\ mm$	LDPE – SW $\delta = 76\mu m;\ r_p = 0.3\ \mu m, \epsilon = 85\%;\ \delta_p = 0.88\ mm$ $A = 7.2\ m^2$	$A = 24\ m^2$	PTFE – FS $r_p = 0.2\ \mu m; \epsilon = 85\%; A = 0.0041\ m^2$		PVDF – HF $d_i = 0.81\ mm; d_o = 1.11\ mm; \epsilon = 81.7\%;\ r_p = 0.15\ \mu m; L = 0.425\ m; A = 0.0102\ m^2$	
		Marine salts 0.6 M		Reactive black	Disperse black	$T_f = 70\ °C; v_f = 0.81 \frac{m}{s}$	
Operational parameters	$Q_f = 500 \frac{L}{h}; T_f = 70\ °C; T_p = 30\ °C$	$Q_f = 600 \frac{L}{h}; T_f = 80\ °C; T_p = 20\ °C$	$Q_f = 500 \frac{L}{h}; T_f = 70\ °C; T_p = 20\ °C$	$T_f = 90\ °C; T_p = 20\ °C; Q_f = 4.7 \frac{L}{min}; Q_p = 1.2 \frac{L}{min}$		8 Gap channels HDPE $d_i = 2.84\ mm; d_o = 3.40\ mm$	8 Gap channels SS 316 $d_i = 4.55\ mm; d_o = 6.35\ mm$
Permeate flux $\frac{kg}{m^2 h}$	≈ 1.5	≈ 2.7	≈ 1.3	≈ 75	≈ 60	≈ 9.41	≈ 11.2
Reference		[136]		[135]		[134]	

FS: Flat sheet; SW: spiral wound; HF: Hollow Fiber

2.2.4. Heat transfer mechanisms in membrane distillation

Heat transfer is very important and is more likely believed to be rate controlling in the MD process. It is carried out in four steps: (i) heat transferred from the heated feed solution across the thermal boundary layer to the membrane surface; (ii) the heat transported by conduction through both the membrane matrix and the gas filled pores, which is considered a heat loss in MD; (iii) heat associated to the mass transfer of the vaporized components through the membrane pores, which is expressed as latent heat; and (iv) heat transfer from the membrane surface to the permeate solution across the thermal boundary layer in the permeate side [32,83].

The heat transfer boundary layer formed at each side of the membrane surface imposes resistances to heat transfer and makes the temperature difference at the liquid/membrane interfaces lower than that applied at the bulk phases and this affects negatively the driving force for mass transfer [83]. A schematic representation of the heat transfer, represented by the model of resistances is shown in

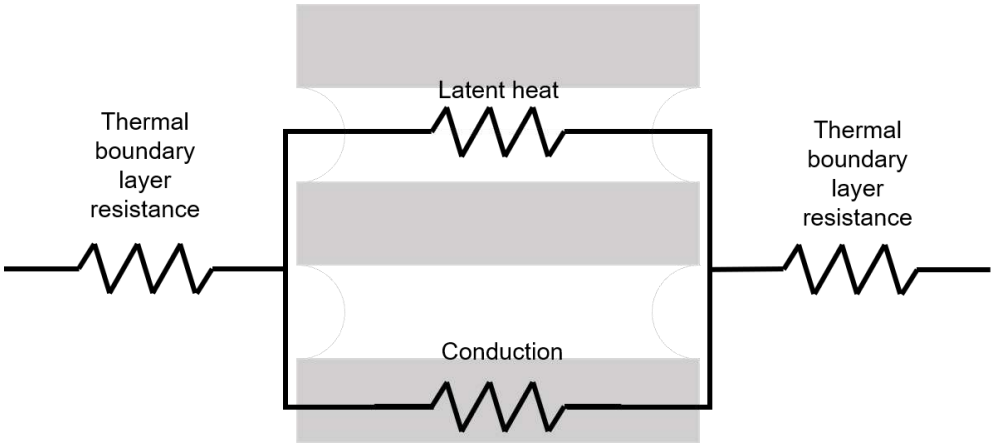

Figure 4. Model of resistances for the heat transfer in DCMD

Temperature difference between the feed/membrane interface temperature (T_f^m) and the permeate/membrane interface temperature (T_p^m) is the driving force for water transport through the membrane. However, due to heat losses in DCMD process, there are differences between the bulk temperatures (T_f^b and T_p^b, feed and permeate, respectively) and the membrane/interfaces temperatures. This difference constitutes one of the main drawbacks of this configuration since it results in the drop of the DCMD

driving force. This phenomenon is known as temperature polarization and it is measured by the temperature polarization coefficient (TPC) as given by Eq. 4 [137]:

$$TPC = \frac{T_f^m - T_p^m}{T_f^b - T_p^b} \tag{4}$$

where T_f^m, T_p^m, T_f^b and T_p^b are membrane surface temperatures and fluid bulk temperatures at the feed and permeate side, respectively.

Feed and permeate thermal boundary layers are function of fluid properties and operating conditions, as well as the hydrodynamic conditions. TPC was observed to decrease generally with increasing operating temperatures. Working at high flow velocities is always an option that is usually considered by MD investigators to achieve better mixing conditions and minimizing the effect of temperature polarization [30,83].

In the feed boundary layer, there is heat transfer due to mass transport across the feed thermal boundary layer, $q_{f,M.T.}$; and convection-heat transfer, $q_{f,conv}$, that depends on the heat transfer film coefficient of the boundary layer, h_f, and the temperature difference between the feed bulk and membrane surface, i.e. [30,83]:

$$q_f = q_{f,conv} + q_{f,M.T.} = h_f\left(T_f^b - T_f^m\right) + NH_{L,f}\{T\} \tag{5}$$

where the $H_{L,f}\{T\}$ is the enthalpy at temperature T. $H\{T\}$ is given by $H\{T\} = CpT + (H\{T_0\} - CpT_0)$ and T_0 is the reference temperature (generally, equal to 273 K) [109].

The combination of conductive heat transfer ($q_{m,cond}$) and heat transfer due to water vapor transport through the membrane pores ($q_{m,M.T.}$) is described by [30,137]:

$$q_m = q_{m,cond} + q_{m,M.T.} = h_m\left(T_f^m - T_p^m\right) + NH_v\{T\} \tag{6}$$

where h_m is the heat transfer coefficient, which can be evaluated as follows:

$$h_m = \frac{\kappa_m}{\delta_m} \tag{7}$$

The thermal conductivity of the membrane (κ_m) can be evaluated as a combination of properties of two-phase composite material. Basically, two models are applied the isostrain or parallel model, and the isostress or series model. In both models, the thermal conductivity is calculated as the volume-average of both conductivities, the solid one, κ_S and the gas phase one, κ_g. The parallel model assumes that solid material is orientated in same direction of heat flux, while the series model the orientation is perpendicular to heat flux. Eqs. 8 and 9 describe the thermal conductivity of the membrane using parallel and series models, respectively [109,138–140].

$$\kappa_m = \epsilon\kappa_g + (1-\epsilon)\kappa_S \tag{8}$$

$$\kappa_m = \left[\frac{\epsilon}{\kappa_g} + \frac{(1-\epsilon)}{\kappa_s}\right]^{-1} \tag{9}$$

where ϵ is the membrane porosity.

The thermal conductivity at 298 and 348 K of air are reported as 0.026 and 0.03 $W/m \cdot K$, respectively. While the thermal conductivity of water vapor in the same temperatures are 0.020 and 0.022 $W/m \cdot K$, respectively [109]. As one may observe, there is a very small difference between the water vapor and air thermal conductivities and, therefore, it is possible to assume that the gases in the pores behave as one single component. Besides, the thermal conductivity of air/gases is an order of magnitude lower than that of the membrane material. Hence, the heat lost by conduction through the membrane can be minimized by using membranes with high porosity [28,83,106].

The fraction of heat transferred by conduction through both the membrane matrix and the gas filled pores is considered heat lost and should be minimized in order to decrease the temperature polarization effect and increase the efficiency of the MD process [83].

In permeate side, heat transfer also occurs by convective flow and due to mass transfer from the membrane surface to the bulk phase, across the thermal boundary layer, generating the temperature polarization effect. The heat flux that takes place in this case is written as [137]:

$$q_p = q_{p,conv} + q_{p,M.T.} = h_p\left(T_p^m - T_p^b\right) + NH_{L,p}\{T\} \quad (10)$$

At steady state conditions, the following expression is considered [83]:

$$q_f = q_m = q_p \quad (11)$$

Phattaranawik *et al.* (2003) [109] found that the maximum effects of mass transfer on heat transfer rates in the feed and permeate streams were only 7.2 and 3.2%, respectively. Qtaishat *et al.* (2008) [137] reported that the effect of mass permeate flux on both temperature polarization layer is much lower than thermal factors and can be neglected. The authors also considered that the vapor enthalpy (H_v) is nearly equal to the latent heat of vaporization (ΔH), and Eqs. 5, 6 and 10 can be rewritten as follows:

$$q_f = h_f\left(T_f^b - T_f^m\right) \quad (12)$$

$$q_m = h_m\left(T_f^m - T_p^m\right) + N\Delta H \quad (13)$$

$$q_p = h_p\left(T_p^m - T_p^b\right) \quad (14)$$

Since it is very difficult to measure the membrane/interface temperatures experimentally; usually these temperatures are evaluated by performing a heat balance that relates them to the bulk temperatures. Most of the theoretical models are based on the adjustment of at least one parameter, frequently the pore tortuosity factor, to predict the permeate flux. Heat transfer coefficients in the boundary layers are usually estimated by empirical correlations that relate the dimensionless Nusselt number with the Reynolds and Prandtl numbers. However, these empirical models are based on the applicability of the heat transfer correlations that were originally developed for rigid nonporous heat

exchangers, and care has to be taken for selecting the proper correlation [106,141,142]. Moreover, by using this approach very different values are predicted even under the same conditions but with different correlations [106,110].

2.2.5. Mass transfer mechanisms in membrane distillation

Mass transport of the volatile species is taking place (i) from the bulk feed to the membrane surface; (ii) through the membrane pores in the gaseous phase; and (iii) from the membrane surface at the permeate side to the bulk permeate phase [83]. The non-volatile components accumulate in the membrane surface in the feed side.

In MD, the diffusive mass transfer resistance in the liquid phase is given by the concentration polarization of the less volatile component in a mixture near the membrane surface. The concentration of the less volatile components will rise at the entrance of the membrane pores, reducing the driven force of the more volatile components. As the concentration of the non-volatile (or less-volatile) solute at the membrane surface becomes higher than that at the bulk feed solution care must be taken as supersaturation states may eventually be achieved affecting the efficiency of the membrane process [83]. The term concentration polarization coefficient (CPC) is usually defined to quantify the concentration increase in the boundary layer at the feed side (Eq. 15):

$$CPC = \frac{C_m}{C_b} \tag{15}$$

Mass transfer through the feed liquid phase can be usually described by the film theory model, which assumes that the drop in concentration is located in a thin layer close to the membrane [143]. Based on this, molar flux of species A (volatile component) through the concentration boundary layer, assuming total retention of non-volatile component B, may be calculated from the following mass balance equation (Eq. 16) [33]:

$$N_A = C k_f \ln\left(\frac{C_{B,m}}{C_{B,b}}\right) \tag{16}$$

where N_A is the molar flux of volatile component A, C the bulk liquid phase total molar concentration $(C_A + C_B)$ and k_f is the mass transfer coefficient through the concentration boundary layer.

When MD is used for the separation or removal of volatile compounds from aqueous solutions, the permeate side will have higher solute concentrations (volatile component). In this case, mass transport resistance will be given by concentration boundary layers made of the solvent (water) and not the solute. The molar flux of volatile component, N_A, across the concentration boundary layer and assuming a negligible water flux, can be expressed by Eq. 17 [33,83]:

$$N_A = C k_f \ln\left(\frac{C_{w,b}}{C_{w,m}}\right) \tag{17}$$

where C is the bulk liquid phase total molar concentration $(C_w + C_A)$, C_w and C_A are the water and the volatile component concentrations, and k_f is the mass transfer coefficient in the concentration boundary layer.

In MD with non-volatile solutes, low to moderate flow rates reduce concentration polarization resistance. Additionally, it is considered that the temperature polarization effect is more evident than the concentration polarization. This represents an advantage, since it is possible to operate with higher concentrations than in other membrane processes (mainly, pressure driven) such UF, which concentration polarization is usually considered a major cause of flux decline [83,99,100].

The overall mass transfer resistance is the sum of the liquid boundary layer resistance and the resistances to mass transfer in the membrane pores and in the permeate boundary layer. However, it has been demonstrated that the mass transfer boundary layer resistance in the feed and permeate sides, generally, result in a negligible contribution to the overall mass transfer resistance [33,144].

The Stefan-Maxwell model describes the vapor diffusion through the membrane pores to determine the diffusive fluxes as shown in Eq. 18, since it allows to take into account the diffusional interactions. At constant pressure, the driving force of the mass

transfer is equal to the composition gradients. For ideal gas mixtures the diffusive fluxes are given by [112,145–147]:

$$(J) = -c_t[B]^{-1}(\nabla x) \tag{18}$$

Due to the hydrophobic nature of the membrane used in MD, a liquid-gas interface is formed at the membrane surface in the feed side (in the entry of the membrane pores) where the evaporation of the volatile species takes place. For the DCMD, another gas-liquid interface is formed at the membrane surface in the permeate side, where the volatile species condensation occurs. Regarding the two phases, it is considered that the interface compositions are $x_{i,L}$ at the interface in the liquid phase and $y_{i,L}$, at the interface in the gas phase. Besides, the interface is a surface that offers no resistance to mass transfer and where equilibrium prevails. The mass transfer takes place in a direction normal to this interface. It is way, there is continuity of molar fluxes.

$$N_i^v = N_i^L = N_i \tag{19}$$

$$N_t^v = N_t^L = N_t \ = \sum_{i=1}^{n} N_i \tag{20}$$

The molar flux N_i is important because it is this flux that allows calculating the heat flux in the membrane distillation process where both mass and heat transfer takes place simultaneously. In this way, even if the diffusion fluxes of the n components are known, it is not possible to calculate the molar fluxes immediately, because all n of these fluxes are independent, whereas only $n-1$ of the J_i are independent.

$$J_n = -\sum_{i=1}^{n-1} J_i \tag{21}$$

In this way, for determining N_i knowing J_i (the bootstrap problem), it is considered that the mass transfer occurs inside the membrane pores and one of the components has a zero flux. In this case, it is considered that the zero-flux component is the air stagnant inside the pores. This is known as Stefan Diffusion [146]. Being the zero-flux component, the n^{th} specie.

$$N_n = J_n + x_n N_t = 0 \tag{22}$$

In order to calculate the flux of the i specie from the J_i

$$N_i = J_i + x_i N_t = J_i - \frac{x_i J_n}{x_n} \tag{23}$$

where $N_t = -J_n/x_n$ from Eq. 22. Thus, Eq. 23 can be rewritten as:

$$N_i = \left(1 + \frac{x_i}{x_n}\right) J_i + \frac{x_i}{x_n} \sum_{\substack{k=1 \\ k \neq i}}^{n-1} J_k \tag{24}$$

A general expression for the relationship between N_i and J_i is written in terms of the generalized determinacy condition as:

$$\sum_{i=1}^{n} \nu_i N_i = 0 \tag{25}$$

where ν_i are the determinacy coefficients. N_i related to J_i is written as in Eq. 26 and the sum over all species as in Eq. 27:

$$\nu_i N_i = \nu_i J_i + x_i \nu_i N_t \tag{26}$$

$$0 = \sum_{i=1}^{n} \nu_i J_i + N_t \sum_{i=1}^{n} x_i \nu_i \tag{27}$$

The total flux N_t can be expressed as:

$$N_t = -\sum_{k=1}^{n-1} \Lambda_k J_k \tag{28}$$

where $\Lambda_k = (\nu_k - \nu_n) / \sum_{j=1}^{n} \nu_j x_j$

Finally, the N_i can be written as:

$$N_i = -\sum_{k=1}^{n-1} \beta_{ik} J_k \tag{29}$$

where $\beta_{ik} \equiv \delta_{ik} - x_i \Lambda_k$. In this expression, δ_{ik} is the Kronecker delta which for $i = k$ is equal to 1 and for $i \neq k$ is equal to 0.

Stefan-Maxwell relations allow to study the diffusion interaction between the components. (Eq. 30) The Stefan-Maxwell equations are written in the matrix form as expressed in Eq. 31.

$$\frac{dy_i}{dr} = \sum_{j=1}^{n} \frac{y_i N_j - y_j N_i}{c_t D_{ij}} \tag{30}$$

$i = 1, \dots, n$

$$\frac{dy_i}{d\eta} = \Phi_{ii} y_i + \sum_{\substack{j=1 \\ j \neq i}}^{n-1} \Phi_{ij} y_j + \phi_i \tag{31}$$

where for $i = 1,2, \dots, n-1$ and η is the dimensionless coordinate expressed as:

$$\eta = \frac{r - r_0}{\ell} \tag{32}$$

where ℓ is the film thickness and it is given by $\ell = \tau \delta_m$ in order to include the membrane tortuosity.

The elements of the Φ matrix are given by Eqs. 33 and 34.

$$\Phi_{ii} = \frac{1}{c_t} \left(\frac{N_i}{k_{in}} + \sum_{\substack{k=1 \\ i \neq k}}^{n} \frac{N_k}{k_{ik}} \right) \tag{33}$$

$$\Phi_{ij} = -\frac{N_i}{c_t}\left(\frac{1}{k_{ij}} - \frac{1}{k_{in}}\right) \tag{34}$$

ϕ_i is defined by:

$$\phi_i = -\frac{N_i}{c_t k_{in}} \tag{35}$$

The mass transfer coefficient k_{ij} is given by Eq. 36.

$$k_{ij} = \frac{D_{ij}}{\ell} \tag{36}$$

where ℓ is the film thickness.

Using the bootstrap solution, the fluxes N_i can be evaluated from one of two equivalent expressions which are evaluated at $r = 0$ and $r = \ell$, respectively [146,147]:

$$\begin{aligned}(N) &= c_t[\beta_0][k_0][\Xi_0](y_0 - y_\delta) \\ (N) &= c_t[\beta_\delta][k_\delta][\Xi_\delta](y_0 - y_\delta)\end{aligned} \tag{37}$$

where $[k] = [R]^{-1}$. The R array's elements are given by Eqs. 38 and 39.

$$R_{ii} = \frac{y_i}{k_{in}} + \sum_{k=1,k\neq i}^{n} \frac{y_k}{k_{ik}} \tag{38}$$

$$R_{ij} = -y_i\left(\frac{1}{k_{ij}} - \frac{1}{k_{in}}\right) \tag{39}$$

The matrices of correction factors are given by Eqs. 40 and 41 according to whether the molar flux is evaluated at $\eta = 0$ and $\eta = 1$, respectively.

$$[\Xi_0] = [\Phi]\left[\exp[\Phi] - [I]\right]^{-1} \tag{40}$$

$$[\Xi_\delta] = [\Xi_0] \exp[\Phi] \tag{41}$$

Effective fluxes are calculated considering the membrane porosity [147].

$$(N)_e = \epsilon(N) \tag{42}$$

Banat *et al*. (1999) considered the effect of the concentration polarization and in order to calculate the membrane concentration proposed Eq. 43:

$$x_{im} = x_{ip} - \left(x_{ip} - x_{ib}\right) \exp\left[\frac{N_t}{c_t k_{in}}\right] \tag{43}$$

The temperature and concentration polarization effects can be seen schematically in the Figure 5. At the feed side it is shown the temperature drop ($T_f^b - T_f^m$) and the thickness of the thermal boundary layer (δ_f^t). Also, it shows the concentration drop of volatile component ($C_A^{b,f} - C_A^{m,f}$) and the opposite for the non-volatile component ($C_B^m - C_B^b$). The thickness of the mass transfer boundary layer is also illustrated (δ_f^c). Similar situation is shown at the permeate side, the temperature drop between the membrane surface and the bulk ($T_p^m - T_p^b$) and there is a thermal boundary layer thickness (δ_p^t). The volatile component also exhibits a concentration polarization layer (δ_p^c) and a concentration drop to the bulk phase ($C_A^{m,p} - C_A^{b,p}$). The membrane thickness (δ_m) and the membrane pores are also shown. Further, the mass (N) and the heat (q) fluxes directions are shown.

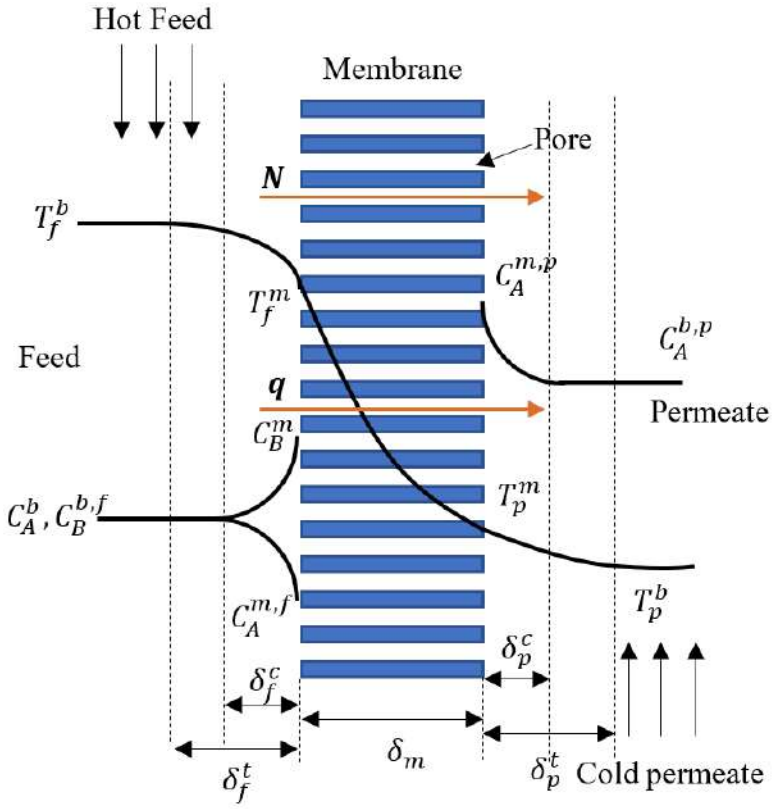

Figure 5. Temperature and Concentration Polarization Effects.

2.2.6. Modelling approach for direct contact membrane distillation

In the membrane distillation process, several different operation conditions are possible by varying both feed and permeate temperatures, flow rates, concentrations, and even modules and membranes. In this way, modelling is widely proposed in order to study these parameters saving time, energy and money. Several approaches are found in the literature for describing the heat and mass transport in the membrane distillation process. The models can describe the phenomena in the liquid phase, inside the porous membranes (vapor phase) or in the whole system [140,148].

Models using Nusselt and Sherwood equations are focused on the liquid phase [99] while the Dusty gas model considers the transport of the volatile component inside the membrane pores [105]. Computational Fluid Dynamics (CFD) has been widely used for describing the whole system by simultaneously solving the momentum, heat and mass equations [148]. Other approaches include the use of artificial neural networks (ANN) and design of experiments (DOE) toolbox [149–151]. These last two approaches are empirical models and do not allow to describe the physical phenomena. A large amount

of data is needed to make conclusions and to perform optimizations. In this regard, the results obtained cannot be extrapolated to other systems [140].

The heat transfer evaluation is usually based on the Nusselt number as a function of the Reynolds and Prandtl numbers in the feed and permeate liquid phase. Several correlations have been obtained and used [109,140,152]. This approach allows to calculate the temperatures at the membrane surfaces, which will be used to calculate the mass transfer [96,140,153,154]. Khayet *et al.* (2011) [106] presented the most used Nusselt correlations. However, the authors warn about the use of these correlations that were originally developed for heat exchangers in which there is no mass transport.

Similarly to the use of Nusselt correlations to describe the heat transfer, Sherwood correlations have been used to describe the mass transfer in the process [96,154]. In many cases, the analogy between heat and mass transfer is assumed, using the Sherwood and Schmidt numbers in an equivalent way of Nusselt and Prandtl [109]. This approach has been widely used to determine the concentration polarization in the liquid phase [99].

Once the temperatures and concentrations at the membrane surfaces are determined, the vapor pressures could be determined. In this point, it is important to consider the reduction of the vapor pressure as a result of the salt presence which affects water activity. With all these data, it is possible correctly evaluate the mass transfer [140,155].

It is worth mentioning that these approaches are considered semi-empirical and an adequate choice of the Nusselt and Sherwood correlations is a determining factor for a good prediction of the permeate flux once there is a great dependence on the flow regime and module geometry [140,155,156]. Another matter to consider is that these correlations are evaluated considering average values for temperatures and concentrations, instead of using continuous distributions. Nevertheless for estimating the permeate flux values, average errors lesser than 5% between the model proposed using these approaches and the experimental data have been reported [157].

The Fick's law and the Dusty Gas Model describe the mass transfer inside the membrane pores. The first one does not take into account the membrane structure while the second one does. This is why the Dusty Gas Model has been extensively proposed in the literature for describing the transport of the volatile components inside the pores. In

this model, the effect of viscous, molecular and Knudsen diffusion are taken in account [152,158].

The Stefan-Maxwell approach for describing the mass transfer in multicomponent ideal gas mixture is hardly found in the membrane distillation literature. Stefan-Maxwell equations consider all coupling interactions between the transporting molecules. This model has been used mainly to describe the mass transport of the volatile components in AGMD [147,159].

Computational fluid dynamics have been considered the most appropriate technique for solving simultaneously momentum, heat and mass equations using a numerical approach, in models that have been developed for one, two or three dimensions [160,161]. Three types of CFD models are generally used: 1) focused on improving just the hydrodynamic conditions and the heat transfer in the module; 2) on the module design and 3) on the whole system, including the mass transfer inside the membrane [140,155]. In the last case, the Dusty Gas Model has been proposed to calculate the membrane coefficient along the membrane length [105].

CFD models can be used to predict the velocity, temperature and concentration profiles allowing the determination of the local temperature and concentration polarization, flux and pressure drop along the modules. CFD models were also proposed for the evaluation of spacers or other turbulence promoters to achieve better performance in the process [162].

Lou *et al.* (2019) [155] developed a two-dimensional CFD model for the heat and mass transfers of hypersaline brines that was validated with experimental data and it was compared with the most commonly used Nusselt and Sherwood correlations. The authors found that these correlations do not allow to predict local membrane conditions due to the temperature and the concentration variation along the module, which can lead to great errors. For example, they do not allow the determination of when concentrations that could cause scaling would be reached.

Experimentally, DCMD process has been proposed for many applications, however, DCMD modelling approach has only focused in feed streams containing non-volatile components, which are concentrated in the feed side [155]. Models considering volatile

and non-volatile mixture are more commonly developed for other configurations rather than DCMD [147,163].

Chapter 3

Methodology

This chapter presents the methodology used to carry out experimental tests in the Membrane Process Laboratory (PAM) at PEQ/COPPE/UFRJ, as well as the model development used to simulate the treatment of a multicomponent solution using direct contact membrane distillation.

3.1. Experimental

A commercial direct contact membrane distillation module (MD020CP-2N, Microdyn®) was chosen for the simplicity to operate and control the process parameters. The MD module contains 40 hydrophobic polypropylene capillary tubes with 0.1 m^2 total area and its characteristics are resumed in Table 5. These data were taken from the literature [81,153,157] and from the data sheet of membrane module. The thermal conductivity of polypropylene membrane considered in this work is an average of the values 0.11 $\frac{W}{m \cdot K}$ at 296 K and 0.2 $\frac{W}{m \cdot K}$ at 348 K, found in Khayet (2011) [106]. A single module was used for all the experiments performed.

Table 5. Membrane distillation module characteristics.

Symbol	Parameter	Value
r_s	Tube external radius (hollow fiber)	1.35 mm
r_l	Tube internal radius (hollow fiber)	0.9 mm
N_{fibers}	Number of tubes	40
d_{mod}	Shell internal diameter	2.1 cm
L	Module length	0.45 m
r_P	Nominal pore diameter	0.20 μm
ϵ	Porosity	73%
κ_S	Thermal conductivity of polypropylene	0.155 $W/m \cdot K$

The experimental set up, as presented in Figure 6, consists in two acrylic tanks, one for water that will flow in the permeate side (outside the tubes) and another for the feed solution (flowing inside the tubes). Feed tank is heated using a glycerol bath in order to achieve high temperatures. The permeate mass is registered in a balance and the water flux is calculated as a ratio of the permeate flow per membrane permeation area. Both tanks are thermally insulated to avoid heat losses. At the top of the tanks there are three holes to allow sampling, temperature and conductivity measurement and the recirculation flow.

Despite the most commonly mode of operation found in the literature being the one performed by feeding the solution to be treated in the shell side and the permeate in the lumen, in this work the opposite mode of operation was chosen. This mode of operation is suggested in the data sheet of the module used in the experiments (MD020CP-2N, Microdyn®). Furthermore, for the same flow rate, the hydrodynamic conditions (axial velocity) will be better in the lumen than in the shell side. Al-Obaidani *et al.* (2008) [157] also reported that there is a fluid maldistribution in the shell side, which affects the mass and heat coefficients of the process.

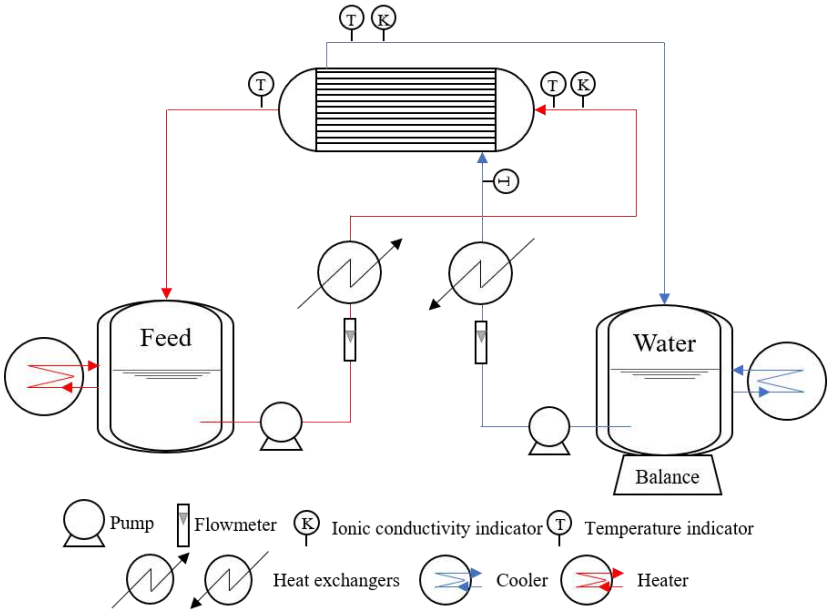

Figure 6. Schematic representation of the DCMD set-up.

Solutions are pumped to the membrane module in counter-current flow, flowing by heat exchanger before entering the module. Positive displacement pumps are used for

this, while the temperatures of the solutions are maintained using thermostatic baths to cool and heat the permeate and feed streams, respectively.

For each experiment, initially a volume of $1000\ mL$ of distilled water with an ionic conductivity of $2 \pm 1\ \mu S/cm$ is putted in the water tank and the balance is putted in zero. The mass increment in the water tank represents the mass of the permeate that permeates the membrane along the experiment. For all experimental tests, the permeate flux is reported as the mean permeate flux given by the total mass of permeate divided by the test time and the permeation membrane area.

In order to monitor and ensure that no pore wetting occurred, the ionic conductivity was measured in both streams during all MD experiments. In the case of pore wetting, permeate conductivity would rise sharply and the MD experiment should be stopped.

3.1.1. Cleaning

After the MD experiment, the set-up was first cleaned by filling the tanks with distilled water (DW) to rinse the module and the whole set-up. Thus, DW was recirculated for 20 minutes, measuring the ionic conductivity. This procedure was repeated until the same conductivity of the original DW was reached. Following this, membrane drying was carried out by passing compressed air by the lumen, by the shell and through the membrane. The drying efficiency was checked by measuring the nitrogen permeability at a pressure difference of 0.1 kgf/cm^2.

Before and after operating with industrial stillage the MD experiment set up was cleaned using a CIP process with a caustic soda solution at pH 9 and a citric acid solution at pH 3. First, the caustic soda solution was recirculated for 20 min. Then, a rinsing with DW was performed to remove the caustic soda solution. Following this, the citric acid solution was recirculated for 20 min. Finally, the module was rinsed with DW, dried and measured the nitrogen permeability. This process was made to ensure that all organic and inorganic material at membrane surface was removed. The nitrogen permeability was also checked after this cleaning procedure.

3.1.2. Synthetic stillage solution

First, MD experimental test was carried out using pure distilled water as feed stream both in the feed side and in the permeate side for the initial evaluations. Each test has been carried out for 2 hours. The permeate mass was registered using a balance and the permeate flux was calculated by dividing the mass by the area and the experiment time.

A synthetic stillage solution was prepared containing alcohol (ethanol), volatile acids (acetic acid), sugars (sucrose) and trace mineral and metals solutions to simulate the wastewater from bioethanol industry [164–167]. Table 6 shows the composition of synthetic stillage with 10,000 mg/L of COD.

Table 6. Composition of synthetic stillage.

Component	Concentration (mg/L)	COD (mg/L)
Ethanol	3194.6	6667
Acetic Acid	624.9	666.6
Sucrose	2374.8	2666.4
$(NH4)_2SO_4$	542.0	
K_2HPO_4	280.6	
KH_2PO_4	219.3	
$(NH_4)HCO_3$	2172.5	
Yeast extract	100	

3.1.3. Study of operational variables influence on the permeate flux.

MD process was tested with water and synthetic stillage as feed solutions in the same conditions in order to determine the concentration polarization effect. Tests were carried out at feed temperatures of 353 K (average temperature of the bioethanol distillation column output), 343 K and 333 K. Permeate temperature was also varied between 293 and 303 K. Flow rates of feed and permeate streams varied from 13 to 36 L/h.

Each experiment was carried out varying only one parameter and maintaining constant the other ones. In this way, it was possible to study the influence of each parameter separately. Table 7 shows the levels of each parameter that were tested.

Table 7. Levels of parameters studied in DCMD tests.

Parameter	Levels		
Feed temperature (K)	353	343	333
Permeate temperature (K)	293	298	303
Feed flow rate (L/h)	13.3	21.3	36.6
Permeate flow rate (L/h)	13.3	21.3	36.6

When the feed temperature is being studied, permeate temperature was maintained at 293 K, feed and permeate flow rates were maintained at 21.3 L/h and the feed concentration at 10,000 mg/L. When another parameter is being studied, feed temperature was maintained at 343 K.

Reynolds number for feed flow rates correspond to 120, 200 and 370 for 13.3 L/h, 21.3 L/h and 36.6 L/h, respectively. For permeate flow rates, number Reynolds correspond to 40, 60 and 100 for 13.3 L/h, 21.3 L/h and 36.6 L/h, respectively. All experiments were conducted in laminar regime.

The feed temperatures were chosen in order to span the temperatures that stillage takes at the distillation column outlet. The typical temperatures found in the plant for water were considered for the permeate temperatures. The flow rates were chosen based in previously work developed in the PAM Laboratory [168].

Results using synthetic stillage served as the basis for deciding the best operational conditions when industrial sugarcane stillage was fed in the system.

3.1.4. Industrial sugarcane stillage.

Industrial sugarcane stillage was provided by USJ Açúcar e Álcool S.A. Unidade São João, a sugar and ethanol production plant located in Araras, São Paulo, Brazil. The results obtained in the previous stage served as the basis for selecting the operational

conditions for the industrial stillage experiments. Due to the high content of total suspended solids, ultrafiltration was used as a pretreatment, with a commercial module – Polyflux® 17L (Baxter). After this pretreatment, the sample was kept refrigerated at 4 ºC. It is worth to mention that this pretreatment was carried out preventively to avoid damage to the experimental system equipment (pumps, heat exchangers, etc.), once they were not suitable for operating samples with high content of suspended solids for long periods of time. However, a short-term experiment (two hours) was performed to determine the performance of the DCMD using raw stillage, without any pretreatment, and the results were similar.

The samples were characterized as received. The sugarcane stillage was treated by membrane distillation and in all cases, feed, concentrated and permeated streams were characterized to determine the removal efficiency and the feasibility of the process as described in Section 3.1.5.

3.1.5. Characterization

Physicochemical and organic characterizations were performed in both synthetic and industrial stillage samples. pH, ionic conductivity, chemical oxygen demand, total phosphorus and ammoniacal nitrogen were measured according to the Standard Methods for Examination of Water and Wastewater ($4500-H^+$, 2520, 5220, $4500-P$ and $4500-NH_3$ methods, respectively) [169]. Organic compounds (sucrose, acetic acid, ethanol and glycerol) were determined using high-performance liquid chromatography (HPLC, Agilent 1260) with a Aminex HPX-87H column at 45 °C, mobile phase consisting of sulfuric acid $5\,mM$ and flow rate of $0.6\,mL/min$. Sucrose and glycerol were analyzed with a refractive index detector (RID) while acetic acid and ethanol were analyzed by ultraviolet (UV) detection at 210 nm. Besides, total (fixed and volatile), suspended and dissolved solids were determined in the industrial sample according the 2540 method of the Standard Methods [169]. The sugar content of industrial stillage samples was also measured using handheld refractometers with automatic temperature compensation (0-32% Brix/ATC and 28-62% Brix/ATC) and the concentration was expressed as degrees Brix (º Brix) [12,170].

It is worth to mention that the characterizations of the permeate stream are presented corrected by the dilution factor given by the mass of the initial volume of distilled water putted in the water tank in order to start the process and the mass of permeate collected during the experiment.

3.1.6. Physicochemical and surface properties of sugarcane stillage

In order to model the sugarcane stillage treatment, it was necessary to determine the physicochemical properties of this effluent. Water activity, thermal conductivity, specific heat, specific mass and viscosity were determined by the procedures described as follows.

The surface free energy was determined to explain the surface phenomena occurred at the membrane surface. All properties were analyzed in duplicate and the results was treated using the Microsoft Excel® software.

3.1.6.1. Specific Heat: this parameter was calculated by Eq. 44, following the work of Larsson and Tengberg [171]. Authors considered that the stillage specific heat could be calculated by pondered average of the specific heat of dry solid content and water:

$$C_{p,stillage} = \left(\frac{100 - Dry\ solid}{100}\right) \cdot C_{p,water} + \left(\frac{Dry\ solid}{100}\right) \cdot C_{p,solid} \quad (44)$$

The dry solid specific heat was considered being 1,270 $J/kg \cdot K$ [171].

3.1.6.2. Specific Mass: was determined by the pycnometer method.

3.1.6.3. Viscosity: this parameter was determined by direct reading at 30°C, using a viscometer model Haake Mars (Thermo Scientific).

3.1.6.4. Water activity: it was measured by direct reading at 20°C, using Aqualab equipment, model Series 3TE (Decagon Devices, USA).

3.1.6.5. Thermal conductivity: it was determined by direct reading using a Thermal Properties Analyzer model KD2 Pro (Decagon Devices, USA).

3.1.6.6. Surface free energy: it was measured using a goniometer equipment (Dataphysics OCA 15). Membrane was fixed in a flat surface, water and stillage drops were delivered onto the membrane surface.

3.2. Mathematical model

Several variables influence the membrane distillation process. It is important to develop a mathematical model that allows their evaluation simultaneously. The same commercial capillary membrane module used in the experiments (MD020CP-2N, Microdyn®) was considered for the simulation. Capillary modules have more uniform distribution of the tubes than the hollow fiber modules. Also, these modules are easier to clean for reuse. However, their packing density is lower [77].

The model was solved for one capillary tube and the same performance was considered in each tube of the module. As presented in Figure 7, axial direction goes from the left to right and the radial direction starts in the center of the fiber, considering a symmetrical condition. The free surface model was considered in the capillary membrane model.

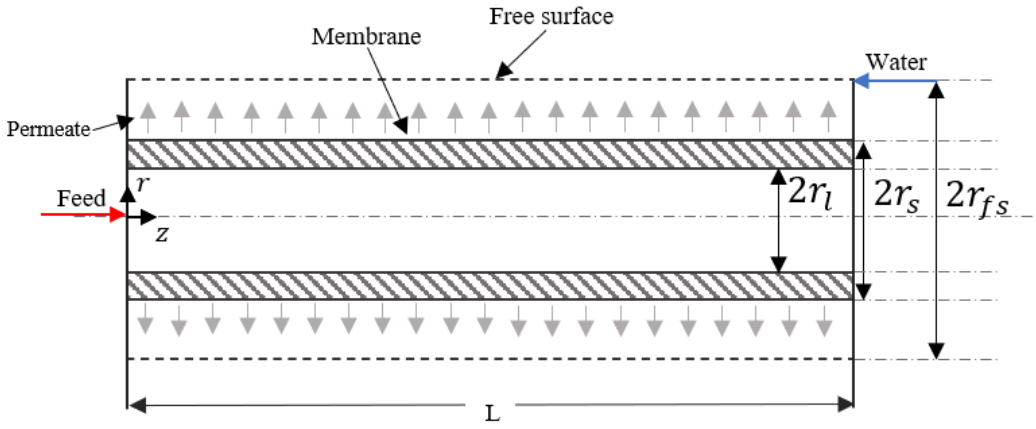

Figure 7. Scheme of a capillary membrane, where r_l, r_s and r_{fs} are the internal, external and free surface radius, respectively and L is the tube length.

In this model, as can be seen in Figure 8, it is considered that the capillaries are organized in a distribution in which the fiber centers coincide with the vertices of an equilateral triangle. In the perimeter of the hexagon formed around each capillary, the thermal and concentration variations are considered to be small. This perimeter is

substituted by a circle with the equivalent area in the annulus between it and the outside capillary diameter. The radius of this circle constitutes the free surface radius (r_{fs}), which is the distance from the center until the heat and mass transfer have influence for a given fiber [172–175].

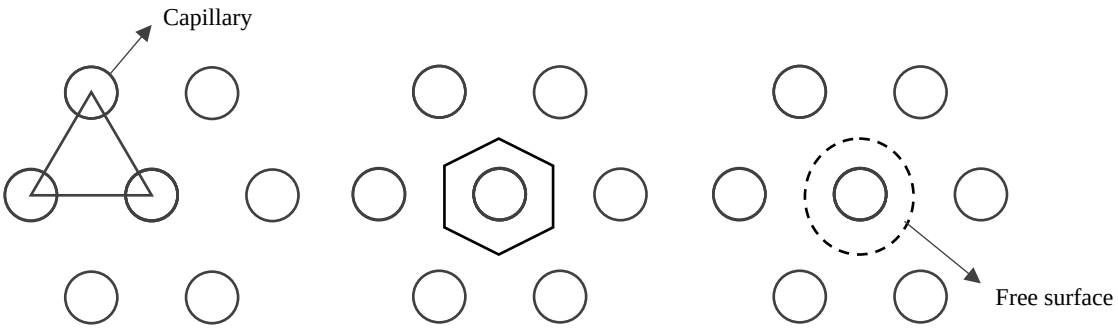

Figure 8. Scheme of capillary tube distribution for the free surface model.

The internal and the external radius of the capillary tube membrane, r_l and r_s, respectively are considered in the model. The free surface radius (r_{fs}) is given by [173]:

$$r_{fs} = \frac{r_s}{\sqrt{\Phi}} \tag{45}$$

where, Φ is the packing density, expressed as:

$$\Phi = \frac{N_{fibers} * (2 * r_s)^2}{d_{mod}^2} \tag{46}$$

The membrane distillation model was simulated in the software EMSO (Environment for Modelling, Simulation and Optimization) which is an equation-based dynamic simulator [176]. The thermal model was discretized using orthogonal collocation method at radial axis and finite difference method at axial axis. The mesh was composed by 41 points at the axial direction. This mesh had small increments in the beginning and at the end and higher increment in the middle, since it was observed that the influence of the parameters is more important in the beginning and at the end of the module. For the radial axis, 9 central points were used and the weight function associated

to the Jacobi polynomials were considered as $\alpha = 2$ and $\beta = 0$, as suggested by Secchi *et al*. (1999) [177]. The computational package OCFEM (orthogonal collocation finite element methods) available in EMSO was used. The solver SUNDIALS, also available in EMSO, was used to solve the resulting equation system [176].

The axial axis in the liquid phase for the concentration model was discretized in the same way as for the thermal model. Radial axis was not considered in the liquid phase. For the radial axis in the gas phase, a mesh of 10 points was used and was discretized by the finite difference method.

VRTherm, a thermodynamic database, coupled to EMSO software was also used in order to predict the equilibrium composition in the interface liquid/vapor at the feed and the permeate sides. For the gas phase, the equations of state considered were *Ideal, Peng-Robinson (PR)* and *Soave-Redlich-Kwong (SRK)*. For the liquid phase, *IdealLiquid* and *UNIFAC* models were considered.

The model developed in this work was included into the library available in EMSO software. This library includes models for mixer, splitter, heater, cooler, energy source, energy sink and the sources and sinks tanks. Thus, it was possible to simulate the integrated process.

3.2.1. Velocity profile.

In this work, the momentum equations were not resolved, and velocities profiles were taken from the literature. Velocity profiles for axial and radial axes are given by Eqs. 47-50 [172,178,179]:

$$v_{z,a}(r_a, z) = 2\left(\bar{v}_{z,a} - \frac{2v_{rm} \cdot z}{r_l}\right)(1 - r_a^2) \tag{47}$$

$$v_{r,a}(r_a, z) = v_{rm}(2r_a - r_a^3) \tag{48}$$

$$v_{z,\ell}(r_\ell, z) = a_1\left(\bar{v}_{z,\ell} + \frac{2r_s \cdot v_{rm} \cdot z}{r_{fs}^2 - r_s^2}\right)\left(\frac{k^2}{2} ln\big(k - r_\ell(k-1)\big) - \frac{1}{4}\big(r_\ell^2 - 1\big)\right) \quad (49)$$

$$v_{r,\ell}(r_\ell, z) = \frac{2a_1 \cdot v_{rm}}{k^2 - 1}\left(\frac{\big(k - r_\ell(k-1)\big)^3}{16} - \frac{k - r_\ell(k-1)}{8} - \frac{k^2}{2}\left(\left(\frac{k - r_\ell(k-1)}{2}\right) ln\big(k - r_\ell(k-1)\big) - \frac{k - r_\ell(k-1)}{4}\right) + \frac{a_2}{k - r_\ell(k-1)}\right) \quad (50)$$

where, $\bar{v}_{z,a} = \frac{Q_a}{Num\cdot(\pi r_l^2)}$, $\bar{v}_{z,\ell} = \frac{Q_\ell}{Num\cdot(\pi r_{fs}^2 - \pi r_s^2)}$, $v_{rm} = \sum_{k=1}^{N} \frac{N_k(z)}{\rho_k}$, $a_1 = \frac{2(k^2-1)}{\left(\left(ln(k) - \frac{3}{4}\right)k^2 + 1\right)k^2 - \frac{1}{4}}$, $a_2 = \frac{\left(\left(ln(k) - \frac{3}{4}\right)k^2 + \frac{1}{2}\right)k^2}{4}$ and $k = \frac{r_{fs}}{r_s}$.

3.2.2. Concentration profile.

The sugarcane stillage is a complex mixture containing volatile and non-volatile components. The development of a mathematical model to study the mass transfer during the sugarcane stillage treatment by membrane distillation process requires the use of the Stefan-Maxwell equation for multicomponent systems. In this work, a liquid mixture of six components was studied. The non-volatile components considered were glycerol, sucrose, and inorganic components expressed as NaCl salt. Ethanol, acetic acid, and water were the volatile components contemplated. Besides, it is considered that in the pores stagnant air is present.

The equilibrium in the liquid-vapor interface is given by Eqs. 51-53.

$$T^v = T^L \quad (51)$$

$$P^v = P^L \quad (52)$$

$$\phi_i^L x_i = \phi_i^v y_i$$
$$i = 1,2,\dots,N\ components \tag{53}$$

where ϕ_i^L and ϕ_i^v are the fugacity coefficient of the liquid and the vapor phases, respectively.

Considering a steady state molecular diffusion and the simplest mass transfer model, the film model, in which the resistance to mass transfer is concentrated to be in a thin film, the diffusion process occurring in the membrane pores (gas phase) is fully determined by the following considerations [146,147]:

- For one dimensional steady state process, the molar flux of each component and the total molar flux are given by:

$$\frac{dN_i}{dr} = 0 \qquad \frac{dN_t}{dr} = 0 \tag{54}$$

where, the molar fluxes (N_i) are given by the contribution of the diffusive and the convective ($N_i = J_i + y_i N_t$)

- The Stefan-Maxwell constitutive relation for each component is given by Eq. 30.

- Considering a Stefan Diffusion, the bootstrap problem can be solved considering a zero-molar flux of air (N_n):

$$\nu_i = 0 \qquad \nu_n \neq 0 \qquad N_n = 0$$
$$\beta_{ik} = \delta_{ik} + y_i/y_n \tag{55}$$

where δ_{ik} is the Kronecker delta

- Last, the boundary conditions are known by combination with the Eq. 53. These boundary conditions are obtained by the simultaneous integration of the equations for the feed and permeate streams in the liquid phase as well as in the gas phase.

$$r = r_0 \qquad y_i = y_{i0}$$
$$r = r_\delta \qquad y_i = y_{i\delta} \tag{56}$$

The Stefan-Maxwell approach allows to solve the mass transfer in the radial coordinate. In order to model a bidimensional mass transfer, it is considered that in the axial coordinate of the liquid phase, the process is given as a plug flow reactor. In this way, the feed solution is modeled as flowing through the membrane module as a series of infinitely plugs that are moving in the axial direction with uniform composition as it is shown in the Figure 9 while the volatile components permeate the membrane (in the radial coordinate). For this reason, it was not possible to considerate the concentration polarization.

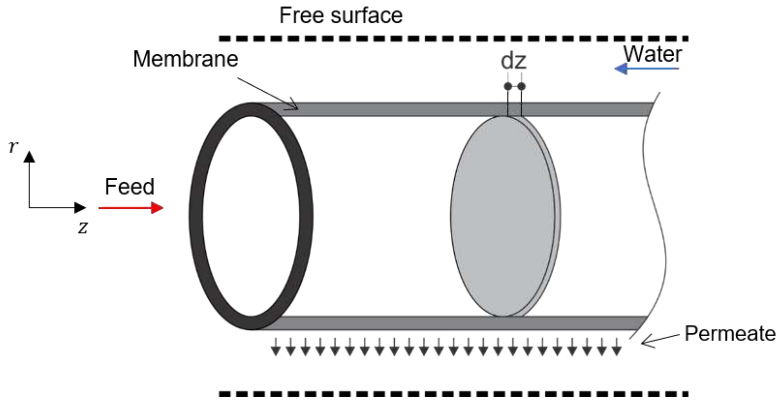

Figure 9. Scheme of concentration variation in the axial direction in the capillary tube.

As previously mentioned, there is a continuity of molar fluxes. Thus, the molar fluxes calculated by the Stefan-Maxwell relations are valid for the liquid phase. The flow rate in the lumen and shell sides in the forward step is calculated from a simple mass balance given by Eqs. 57 and 58, respectively [163]:

$$Q_f(i) = Q_f(i-1) - \left(\frac{N_t(i-1)}{\rho}\right) \cdot (A(i) - A(i-1)) \tag{57}$$

$$Q_p(i) = Q_p(i+1) + \left(\frac{N_t(i+1)}{\rho}\right) \cdot (A(i+1) - A(i)) \tag{58}$$

This allows to calculate the concentration of the non-volatile components at the feed side (Eq. 59). The concentration of volatile components at the feed and permeate sides are given by Eqs. 60 and 61, respectively.

$$C_{i,f}(i) \cdot Q_f(i) = C_{i,f}(i-1) \cdot Q_f(i-1) \quad (59)$$

$$C_{i,f}(i) \cdot Q_f(i) = C_{i,f}(i-1) \cdot Q_f(i-1) - N_i(i-1) \cdot (A(i) - A(i-1)) \quad (60)$$

$$C_{i,p}(i) \cdot Q_p(i) = C_{i,p}(i+1) \cdot Q_p(i+1) + N_i(i+1) \cdot (A(i+1) - A(i)) \quad (61)$$

First, the model was used to simulate the DCMD process using water both in the feed and in the permeate. The model was validated with the experimental results obtained in this work. To validate the model for NaCl solution treatment, literature data were used.

The correction of the water activity coefficient (γ_{water}) due to the presence of NaCl was considered using the following expression [33].

$$\gamma_{water} = 1 - 0.5 \cdot x_{NaCl} - 10 \cdot x_{NaCl}^2 \quad (62)$$

where x_{NaCl} is the mole fraction of the NaCl in the solution. In this case, for the determination of the liquid and vapor composition of water, the modified Raoult's law was considered, given by:

$$x_{water}\gamma_{water}P_f^{sat} = y_{water}P \quad (63)$$

The physical properties used to model the NaCl solution are shown in Table 8 and were taken from Schofield *et al.* (1990) [100]. For water, the same correlations were used considering $x_{NaCl} = 0$.

Table 8. Physical properties of NaCl aqueous solution.

Property	Equation
Density[a] (kg/m^3)	$\rho = 980 + 1950 \cdot x_{NaCl}$
Specific heat[a] ($J/kg \cdot K$)	$C_p = 4180 - 8370 \cdot x_{NaCl}$
Thermal conductivity[b] ($W/m \cdot K$)	$k = (0.608 + 7.64.10^{-4} \cdot T)(1 - 0.98 \cdot x_{NaCl})$

Viscosity[b] $(Pa \cdot s)$	$\mu = (8.7.10^{-4} - 6.3.10^{-6} \cdot T)(1 - 12.9 \cdot x_{NaCl})$

[a] Valid for temperatures from 50 to 90°C

[b] T in °C

The model for multicomponent solution was validated with the experimental results using the synthetic sugarcane stillage solution and the industrial stillage. The VRTherm plugin available in the EMSO software was used. The database of this thermodynamic plugin contains more than 2,000 components and allows to predict the partition coefficient. The value is calculate using the following expression:

$$K_i = \phi_i^l / \phi_i^v \tag{64}$$

where ϕ_i^l and ϕ_i^v are the liquid and vapor fugacity coefficients, respectively. These values are taken from the VRTherm plugin as a function of the temperature, pressure of the system and the liquid and vapor compositions, respectively.

The vapor fugacity is easily determined using the equations of state (EOS), like Ideal Gas, Peng-Robinson (PR) and Soave-Redlich-Kwong (SRK) equations. These models are available in the VRTherm. For the liquid phase is more complicated to model the fugacity of each component in the mixture. For this reason, the modified Raoult's law is more commonly used and, in this case, the activity coefficient is important to be estimated [180].

A complex mixture is considered in this work to represent the synthetic stillage which contains sucrose, acetic acid, ethanol, salts (represented by NaCl salt) and water. For the industrial stillage, besides these components, glycerol was also included in the mixture. All the information needed for the calculation of the vapor liquid equilibrium (VLE) of glycerol, acetic acid, ethanol, and water is available in the VRTherm plugin. The non-volatile components can have influence in the VLE [181–183]. However, neither the sucrose data nor the salts (which was considered as NaCl) are available in the VRTherm. For this reason, their effect in the VLE were not considered in the model. This causes the model to have limitations to correctly estimate the process. Besides, the fact of considering NaCl salt for representing all the inorganic salts present in the stillage clearly contributes to the estimation error.

For the synthetic stillage, as a first approximation, it was considered that the system ethanol, acetic acid and water forms an ideal liquid mixture. In this way, the *IdealLiquid* model available in the VRTherm was used for the liquid phase. Then, the UNIFAC model was used for the liquid phase in order to compare both models. These models allowed to determine the composition of the volatile components at the liquid and the vapor phases by the partition coefficient available in the VRTherm plugin with the limitations already mentioned. For the vapor phase, the *Ideal, SRK* and *PR* models were compared. The industrial stillage also contains glycerol, and this component, as it was mentioned, is also included in the VRTherm database and it was considered for the calculation of the VLE. In this case, for the liquid phase, the *IdealLiquid* and UNIFAC models were also compared. For the vapor phase, the *Ideal* model and the *SRK* model were compared.

Besides, the effect of the non-volatile components in the water coefficient activity (γ_{water}) was also considered. This impacts directly in the permeate flux value, since the vapor pressure is the driving force of the process. However, this has effect only for the water not so for the other volatile components, which causes difference between the experimental data and the simulation results. The following expression obtained experimentally, as described in the Section 3.1.6.4 from the industrial stillage data, was considered in the modified Raoult's law (Eq. 63) for determining the water vapor pressure:

$$\gamma_{water} = 1.0032 - 0.0013 \cdot c_{glycerol} \tag{65}$$

The diffusivity of air-water vapor is 0.219, 0.242 and 0.399 cm^2/s at 273, 293 and 373 K, respectively [184]. The curve fitted using these data was used in this work. The diffusivities of acetic acid-air (0.1064 cm^2/s at 273 K [185]) and of ethanol-air (0.145 cm^2/s at 313 K [186]) found in the literature were corrected to consider the effect of temperature using the following expression:

$$D_{ij}|_{T_2} = D_{ij}|_{T_1} \cdot \left(\frac{T_2}{T_1}\right)^{3/2} \tag{66}$$

In order to estimate the diffusivity of the other pair of gases and vapors Eq. 67 was used.

$$D_{AB} = 0.0018583\sqrt{T^3\left(\frac{1}{M_A}+\frac{1}{M_B}\right)}\left(\frac{1}{P\sigma_{AB}^2\Omega_{D,AB}}\right) \quad (67)$$

where P is the pressure in atm, T is the temperature in K. For binary mixtures containing polar components, the $\Omega_{D,AB}$, σ_{AB} and ε_{AB} parameters were estimated using the following expressions suggested by Brokaw [187].

$$\Omega_{D,AB} = \Omega_D + \frac{0.19\delta_{AB}^2}{T^*} \quad (68)$$

$$\Omega_D = \frac{A}{T^{*B}} + \frac{C}{\exp(DT^*)} + \frac{E}{\exp(FT^*)} + \frac{G}{\exp(HT^*)} \quad (69)$$

where $A = 1.06036$, $B = 0.15610$, $C = 0.193$, $D = 0.47635$, $E = 1.03587$, $F = 1.52996$, $G = 1.76474$, $H = 3.89411$ and $T^* = kT/\varepsilon_{AB}$.

$$\delta_{AB} = \frac{1.95.10^3\mu_P}{V_b T_b} \quad (70)$$

$$\sigma = \left(\frac{1.585V_b}{1+1.3\delta^2}\right)^{1/3} \quad (71)$$

$$\delta_{AB} = (\delta_A\delta_B)^{1/2} \quad (72)$$

$$\frac{\varepsilon_{AB}}{k} = \left(\frac{\varepsilon_A}{k}+\frac{\varepsilon_B}{k}\right)^{1/2} \quad (73)$$

$$\sigma_{AB} = (\sigma_A\sigma_B)^{1/2} \quad (74)$$

where μ_P is the dipole moment (in debyes), V_b is the liquid molar volume at the normal boiling point (in cm^3/mol) and T_b is the normal boiling point (in K).

3.2.3. Temperature profile.

In the MD process, heat transfer at the membrane is a combination of heat conduction, that takes place through the membrane matrix and the gases within the

membrane pores, and the heat related to the mass transfer due to the water vapor and the other volatiles components transport through the pores [28,32,83,99,106,178,188]. It is worth to mention that in this expression, the enthalpy of the vapor transported through the membrane is approximated to the latent heat of vaporization [137].

$$\kappa_i \left(\frac{1}{r_i} \frac{\partial}{\partial r_i} \left(r_i \frac{\partial T_i(r_i, z)}{\partial r_i} \right) \right) = \rho_i C_{p,i} \left(v_{z,i} \frac{\partial T_i(r_i, z)}{\partial z} + v_{r,i} \frac{\partial T_i(r_i, z)}{\partial r_i} \right) \tag{75}$$

$i = a, b$

Thus, boundary conditions for the energy equation considering countercurrent operation are written as follows:

$$\kappa_a \frac{\partial T_a(r_l, z)}{\partial r_a} = -\left(\sum_k^N (\Delta H_k \cdot N_k) + \frac{\kappa_m \left(T_a(r_l, z) - T_b(r_s, z) \right)}{\delta_m} \right) \tag{76}$$

$$T_a(r_a, 0) = T_{a,in} \tag{77}$$

$$\frac{dT_a(0, z)}{dr_a} = 0 \tag{78}$$

$$\kappa_b \frac{\partial T_b(r_s, z)}{\partial r_b} = \left(\sum_k^N (\Delta H_k \cdot N_k) + \frac{\kappa_m \left(T_a(r_l, z) - T_b(r_s, z) \right)}{\delta_m} \right) \tag{79}$$

$$T_b(r_b, L) = T_{b,in} \tag{80}$$

$$\frac{dT_b(r_{fs}, z)}{dr_b} = 0 \tag{81}$$

Eqs. 76 and 79 are related to the thermal balance at the membrane. The entry temperature is considered constant and equal to $T_{a,in}$ and $T_{b,in}$ for the lumen and shell sides, respectively (Eqs. 77 and 80). There are no thermal gradients at the center of the lumen and in the free surface radius (Eqs. 78 and 81, respectively).

The heats of vaporization of acetic acid, ethanol and water were calculated by using the following expressions [185]:

$$\Delta H_k = C_1 \cdot (1 - T_R)^{C_2 + C_3 T_R + C_4 T_R T_R} \quad (82)$$

where T_R is the reduced temperature equal to T/T_c and ΔH_v is expressed in $J/kmol$. Table 9 shows the values of the constants for each component and the critical temperature.

Table 9. Constants for determining the heats of vaporization by Eq. 82.

Component	C_1	C_2	C_3	C_4	$T_c\ (K)$
Acetic acid	$2.0265.10^7$	0.11911	−1.3487	1.4227	591.95
Ethanol	$5.69.10^7$	0.3359	0	0	513.92
Water	$5.2053.10^7$	0.3199	−0.212	0.25795	647.13

It is worth to mention that the values used for the calculation of the heat of vaporization are valid in the range of temperature normally used in membrane distillation process.

3.2.4. Dynamic approach

The sugarcane stillage concentration was simulated using a transient tank for recirculating the concentrated stream to the membrane distillation process. This tank is well-mixed, it has one inlet and one outlet stream, and it is isolated. The global mass balance in the tank is given by Eq. 83 and the component mass balance by the Eq. 84:

$$\frac{dm}{dt} = \dot{m}_{in} - \dot{m}_{out} \quad (83)$$

$$\frac{dm_i}{dt} = \dot{m}_{i,in} + \dot{m}_{i,out} \quad (84)$$

In the same way, the energy balance is given by Eq. 85. The liquid heat capacity is constant for all streams.

$$\frac{d(mH)}{dt} = \dot{m}_{in}H_{in} - \dot{m}_{out}H_{out} \tag{85}$$

3.3. Energy consumption

The specific thermal energy consumption (STEC) for the DCMD system found in the literature is around 1,000 kWh_{th} per m^3 of recovered water, depending on several factors [156,189,190]. In this work, this value was calculated using Eq. 86 [156]:

$$STEC = \frac{q_{T_{in}-T_{f,in}} + q_{T_{f,out}-T_{f,in}}}{\dot{m}_{permeate}} \tag{86}$$

where $\dot{m}_{permeate}$ is the permeate flow (calculated by the product of the permeate flux and membrane area). $q_{T_{in}-T_{f,in}}$ represents the energy needed to heat the feed solution from room temperature to the module inlet temperature. In this work, it is considered that stillage leaves the distillation column at temperatures between 70-90 ºC, thus, in principle, no additional heat source is necessary to start running the treatment. So, this term will be zero in most cases. The term $q_{T_{f,out}-T_{f,in}}$ is the heat lost in the module and it is calculated by Eq. 87 [156]:

$$q_{T_{f,out}-T_{f,in}} = \dot{m}_f Cp_{stillage}(T_{f,in} - T_{f,out}) \tag{87}$$

where $\dot{m}_f$ is the mass flow rate of feed solution, $Cp_{stillage}$ is the specific heat (in $J/kg \cdot K$) and $T_{f,in}$ and $T_{f,out}$ are the feed solution temperatures at the inlet and outlet to the module, respectively. The specific heat of stillage solution was calculated using Eq. 44.

Eq. 86 was used for the experimental data. In the simulation, the STEC was calculated in relation to the feed and to the permeate stream and it is given by Eqs. 88 and 89, respectively:

$$STEC_f = \frac{q_{in}}{Q_{f,in}} \tag{88}$$

$$STEC_p = \frac{q_{in}}{Q_p} \tag{89}$$

where q_{in} is the heat energy provided by the heater and $Q_{f,in}$ and Q_p are the feed and permeate flow rates [191].

The specific electric energy consumption (SEEC) was also evaluated in relation to the feed and to the permeate stream. It was considered that the electricity is used for operating the pumps. A pressure drop (ΔP) of 1 bar and an efficiency (ε) of 80% were considered [192]. SEEC is given by Eqs. 90 and 91:

$$SEEC_f = \frac{\sum W_i}{Q_f} = \frac{W_f + W_p + W_{RR}}{Q_f} \tag{90}$$

$$SEEC_p = \frac{W_f + W_p + W_{RR}}{Q_p} \tag{91}$$

where W_i is the pump power given by $W = q \cdot \Delta P/\varepsilon$ and the subscript express the flow rate of the feed (f), the permeate (p) or the concentrate recycled (RR) streams.

When a heat exchanger for the recovery of the energy contained in the permeate stream is used a global heat coefficient of 1000 $W/m^2 \cdot K$ [193] and an area of 20 m^2 were considered in all cases. This area was chosen to be enough for recovery the maximum energy from the permeate stream.

In a subsequent concentration step by DCMD, it is possible to perform the incineration of the concentrated stillage as biofuel in the boiler of the sugar and ethanol plant. It is estimated that it is possible to obtain 65.2 kg of steam (480ºC/65 bar) per ton of sugarcane processed when the concentrated stillage is incinerated [18]. In this way, it can be considered that the concentrated stillage incineration could be exploited to

partially sustain the thermal requirements of the DCMD process, allowing to reach high concentrations due to the surplus steam obtained.

An integrated process was simulated to evaluate the thermal energy consumption and the average permeate flux considering six permeation modules in series, each one of 1 m of length. Heaters and chillers were also considered and the location of them was evaluated. In all cases, a heater was used to heat the fresh feed stream from 328 K to 353 K. The feed flow rate was 3.33 m^3/h. Water at 293 K was used in the permeate side and it was fed in the last module in order to operate in a countercurrent. The inlet water flow rate was 2 m^3/h.

Each heater is used to heat the concentrate stream until 353 K and each chiller to refrigerate the permeate stream until 293 K. First, the heaters and chillers were placed between each module (Case 1, Figure 10.a). Then, they were placed after 2 (Case 2, Figure 10.b) or 3 (Case 3, Figure 10.c) modules.

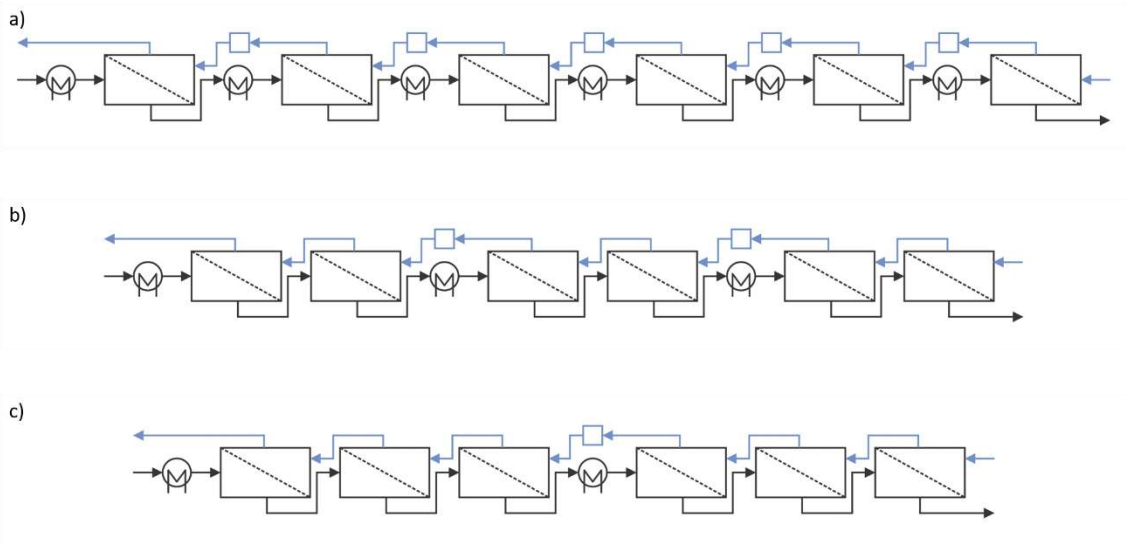

Figure 10. Integrated process arrangement: a) Case 1: heaters and chillers between each module; b) Case 2: heaters and chillers placed after 2 modules; c) Case 3: heaters and chillers placed after 3 modules.

Cases 4 and 5 are shown in Figure 11 a) and b), respectively. In these cases, a heater is used to preheat the feed fresh stream and the chiller was not necessary because the permeate stream left the system. In this respect, in the case 5, a heat exchanger is also included, which is used as a recuperator and it is putted before the heater to preheat the fresh feed stream using the permeate stream that leaves the first module. The heat

exchanger considered here has an area ($20\ m^2$ in this case) enough for the maximum heat recovery possible from the permeate stream.

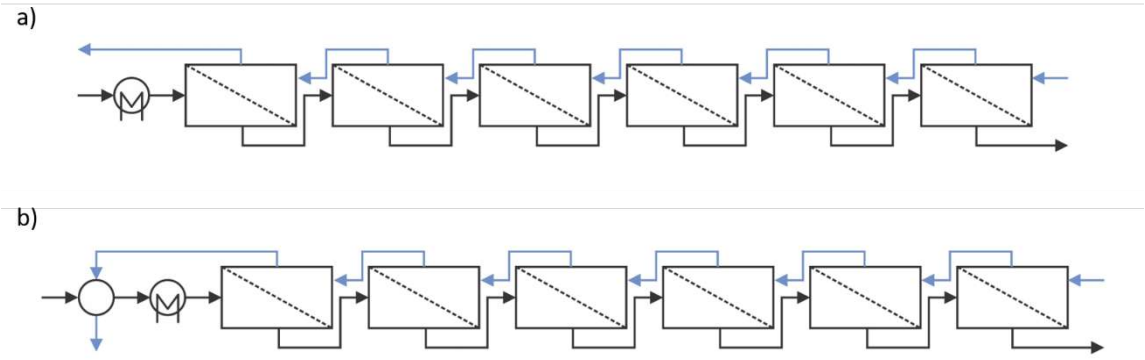

Figure 11. Integrated process arrangement: a) Case 4: without heaters and chillers between each module; b) Case 5: with a heat exchanger as recuperator.

3.4. Integrated process

Aiming to integrate the direct contact membrane distillation in the ethanol production plant as it is shown in Figure 12, different membrane module arrangements were analyzed in terms of permeate flux, permeate recovery and final concentration reached.

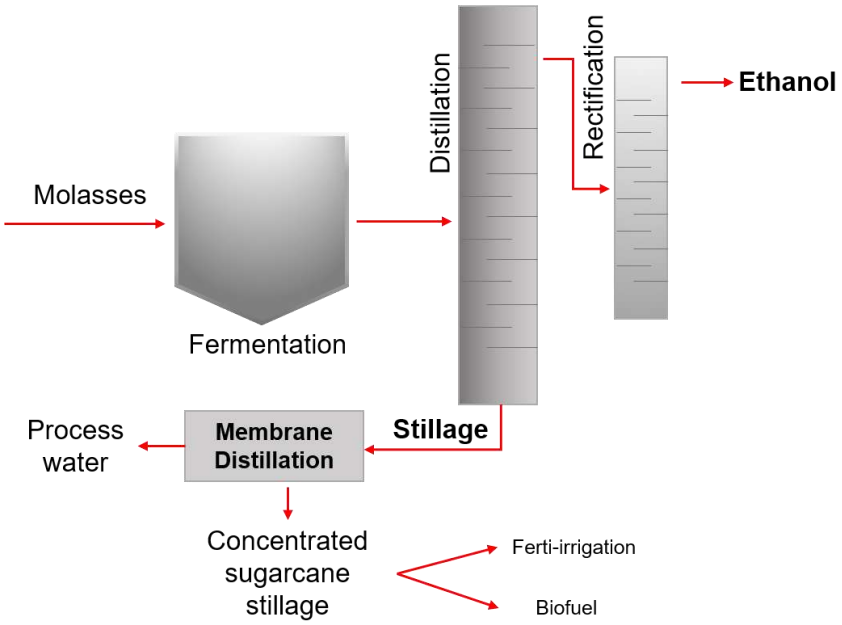

Figure 12. Direct contact membrane distillation process integrated in the ethanol production process.

In Configuration 1, 100 parallel sets of 252 modules in series are considered. Each set is fed with 3.3 m^3/h of fresh stillage of 3.8 $°Brix$. The concentrate recycle was considered for the Configurations 2, 3 and 4. These configurations differ in the position of the mixer/splitter (after 24, 36 or 60 modules placed in series). For Configuration 2, each parallel set was fed with 0.32 m^3/h of industrial stillage. So, 1035 sets are placed in parallel to treat 333 m^3/h. For Configuration 3, 690 parallel sets were considered each one fed with 0.48 m^3/h. And, for Configuration 4, 414 parallel sets were considered each one fed with 0.80 m^3/h.

The last configuration simulated the Christmas Tree arrangement (Configurations 5). The total membrane area required is 48,712 m^2. To achieve a good concentration degree, sets of 36 modules were placed in series. Initially 100 sets were considered that were reduced to 86, 73, 63, 53, 46, 39, 34, 29, 25, 21, 18, 16, 14, 12, 10, 9, 8, 7, 6, 6, 5, 4. This arrangement was chosen such that every set was always fed with $3.3 \pm 0.2\ m^3/h$.

For a membrane distillation process, parallel and series arrangements have already been proposed in the literature [76,194]. However, the Christmas Tree arrangement has not been extensively reported for membrane distillation. This arrangement is widely used in other membrane separation processes because it allows to maintain high feed flow rates through the modules increasing the permeate recovery [195].

3.5. Preliminary economical study

In order to perform an economical study, it was considered 333 m^3/h of stillage to be disposed. This corresponds to a sugarcane plant that processes 687 ton of cane per hour. The recovery rate of the DCMD treatment plant was considered based on the simulation results of Section 3.4. Then, the capacity of the DCMD treatment plant was established to recover the permeate, which was considered as mainly water with a little content of volatile organic compounds. The operating time of the plant was considered to be 4,000 $h/year$ [18]. The interest rate and the plant life were considered 5% and 20 years, respectively [157]. Al-Obaidani *et al.* (2008) [157] suggested that the membrane cost contributed to 50% of the total capital cost (indirect capital costs are 10 % of direct capital cost). The membrane cost was considered at 90 $ per m^2 of membrane area [157]. The membrane replacement rate was considered to be 12% of total membrane cost and

the maintenance cost was 0.5% of the total capital cost [196]. Spares and labor costs were considered 0.033 $\$/m^3$ and 0.03 $\$/m^3$, respectively [157].

The specific electricity consumption for DCMD system is around 1.24-2 kWh_e per m^3 of recovered water, which is relatively low [189,197]. In this work, the specific thermal energy consumption calculated from the experimental data was ranged between 671 and 885 kWh/m^3. As it was already mentioned, if the concentrated stillage is incinerated, the steam obtained can be used to supply the thermal requirements necessary to sustain the process. Besides, residual energy could be also used to produce more electricity. When a low or high grade heat is available, Kesieme *et al*. (2013) [197] considered that the cost of thermal energy is only 10% of the total cost of thermal energy that would be necessary without that heat source available. For these reasons, the costs of steam, electricity, thermal energy, chemical and the concentrate disposal cost were not included in the calculation.

Chapter 4

Results and Discussion

In this chapter, the results obtained using the methodology described in Chapter 3 will be presented. Firstly, the experimental results using water, synthetic stillage solution and the industrial stillage are presented. Tests using the synthetic stillage solution allowed to have a better understanding about the membrane distillation treatment of a multicomponent solution and about mass transfer when a multicomponent solution is treated by DCMD. This solution included volatile and non-volatile components. Also, tests were carried out using industrial stillage to complement the experimental procedure. Thermal properties of the industrial stillage were determined in order to use the data in the simulation approach.

Secondly, the simulation results obtained with the mathematical model proposed are shown. The validation of the model was also presented. Finally, an economic analysis was carried out in order to determine the feasibility of industrial stillage concentration using membrane distillation.

4.1. Experiments results

4.1.1.Cleaning process

Even considering that all experiments were quite simple to carry out, a strict control of the parameters as temperatures and flow rates, is very important for obtaining better results, mainly when a validation test was carried out. The characteristics of the MD module should also remain constant for every experiment test.

After each experiment, a cleaning process was realized in order to ensure the same conditions in the beginning of the next test. The MD system was cleaned following the procedure described in Section 3.1.1. The N_2 permeability of the MD module was measured between each experiment and it is presented at Figure 13. The average nitrogen

permeability was 1.52 m^3/h and varied from 1.48 to 1.54 m^3/h, along the experiments. In Figure 13 two CIP procedures are highlighted.

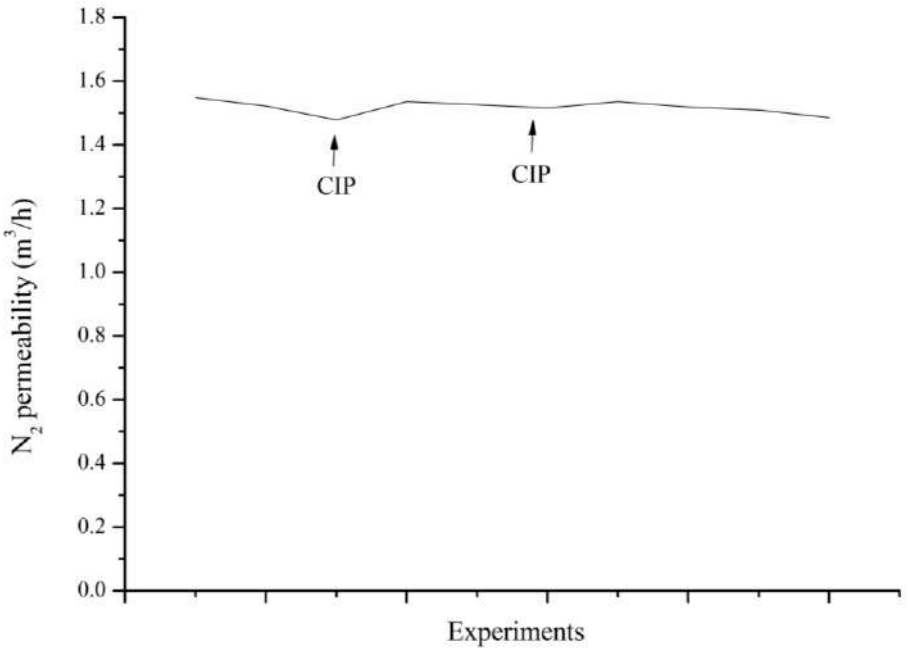

Figure 13. MD module integrity evaluation through the measurement of N_2 permeability, expressed in terms of flow rate, m^3/h. $\Delta P = 0.1\ kgf/cm^2$.

It is worth mentioning that these values show that membrane fouling, if occurred, was reversible during the experiments, since the gas permeability remained practically constant. This also allows to state that the cleaning procedure was efficient for recovery the initial characteristics of the membrane module along the experiments performed.

4.1.2.Study of operational parameters

Distilled water and the synthetic stillage solution were tested in DCMD. For each stream, feed temperature influence on permeate flux was studied. Figure 14 shows the increment in permeate flux because of the hot stream temperature increase. For a given permeate temperature, the feed temperature increment causes an increase in the mass transfer driving force [83]. This is a consequence of the higher vapor pressure at high temperatures due to its exponential relation [198]. Discussion is valid for both feed solutions.

Temperature difference between both sides of the membrane varied from 40 to 60 $°C$ and the permeate flux, from 3.38 to 6.78 $kg/m^2 \cdot h$, respectively, when water was fed to the DCMD process. The permeate fluxes obtained with distilled water are slightly higher than the ones observed with the synthetic stillage. The presence of salts in the synthetic stillage solution could be responsible for a vapor pressure reduction causing a decrement in the driving force of the process and, consequently, in the permeate flux. Besides, the non-volatile components present in the synthetic stillage, due to their concentration at the membrane surface, could also reduce the driving force of the DCMD process.

In addition, the combination of high fluxes of heat and mass, due to the high operational temperatures, provokes a large temperature drop between the bulk and the membrane surface promoting temperature and concentration polarization effects [152]. From Figure 14 to Figure 17, error bars are presented for the permeate flux of the synthetic stillage. Three experimental tests were carried out at the same experimental condition and the standard deviation of them was considered to be the same for all conditions. This value was considered in the error bars.

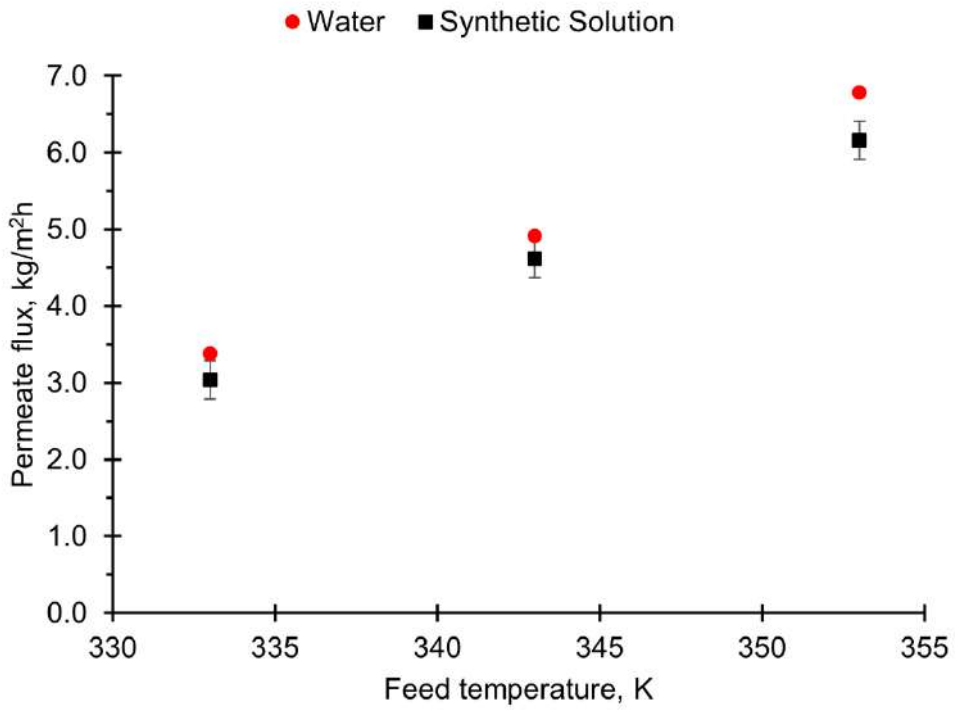

Figure 14. Feed temperature influence on permeate flux: water (●) and synthetic stillage solution (■). $T_p = 293\ K;\ Re_f = 200; Re_p = 60$

The permeate temperature influence on the permeate flux was also studied. As shown in Figure 15, the permeate temperature increase results in a permeate flux decrement. However, this effect is small in the permeate temperature range studied. This could be explained due to the small variation of the water vapor pressure at low temperatures [199]. The same tendency is observed for both feed solutions. The permeate fluxes for synthetic stillage solution experiments operating at 293 K and 303 K are 4.62 and 4.02 $kg/m^2 \cdot h$, respectively. The little decrement on the permeate flux when operating at 303 K shows that an additional cost related to the refrigeration of the permeate stream may be not compensated for the effort of increasing water recovery. On this matter, a better alternative would be to invest in the hot stream, since the feed temperature effect in the permeate flux is greater.

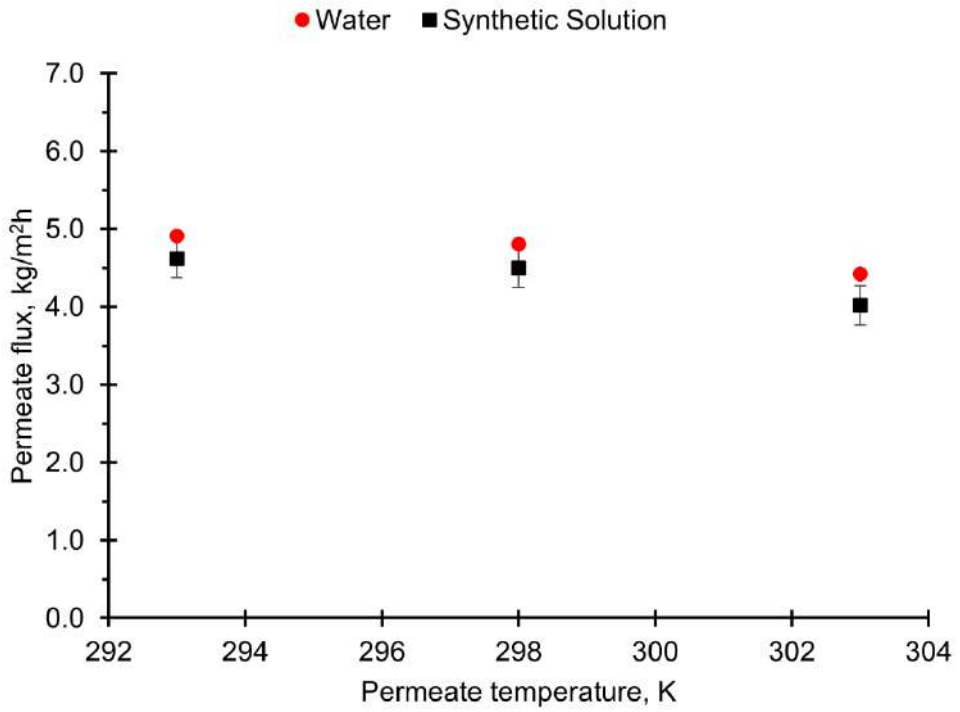

Figure 15. Permeate temperature influence on permeate flux: water (●) and synthetic stillage solution (■). $T_f = 343\ K;\ Re_f = 200; Re_p = 60$

Figure 16 shows the feed flow rate influence on the permeate flux. The increment in the feed recirculation rate results in higher permeate fluxes. This behavior is related to an increase in the mass and heat transfer coefficients in the liquid phase, which leads to the reduction in both concentration and temperature polarization [200]. The reduction in the polarization effects makes both concentration and temperature at the membrane surface

to approach the bulk liquid values. Therefore, a greater driving force is obtained and, consequently, higher permeate fluxes are observed [99,142,201]. In addition, high flow rates make the residence time in the module shorter and, consequently high driving force is maintained along the module, allowing to reach higher permeate fluxes [202].

For the experiments presented in Figure 16, the temperature difference was 50 K. Even so, for a feed Reynolds number of 370, the permeate flux obtained was higher than that achieved for a temperature difference of 60 K when the feed Reynolds number was only 200 (Figure 14). This shows that feed Reynolds number has an important effect on the permeate flux. However, the increase in the driving force tends to reach asymptotic values due to the reduction of boundary layer to a thickness below which the feed Reynolds number increment has no effect [125,200]. In that case, the feed temperature variation is a better strategy to increase the permeate flux.

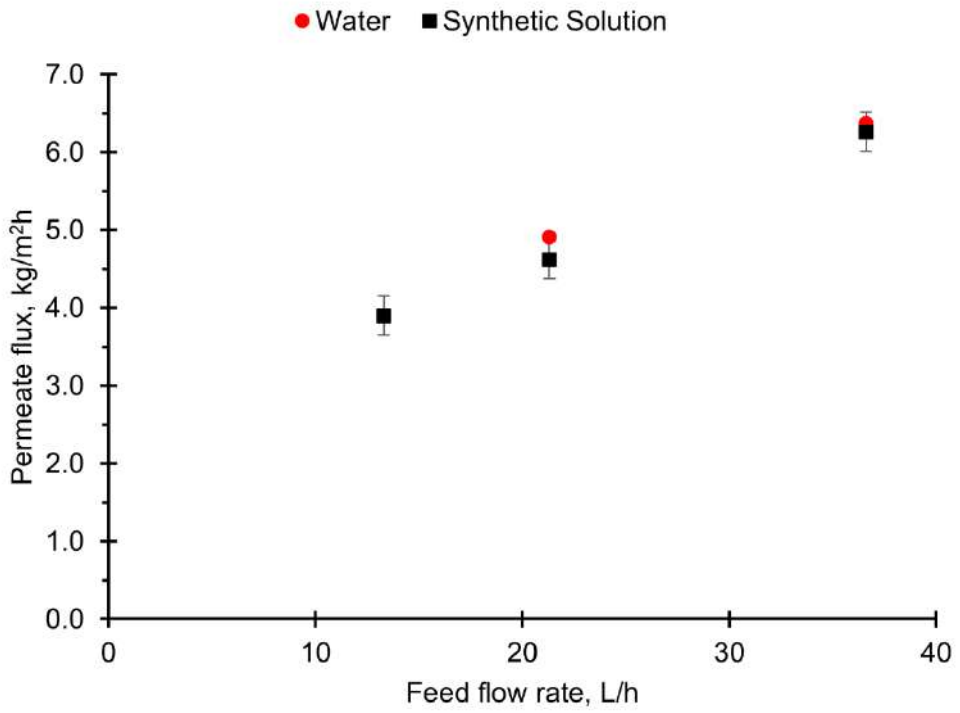

Figure 16. Feed flow rate influence on permeate flux: water (●) and synthetic stillage solution (■). $T_f = 343\ K; T_p = 293\ K;\ Re_p = 60$

On the other hand, Figure 17 shows that permeate flow rate increment has a little effect in the permeate flux. Although the organic volatile components (ethanol and acetic acid present in the synthetic stillage) can also be found in the permeate side, their

concentration, as well as their concentration polarization, are low. For this reason, the permeate fluxes obtained for water and synthetic stillage are quite similar.

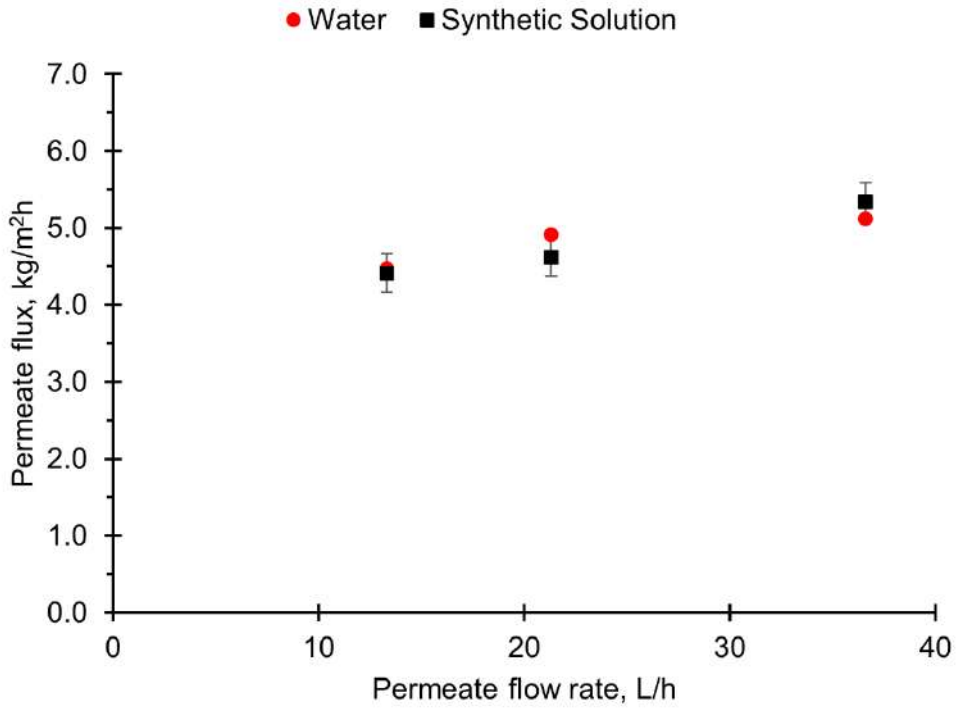

Figure 17. Permeate flow rate influence on permeate flux: water (●) and synthetic stillage solution (■). $T_f = 343\ K; T_p = 293\ K;\ Re_f = 370$

The influence of these parameters on the DCMD performance has been widely studied. In the literature, reported permeate flux values are similar to those observed in the present work. Pantoja *et al.* (2015) [81] used high flow rates and found that permeate flux increased from 3.96 to 12.60 $kg/m^2 \cdot h$ when increasing temperature from 333 K to 353 K, using a saline solution as feed (mass fraction equal to 0.26). As in the present work, when the permeate temperature decreased, these authors did not observe a significant increase in the permeate flux. The permeate flux varied from 8.22 to 7.41 $kg/m^2 \cdot h$ when the permeate temperature increased from 293 K *to* 303 K. Evidently, operating with higher Reynolds numbers than those used in this work might lead to higher permeate fluxes as it is shown in the literature [81,83,152,198].

Feed, permeate and concentrate streams of each experiment with the synthetic stillage solutions were characterized. Table 10 shows the average value and the standard deviation of these characterizations. Composition remained almost constant in the

different experiments performed. In all experiments, the permeate stream presented low ionic conductivity indicating that practically there was no membrane wetting. The absence of phosphorus and sucrose in this stream confirms this statement. The high salt rejection constitutes one of the main advantages of the membrane distillation process [28,30].

The nitrogen content in the permeate stream found in the experiments was low. Regarding this component, it is known that ammonia in aqueous solution exists in two forms: volatile ammonia molecules NH_3 and NH_4^+ ions. Due to the nature of the process, volatile ammonia molecules are removed by DCMD [130]. The amount of ammonia that can be removed depends largely on the pH and temperature [133]. Increasing temperature favors production of volatile ammonia in the aqueous solution. Increasing pH leads to the ammonia dissociation reaction to produce more volatile ammonia in the aqueous solution. The high operational temperatures used in the DCMD process could favor the presence of volatile ammonia in the permeate. Conversely, stillage is predominantly acid, by which ammonia will be present mainly as NH_4^+.

The initial distilled water pH (used on the permeate side) was 6.50 and decrease to 3.72±0.06 along the experiments. This could be explained due to the permeation of acetic acid through the membrane, causing a pH decreasing on the permeate side.

Permeate streams presented total organic carbon (TOC) as well as chemical organic demand (COD) above zero due to the partial permeation of volatile components. Ethanol and acetic acid, present in the synthetic stillage solution, permeate the membrane as a result of its vapor pressure difference. The TOC and COD content in concentrate streams is due to the concentration of the remaining sucrose, ethanol and acetic acid.

Table 10. Characterization of feed, permeate and concentrate streams from synthetic stillage solution treated by DCMD process

	Feed		Permeate		Concentrate	
Ionic conductivity ($\mu S/cm$)	4,489.6	±142.9	199.08	±10.5	7,328.4	±156.8
Phosphorus (mg/L)	100.5	±12.9	ND	±0	236.3	±40.9
Sucrose (mg/L)	2,394	±42	ND	±0	3,424	±397
Nitrogen (mg/L)	496.0	±21.5	6.09	±1.90	933.3	±99.9
pH	3.82	±0,11	3.72	±0.06	3.93	±0.14
TOC (mg/L)	3,200.9	±74.0	2,867.6	±285.6	3,181.7	±237.9

COD (mg/L)	9,992.6	±377.1	9,126.9	±1,270.8	9,468.6	±1,085.8
Acetic acid (mg/L)	1,377	±538	512	±245	1,515	±614
Ethanol (mg/L)	3,783	±254	6,800	±919	1,543	±383

ND: not detected

These experiments served as reference to perform the DCMD experiments using the industrial stillage.

4.1.3.Industrial stillage solution

Industrial stillage provided by USJ Açúcar e Álcool SA (Araras, São Paulo - Brazil) was characterized and the results are summarized in Table 11. The COD content is high and comparable with the values found in the literature [7,52]. The main volatile organic components found in this industrial stillage sample are ethanol and acetic acid. Sucrose and glycerol are the main organic components in this solution. The stillage has an acidic nature and high ionic conductivity. The solids present in industrial stillage are mainly volatile and dissolved. The initial degree Brix was 3.5.

Seasonal characterization of stillage shows that there is an important variability of the compounds in this effluent [7,52]. Other organic components also reported in the literature are fructose, glucose, citric acid, succinic acid, aconitic acid, propionic acid, lactic acid, malic acid, butyric acid, methanol, among others [7,51,52]. However, in this work only the components showed in Table 11 were identified. Nevertheless, these concentrations agree with the characterization presented in the literature and could be considered as a representative sample.

Table 11. Industrial sugarcane stillage characterization as received.

Parameter	Value
COD (mg/L)	35,000
Ethanol (mg/L)	213.6
Acetic Acid (mg/L)	411.6
Sucrose (mg/L)	2,724
Glycerol (mg/)	4,622

pH	4.48
°Brix	3.5
Ionic conductivity (μS/cm)	10,098
Total solids (mg/L)	35,920
Total fixed solids (mg/L)	2,193
Total volatile solids (mg/L)	33,727
Total suspended solids (mg/L)	1,510
Total dissolved solids (mg/L)	34,410

Regarding the DCMD experiments, Table 12 shows the permeate flux values for three different feed streams: water, synthetic sugarcane stillage (10,000 $mg/L\ COD$) and industrial sugarcane stillage (3.5° Brix). The experiments were performed at the same operational conditions and for the same time (two hours). There is no appreciable difference among the permeate fluxes achieved for each feed stream at these concentrations. Although concentration polarization effects are expected in the synthetic and industrial stillage with a consequent permeate flux decrement, it is considered that the contribution of this effect is lesser than temperature polarization effect, which depends on the operational temperatures [200]. Besides, industrial stillage presents large quantity of volatile solids (Table 11), so that the eventual permeate flux decrement due to the concentration polarization effect at the feed side could have been compensated by the transport of these compounds through the membrane pores, causing an increment in the total permeate flux and in their concentration at the permeate side. It is worth to mention that these permeate flux values corresponding to average permeate flux.

Table 12. Average permeate flux for water, synthetic and industrial sugarcane stillage for the same DCMD operational conditions ($T_f = 343\ K, T_p = 293\ K$, feed and permeate flow rates: 36.6 L/h and 21.3 L/h, respectively)

Feed solution	Water	Synthetic sugarcane stillage	Industrial sugarcane stillage
Permeate flux (kg/m^2h)	6.37	6.26	6.67

Synthetic stillage experiments showed that temperature and flow rate of the feed streams were the operational parameters with the greatest influence on the permeate flux (Section 4.1.2). For this reason, experiments using industrial stillage were performed at higher flow rates than that for synthetic stillage solution. The influence of the feed flow rate on the permeate flux and on the specific thermal energy consumption (STEC, which was calculated as describe in Section 3.3) is shown in Table 13. The increment in the permeate flux with the feed flow rate was already explained in Section 4.1.2. As it was mentioned, higher feed flow rates allow the maintenance of a higher temperature in the feed side, resulting in higher permeate fluxes. This also results in a smaller temperature drop between the inlet and the outlet of the module. The permeate flux increment and the decrement in the temperature drop along the module achieved when the flow rate increased allow to reach a smaller STEC [156].

Table 13. Flow rate influence on permeate flux and STEC during DCMD process with industrial sugarcane stillage as feed stream ($T_f = 333\ K,\ T_p = 298\ K$, permeate flow rate: 36.6 L/h)

Experiment	1	2	3
Feed flow rate (L/h)	40	60	80
Permeate flux (kg/m^2h)	4.65	5.22	5.46
$T_{f,in} - T_{f,out}$ (K)	11	8	6
STEC (kWh/m^3)	885	860	822

Regarding the feed temperature, Table 14 shows the permeate flux and the STEC achieved with the temperature increment. These experiments were performed at a feed flow rate of 80 L/h. As it was expected, this allowed the achievement of higher permeate fluxes. Besides, it is possible to see that for higher feed temperatures the STEC is lesser, due mainly to the high permeate flux achieved [203]. STEC values found in this work are lower than typical values found in the literature for membrane distillation processes [156,190,203]. This could be due to the fact that the sugarcane stillage leaves the distillation column at temperatures between 70-90 $°C$, thus an additional heat source is not necessary to start running the DCMD process, which allows savings in thermal energy to carry out the process. In this regard, for the calculation of STEC, the first term in Eq. 86 was considered to be zero.

Table 14. Effect of the feed temperature on the permeate flux and the STEC during DCMD process with industrial sugarcane stillage as feed stream ($T_p = 298\ K$, feed and permeate flow rates: 80 L/h and 36.6 L/h, respectively)

Experiment	1	2	3
Feed temperature (K)	333	343	353
Permeate flux (kg/m^2h)	5.46	9.26	13.37
$T_{f,in} - T_{f,out}$ (K)	6	9	12
STEC (kWh/m^3)	822	727	671

In order to perform a long-term experiment, a volume of 15 L of industrial stillage was concentrated using the direct contact membrane distillation process. Distilled water was used in the permeate side and recycled throughout the experiment. Figure 18 shows the total permeate flux along the sugarcane stillage concentration experiment. After reaching a concentration of 20º Brix, the permeate flux decrement could be explained due to concentration polarization effects owing to the concentration increase of the treated solution. The decrement in the permeate flux may also be attributed to the modification in the hydrodynamic properties of stillage (increase in both viscosity and density). It was reported that the viscosity increment affects the heat transfer coefficient causing a thermal resistance which results in a decrement in the driving force of the process, mainly in solutions containing sucrose [200]. Nevertheless, it is worth mentioning that the permeate flux decreased only 1.8-fold when the ºBrix concentration increased by 17-fold. The water recovery rate achieved in this experiment was 86%. As it is indicated in Figure 18, rapid module cleanings, not more than 1 min, were performed by flowing pure water by the feed side. Permeate was discarded during these cleanings. In the first cleaning, permeate flux showed an important increment. In the second case, the permeate flux increment was smaller.

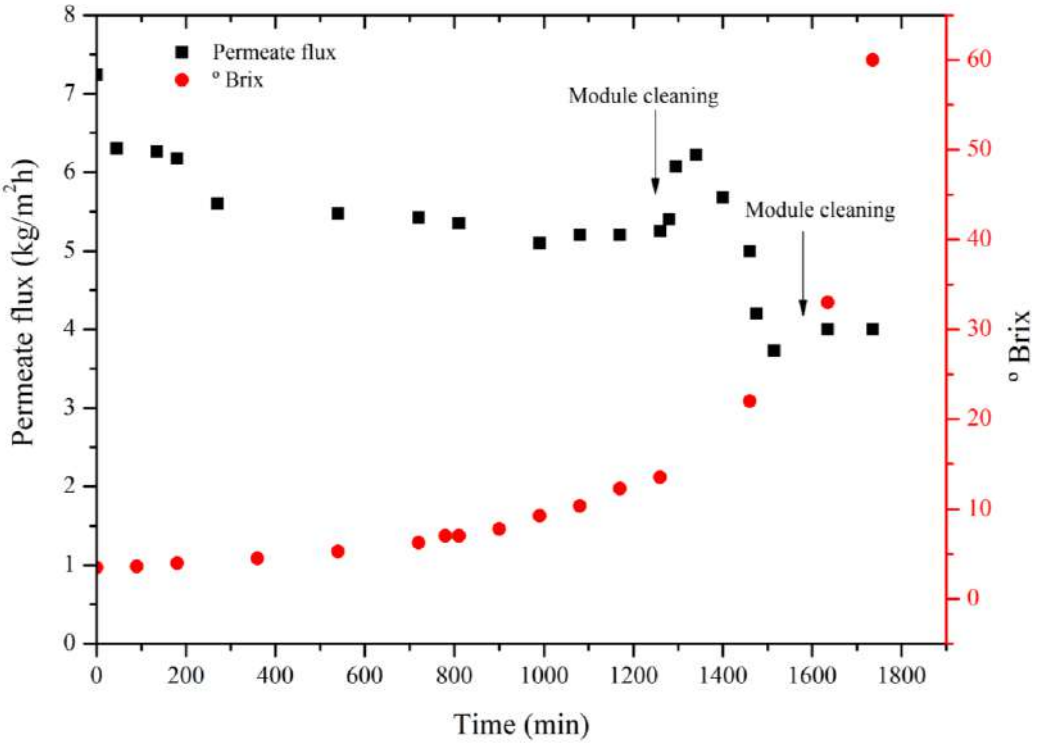

Figure 18. Permeate flux and ºBrix concentration along the industrial sugarcane stillage concentration by DCMD ($T_f = 65 \pm 5°C, T_p = 20 \pm 2°C$, feed and permeate flow rates: 40 L/h and 36.6 L/h, respectively)

Table 15 presents the characteristics of feed, permeate and concentrated streams. In this experiment, an average permeate flux of 5.50 $kg/m^2 \cdot h$ was achieved, using operating conditions far from optimal. The feed temperature and Reynolds number were 65±5 ºC and 410, respectively. Higher feed flow rates and temperatures could not be used due to the limitations of the heat source of the DCMD system due to the high volume of stillage to be treated.

ºBrix was used as an indicative of the concentration degree. The ºBrix varied from 3.5 to 60 during the DCMD concentration. In the permeate side, the ºBrix was zero. Thus, the concentration degree was approximately 17-fold. Besides, sucrose and glycerol were concentrated and none of these compounds were detected in the permeate stream. The ionic conductivity in the permeate stream was only 144.4 $\mu S/cm$. For a binary mixture of water and acetic acid at the concentration found in this work, the ionic conductivity is approximately 97 $\mu S/cm$ [204]. Thus, the ionic conductivity could be attributed mainly due to the presence of acetic acid and other no identified organic acids rather than the wettability of certain pores caused by the acetic acid [205]. Figure 19 shows the increment in the ionic conductivity as well as the acetic acid concentration at the permeate

stream. Nevertheless, this ionic conductivity value shows the high rejection of non-volatile compounds that could be achieved using the direct contact membrane distillation process.

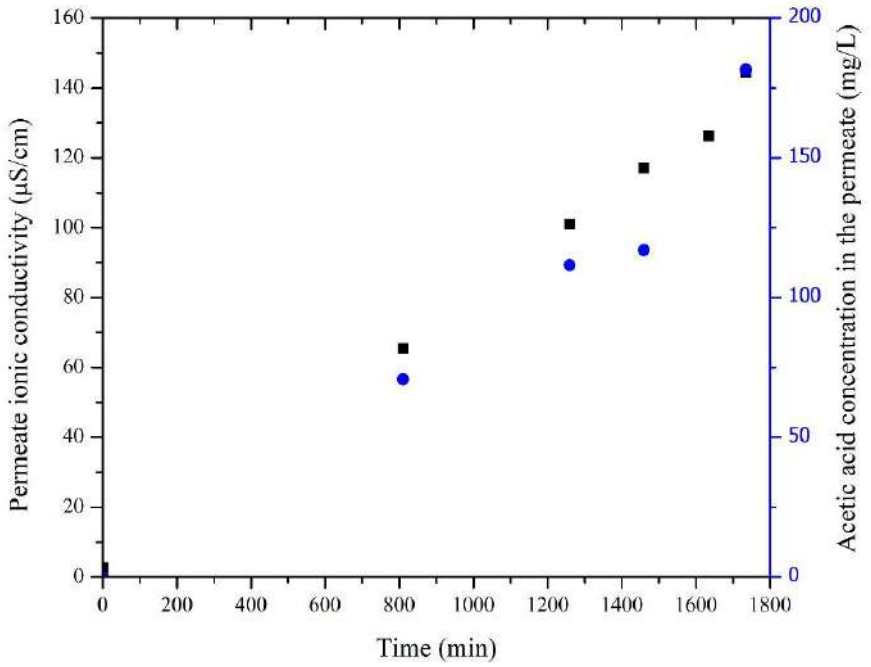

Figure 19. Permeate ionic conductivity and acetic acid concentration in the permeate stream along the industrial sugarcane stillage concentration by DCMD ($T_f = 65 \pm 5°C, T_p = 20 \pm 2°C$, feed and permeate flow rates: 40 L/h and 36.6 L/h, respectively)

Regarding the pH, it is worth mentioning that the water used at the permeate side initially had a pH value equal to 6.50. During the experiment, permeate pH decreased as result of the passage of volatile acids from the industrial stillage. The main component present in the permeate stream was acetic acid. Ethanol content in the permeate stream was so low that it was below the detection limit [206,207].

Acetic acid is also responsible for the COD content in the permeate stream. At the feed and concentrate streams, the sucrose and glycerol concentration as well as the residual acetic acid are responsible for the COD content. Nevertheless, the COD rejection was around 83.5%. It is worth mentioning that the COD removal reached by membrane distillation is comparable with that obtained using physicochemical processes. However, these processes require the use of high quantities of chemicals as flocculants or oxidants, which is a great disadvantage [9,11]. On the other hand, COD removal is lower than that achieved by anaerobic digestion (AD). AD is widely used because of the advantage of

biogas production. However, AD is more efficient when it is performed with a co-substrate because of the lack of macro and micronutrients in the stillage [25,27]. Besides, stillage represents some challenges for AD process due to the high ions content, mainly potassium and sulfate (which are responsible for the production of a sulfur-rich biogas), and to the melanoidins compounds (responsible by the dark color) present in this effluent [9,19]. About this, Yang *et al.* (2017) [208] reported that after of the anaerobic-aerobic digestion of the stillage, it was also necessary to treat the effluent using an ion exchange resin to remove the effluent color.

Table 15. Characterization of DCMD streams for sugarcane stillage concentration.

	pH	Ionic conductivity ($\mu S/cm$)	ºBrix	COD (mg/L)	Sucrose (mg/L)	Glycerol (mg/L)	Acetic acid (mg/L)	Average permeate flux (kg/m^2h)
Feed	4.45	10,098	3.5	35,000	2,720	4,620	411.6	
Permeate	3.79	144.4	ND	5,759	ND	ND	181.5	5.50
Concentrate	4.55	37,130	60	240,000	32,462	76,099	ND	
Rejection	-	98.5%	100%	83.5%	100%	100%	56%	

Photographs of samples collected from the streams of the industrial sugarcane stillage concentration by membrane distillation are presented in Figure 20. Regarding the permeate stream from the membrane distillation test, a decolorization process is not necessary. This stream could be reused in the ethanol production process, for example, recycling it into the fermentation process as make-up water. This practice was studied by many authors in order to take advantage of the effluent obtained after the anaerobic digestion or of the condensate obtained from stillage concentration by evaporation [9,11,51,55,208–210]. Recycling is only limited by the accumulation of inhibitory compounds [208,209,211]. Due to the presence of acetic acid in the permeate stream, it is possible to consider the recovery of this compound. In this way, the acetic acid free permeate stream could be recuperated as process water. Rai *et al.* (2008) proposed a nanofiltration process as a tertiary treatment of aerobically treated stillage achieving high

removal degree of COD, total dissolved solids and color [212]. This could be an alternative for recovery water to the ethanol production process.

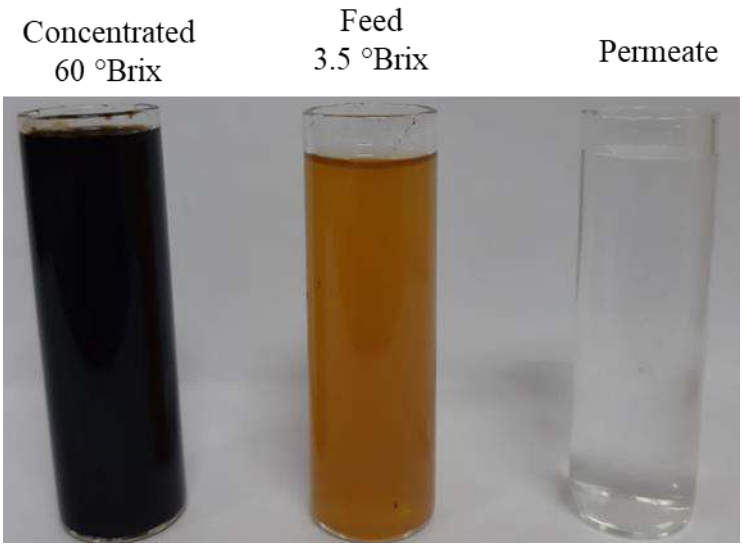

Figure 20. Feed, permeate and concentrated streams of industrial sugarcane stillage concentration by DCMD process.

Membrane separation processes, such as micro (MF), ultra (UF) and nanofiltration (NF) and reverse osmosis (RO) or a combination of them, were proposed to treat the industrial stillage aiming the stillage concentration or the recovery of water for its recycling.

Nataraj *et al*. (2006) used a combination of NF and RO to treat distillery spent wash achieving a permeate stream that meets the requirements for its discharge. However, pressures higher than 70 bar are necessary for reaching high percent rejection of contaminants by RO process [21]. The combination of UF and RO processes, proposed by Murthy *et al.* (2009), allowed to obtain a permeate stream that could be recycled to the process, reducing the consumption of fresh water [213].

Arora *et al.* (2011) concentrated from 7% to 35% using a 5 stages MF system. The authors estimated that this system could treat more than twice the amount of feed flow rate than a four effect evaporator system for the same cost [214].

Despite the fact that the permeate characteristics obtained by RO has a slightly better quality compared to the obtained in this work it is worth to mention that in the former process a pretreatment is quite required.

The STEC in this case was 846 kWh/m^3. Although, the heat requirements for DCMD are higher than other concentration processes (for example, reverse osmosis [215]), the concentrated stillage (60 $°Brix$) could be used as a biofuel to produce more energy. Cortes-Rodriguez *et al*. (2018) [68] suggested a heat integration between juice and stillage concentration processes. Stillage concentration was carried out in a multiple-effect evaporator system and a final concentration of only 25 $ºBrix$ was achieved with this approach. Recently, Fukushima *et al*. (2019) [18] proposed the same integration, however, they achieved to concentrate stillage until at least 60 $ºBrix$. This was possible due to the incineration of the concentrated stillage. In this way, 65.2 kg of steam ($480ºC/65\ bar$) was obtained for each ton of cane processed, which were used in the stillage evaporation process and in the cogeneration system to obtain more electrical energy. This resulted in a power generation capacity of 49 MW, considering the processing of 500 ton of cane per hour. This implies in an electricity supply of more than 190 $GWh/year$ considering 4,000 operating hours per year. This power generation capacity is higher than the one achieved in a plant of sugar and ethanol integrated with AD process for the stillage treatment, as reported by Fuess *et al.* (2018) [52]. These authors concluded that a plant with a capacity of almost 1,900 ton per hour can recover 116.8 GWh/harvest when stillage is treated in two-phase AD systems.

Any of these cases involve large investments. Peiter *et al*. (2019) [17] estimated the investment costs for an anaerobic bioreactor (coupled to gas treatment) and an evaporator system (21° Brix of final concentration), separately. They found that an AD system had a cost of 1.94 USD/m^3 of biogas produced while for an evaporator system, the investment cost was 0.73-1.03 USD/m^3 of water recovered depending on, among other factors, the attachment of the stillage treatment to an ethanol or sugar and ethanol production plant.

4.1.4.Physicochemical and surface properties

Along the concentration process of industrial stillage samples of concentrated stream were collected and characterized. These data were used to determine the physicochemical properties of the industrial sugarcane stillage as a function of the total solids content. These properties are shown from Figure 21 to Figure 30. Some of these experimental values were fitted and the relations were used in the mathematical model, as it is shown

below. It is worth to mention that all thermal properties were measured only at room temperature.

The ionic conductivity does not show a linear increment with the total solids content (Figure 21). This could be due to the ionic interactions at high concentrations of stillage.

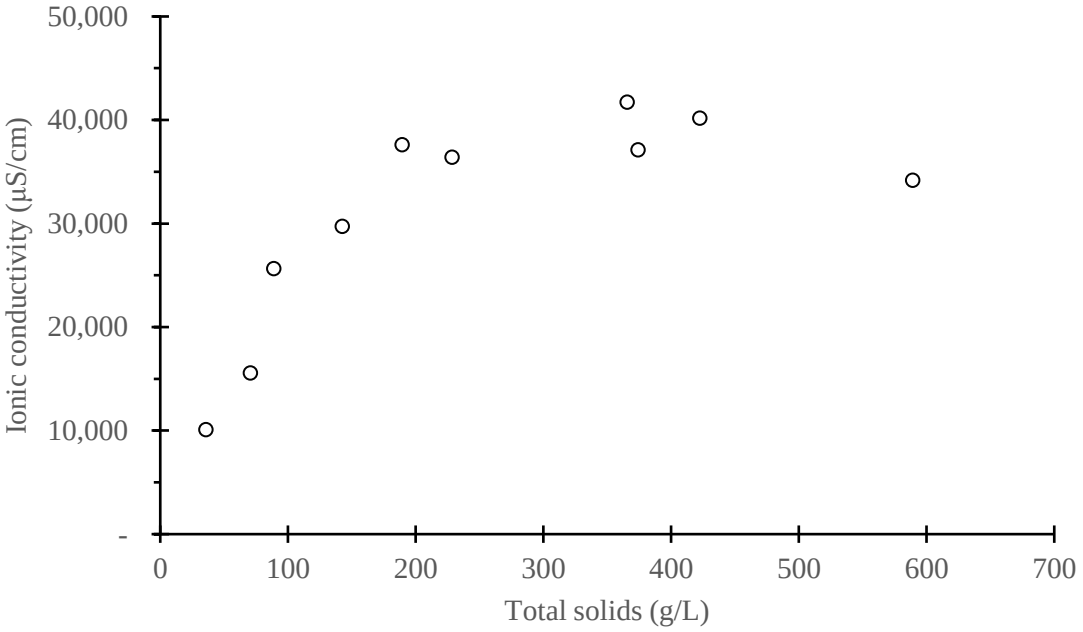

Figure 21. Ionic conductivity (○) as function of the total solids content in the concentrated stillage.

Figure 22 shows that °Brix content increases linearly with the concentration degree. This tendency it is expected since $°Brix$ measures the sugars content. Sugars are non-volatile components (as glycerol) and are concentrated at the concentrated stream along the test. Sucrose concentration increment is shown in Figure 23.

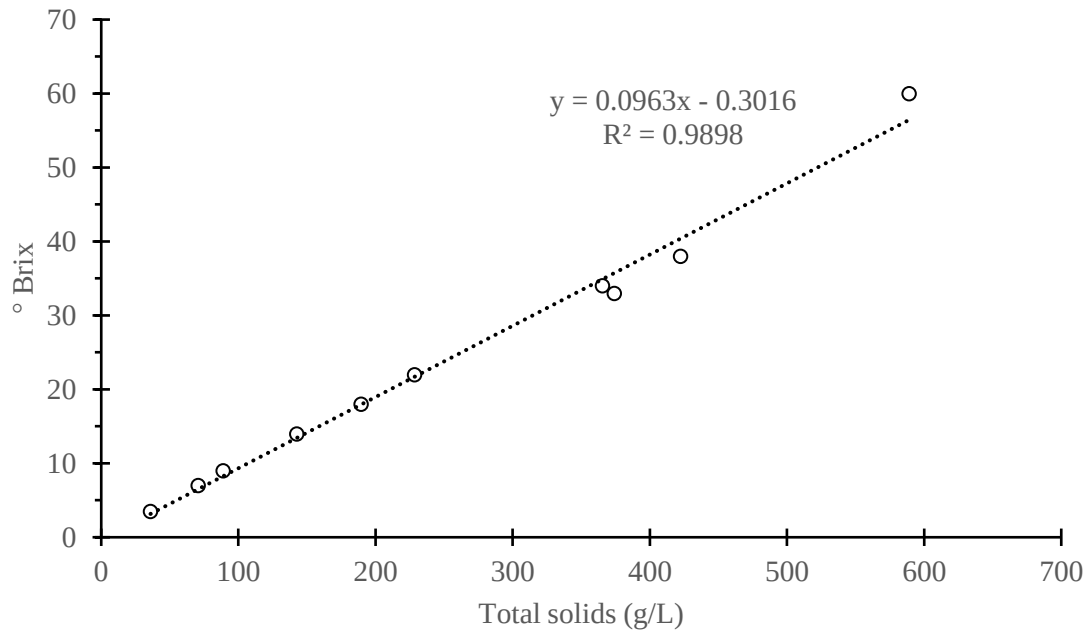

Figure 22. °Brix (○) as function of the total solids content in the concentrated stillage. Trend line: dotted line

The sucrose concentration shows a high dispersion. This could be explained due to HPLC method used to determine this component, in which the retention time of sucrose could be overlapped with other sugars [216]. Besides, the acid nature of the stillage could cause sucrose hydrolysis producing fructose and glucose which is favored by the high temperatures used [217].

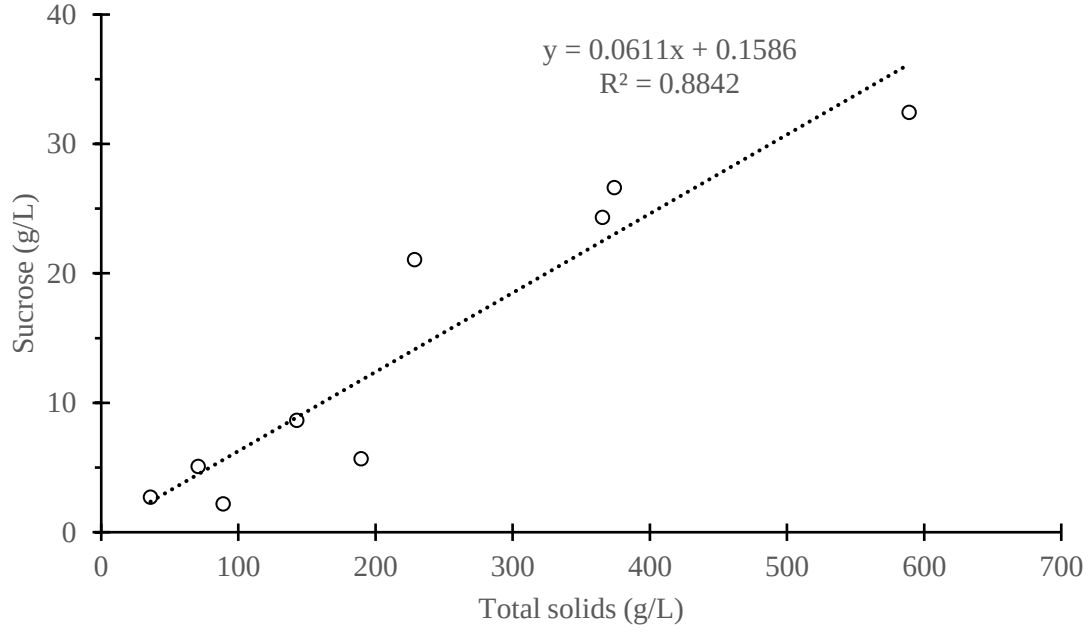

Figure 23. Sucrose concentration (○) as function of the total solids content in the concentrated stillage. Trend line: dotted line.

On the other hand, the glycerol concentration presents a linear relation with the stillage total solids content, as shown in Figure 24.

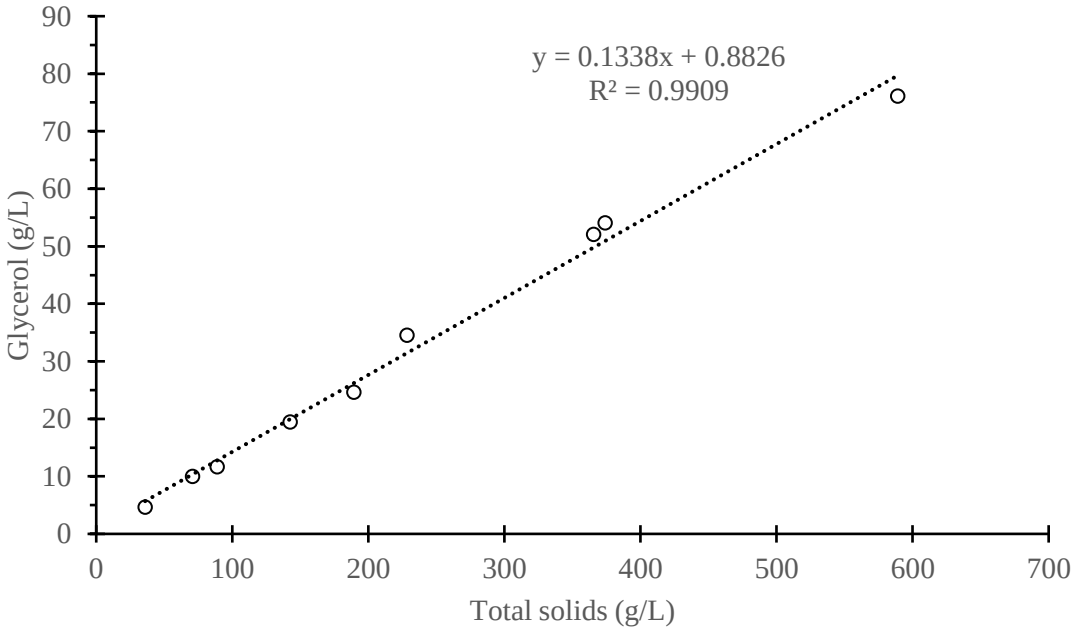

Figure 24. Glycerol concentration (○) as function of the total solids content in the concentrated stillage. Trend line: dotted line.

Table 16 shows the COD and the total volatile components at different concentrations of stillage. The total volatile solids values do not represent the content of organic matter because the losses due to volatilization or decomposition of some salts are also included. The COD is better to characterize the organic matter of the samples [169]. It is way, as it can be seen in the Table 16 the different between these values is minimal and it could be said that stillage contains mainly volatile organic matter. Gouvêa de Godoi *et al*. (2019) found that 45 to 80% of the total solids are volatile solids.

Table 16. Characterization of DCMD streams for sugarcane stillage concentration.

º Brix	TS (g/L)	COD (g/L)	TVS (g/L)
3.5	35.92	35.00	33.73 ± 1.36
7	70.73	49.92	47.12 ± 2.35

9	88.94	32.34	59.08 ± 2.93
14	142.68	90.83	95.90 ± 5.05
18	189.48	-	139.67 ± 3.03
22	228.43	148.33	153.21 ± 8.16
33	374.13	240.00	254.13 ± 11.8

Water activity is an indirect indicative of the vapor partial pressure of the water in the solution and it is important to determine because the vapor pressure is the driving force of the membrane distillation process. The water activity was determined by direct reading as function of the stillage concentration. A decrement of almost 10% was observed when the content of total solids increased from 36 to 590 g/L (Figure 25). The equation of the fitting line for the values, showed in Figure 25, was used in the mathematical model developed for the stillage concentration by membrane distillation in order to correct the vapor pressure of the water.

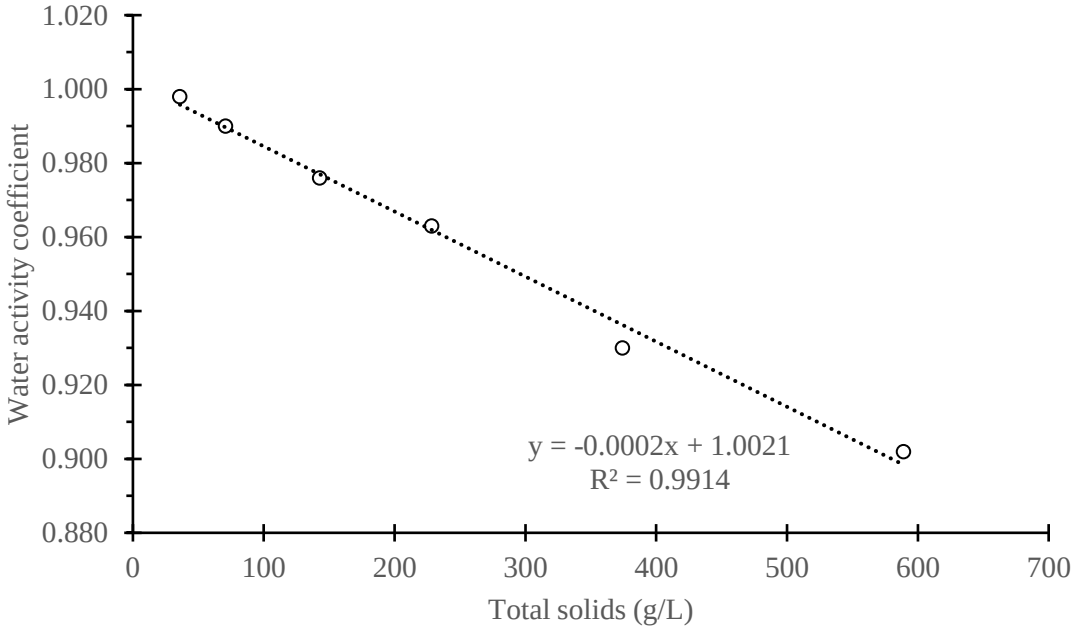

Figure 25. Water activity (○) as function of the total solids content in the concentrated stillage. Trend line: dotted line.

Total solids increment causes an increment on the density and the viscosity of the stillage as can be seen in Figure 26 and Figure 27. These parameters were also used in

the mathematical model. Density values determined in this work are agree with the ones reported by Larsson (2014) [171].

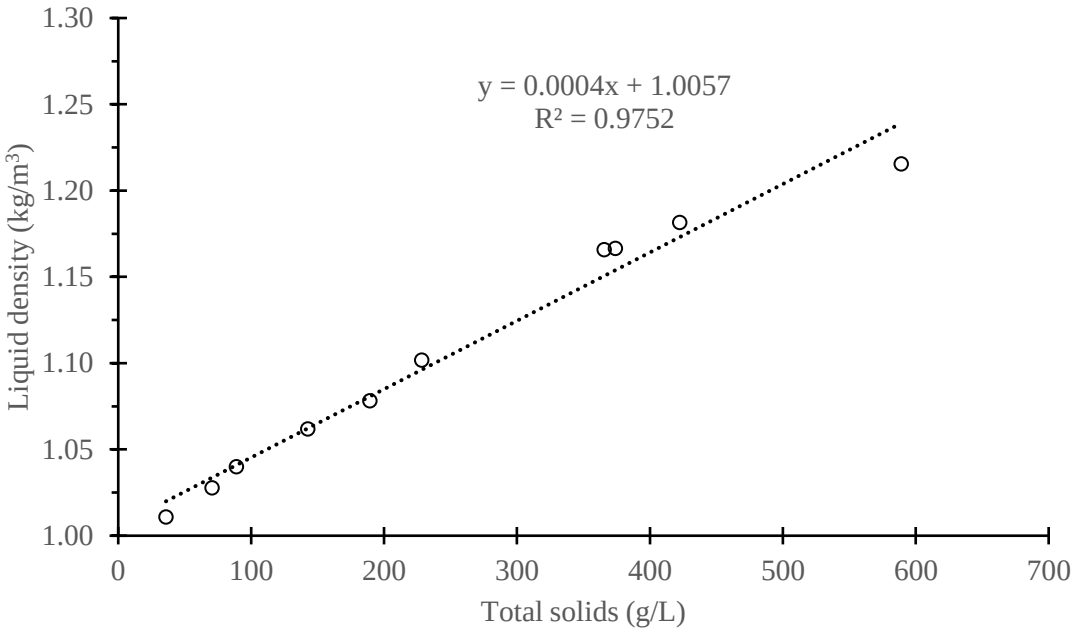

Figure 26. Density (○) as function of the total solids content in the concentrated stillage. Trend line: dotted line.

The viscosity of the stillage is relatively low in the range measured. However, Larsson (2014) [171] and Nair & Taherzadeh (2016) [218] found a high increment of the viscosity for higher concentrations of stillage. Besides, Larsson's data were determined at 100°C. Nevertheless, in the range determined in this work, the values are in agreement with those found by the mentioned authors.

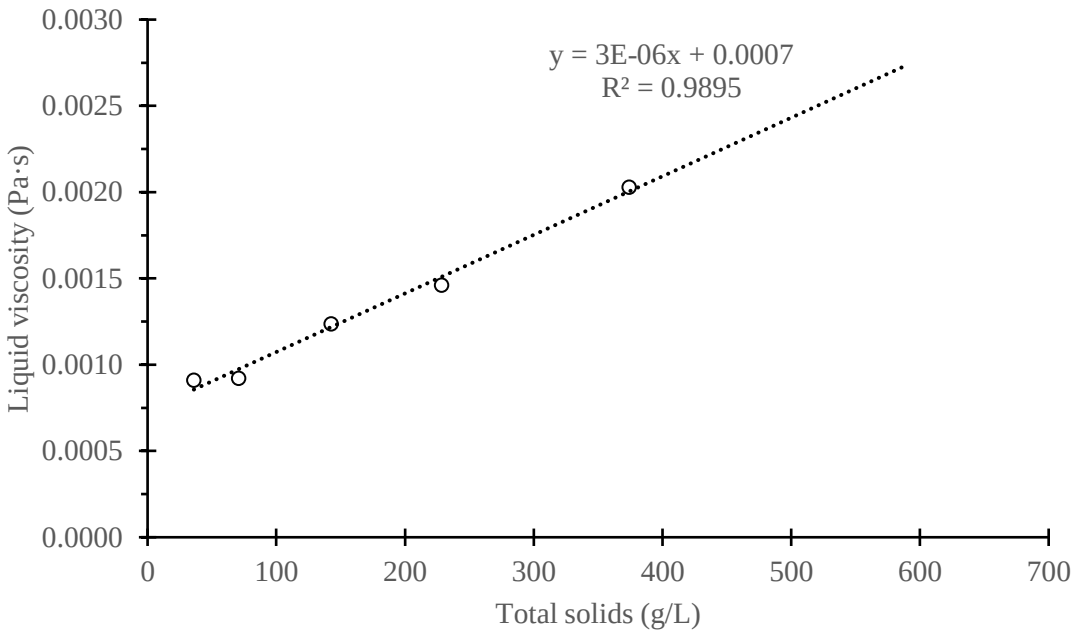

Figure 27. Viscosity (○) as function of the total solids content in the concentrated stillage. Trend line: dotted line.

Thermal conductivity of stillage decreases with the total solids content increment (Figure 28). Specific heat capacity shows the same tendency (Figure 29). This makes the MD process difficult as it affects the heat transfer in the boundary layer at the feed side.

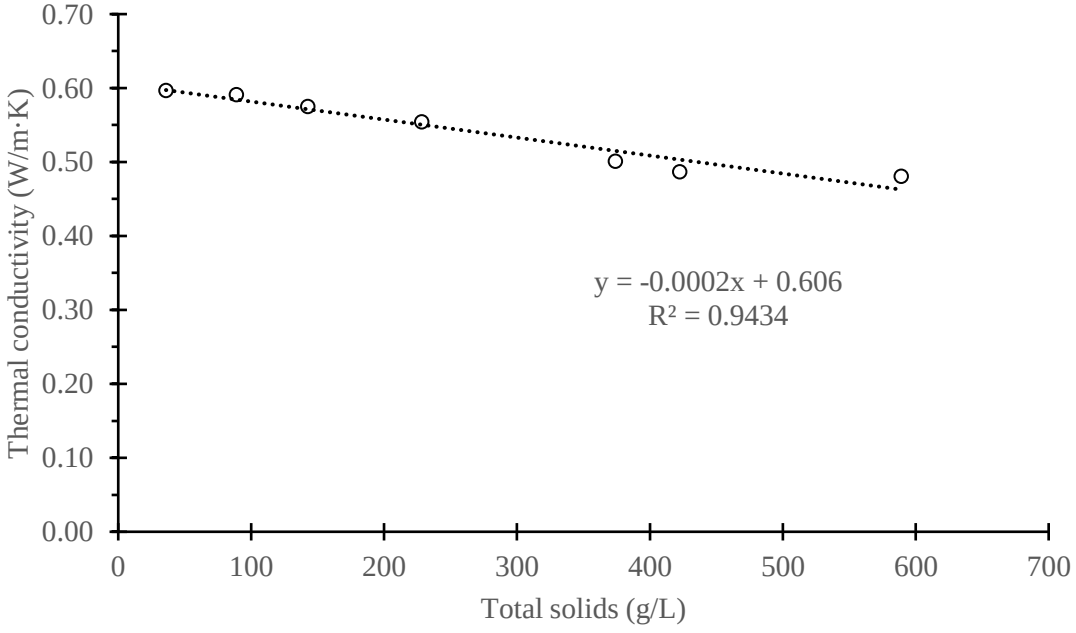

Figure 28. Thermal conductivity (○) as function of the total solids content in the concentrated stillage. Trend line: dotted line.

The specific heat of stillage solution was calculated as a function of dry solid content using Eq. 44 as mentioned in the Section 3.1.6.1 [171]. The trendline showed in the Figure 29 was used in the mathematical model.

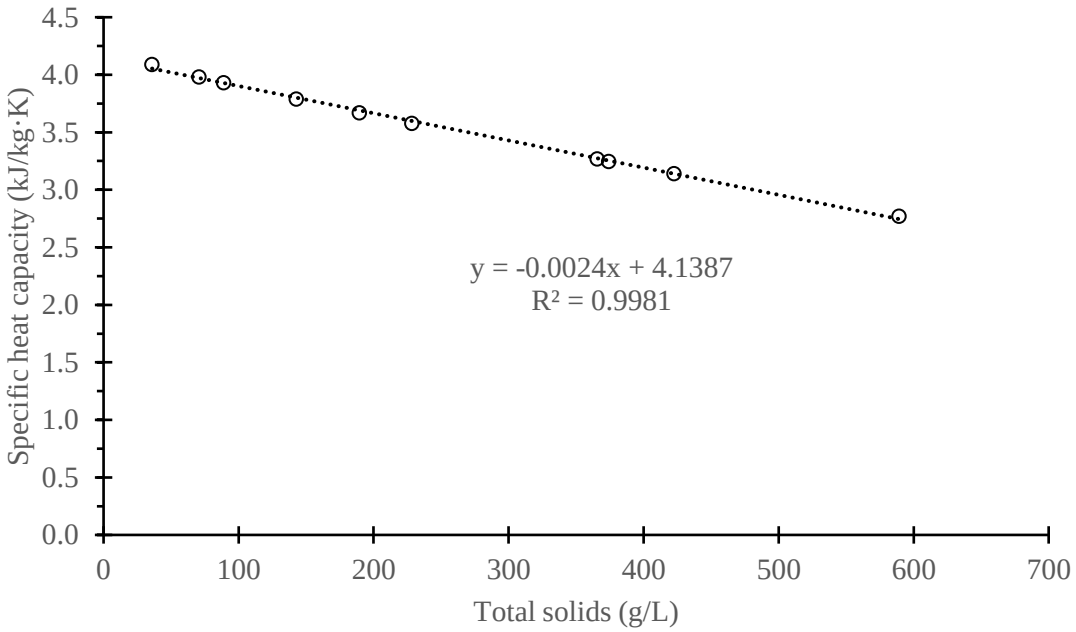

Figure 29. Specific heat capacity (○) as function of the total solids content in the concentrated stillage. Trend line: dotted line.

Surface tension is a measurement of the liquid surface's resistance to an external force, due to its cohesive intermolecular forces. This parameter is directly proportional to the liquid entry pressure, which must be higher than the operational pressure in the MD process. For this reason, it is important to measure it in order to determine if the concentrate stillage could cause membrane wetting. Membrane wetting is a problem in MD distillation because decreases the permeate quality [31,83,219]. Alcohols are liquids with low surface tension that can lead to the wetting of the commonly membranes used in MD [219]. As it can be seen in Figure 30, for concentrations higher than 100 g/L of total solids the surface tension becomes stable, this could be due to the evaporation of the volatile components as ethanol and acetic acid present initially in the sample.

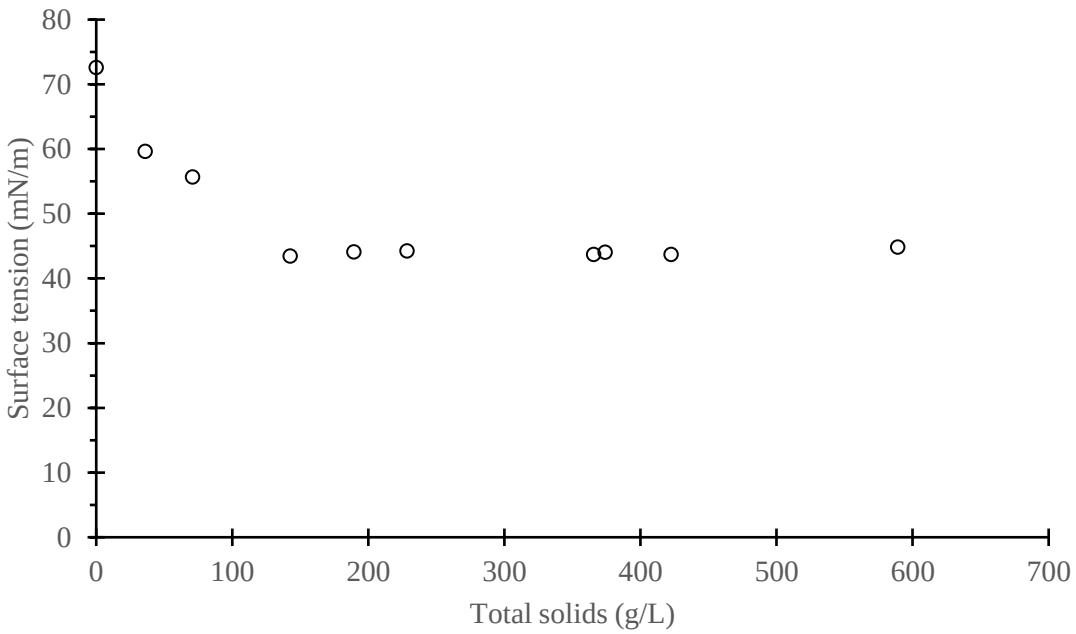

Figure 30. Surface tension (○) as function of the total solids content in the concentrated stillage.

4.2. Simulation results

4.2.1.Sensibility analysis

The influence of the temperature of feed and permeate streams on the permeate flux will be analyzed in this part of the thesis. All the simulations of this section were carried out considering that water is flowing by both feed and permeate sides. The model was simulated for feed temperatures varying from 333 K to 353 K and permeate temperatures from 288 to 308 K. As presented in Figure 31, permeate flux rises exponentially with the feed temperature increment.

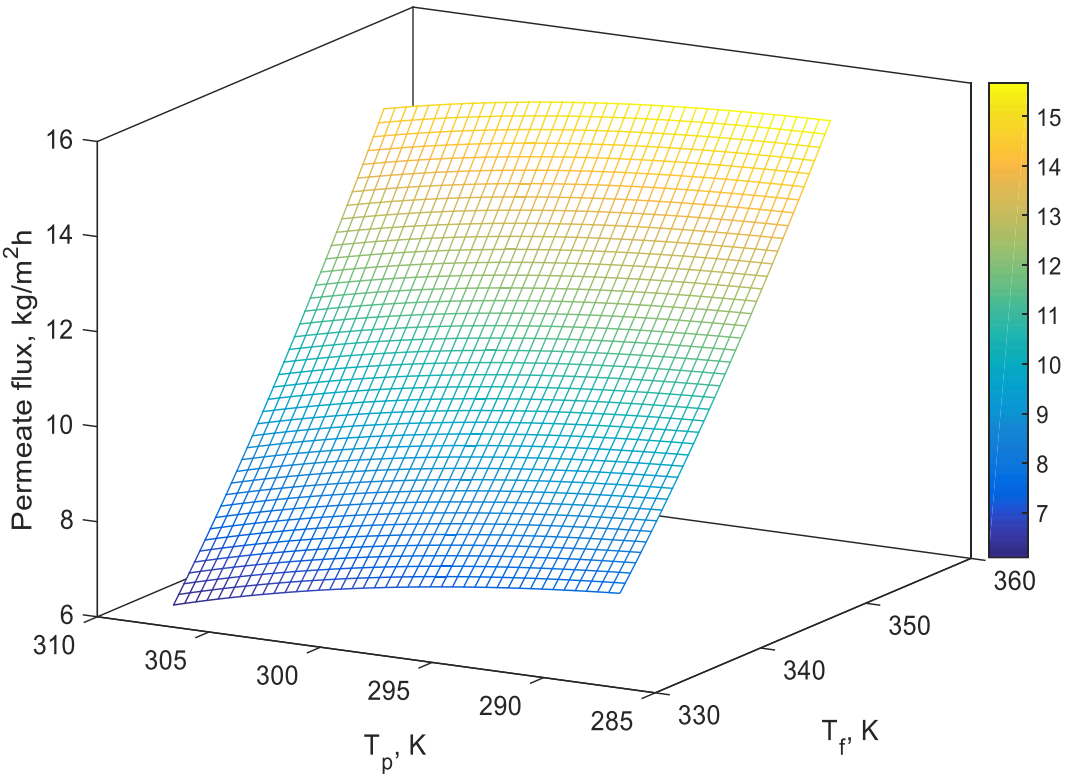

Figure 31. Permeate flux variation with hot (T_f) and cold (T_p) water temperatures for $Re_f = 1500$; $Re_p = 1000$.

When permeate temperature increases from 288 to 308 K, the permeate flux decreases. However, the decrement is 25% for a feed temperature of 333 K and decreases to only 7% for a feed temperature of 353 K. It is worth mentioning that this is mainly important in practical applications when there is no availability of water at temperatures below 293 K.

In the other hand, when the feed temperature varies from 333 K to 353 K, there is an increment of 106% on the permeate flux for a permeate inlet temperature of 288 K and 157% for 338 K.This shows that the feed temperature influence is more important than the permeate one on the permeate flux. This is related to the vapor pressure dependence with temperature, more intense at high temperatures.

Figure 32 shows the permeate flux variation with the feed and permeate Reynolds numbers. The Reynolds number of the hot water stream has a higher effect on the permeate flux. When the Reynolds number of the cold water stream increases from 150

to 1800, the permeate flux increases 0.2% and 6% for feed Reynolds numbers of 150 and 1800, respectively.

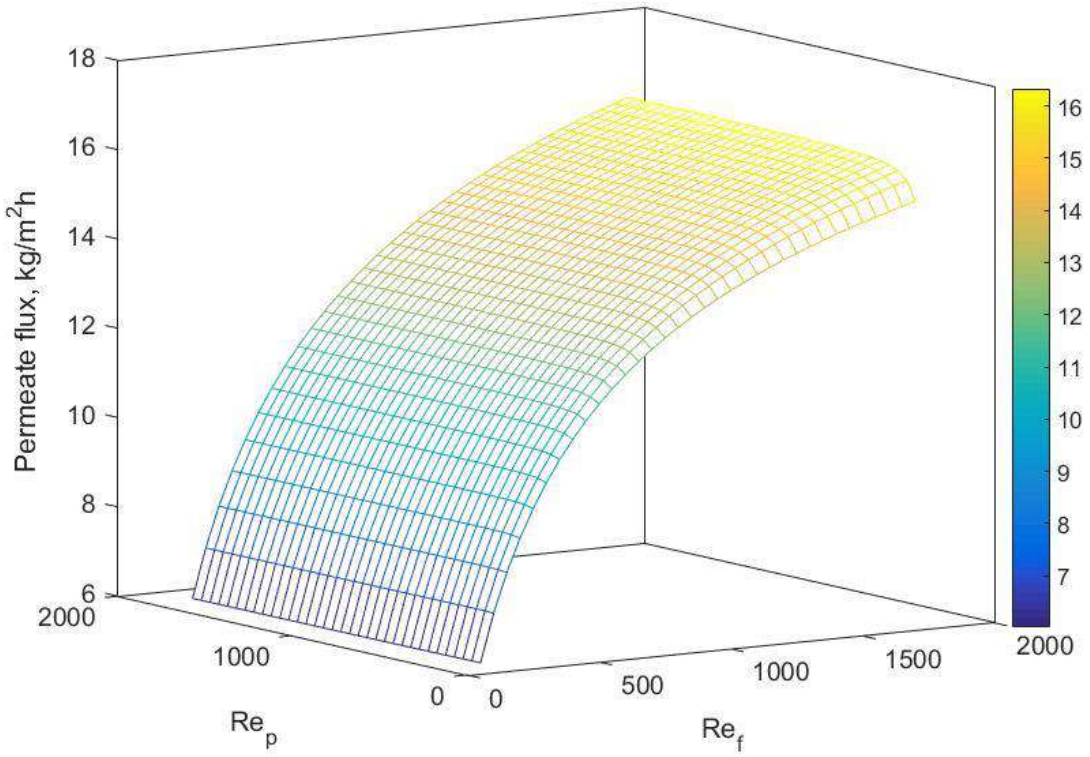

Figure 32. Permeate flux variation with hot (Re_f) and (Re_p) cold water Reynolds number for $T_f = 353\ K$ and T_p = 293 K.

For a given Reynolds number of the permeate stream, the permeate flux tends to reach a plateau despite the feed Reynolds number increase. This indicates the existence of a boundary layer responsible for the temperature polarization. In this way, when the hydrodynamic conditions of the process are enhanced, it is possible to achieve a better mixture at the feed side, which causes the boundary layer thickness to decrease and, consequently, the temperature polarization is reduced. Higher permeate fluxes are then achieved. However, when the boundary layer thickness reaches a minimal value, no enhancement is possible on the permeate flux despite of feed Reynolds number increase.

The driving force of the membrane distillation process is the vapor pressure difference between both sides of the membrane. The permeate flux increases with the increment on the feed temperature and feed Reynolds number, as could be seen in Figure 31 and in Figure 32, respectively. This is due to the increment of the driving force of the

process as can be seen in Figure 33, where it is shown the variation of vapor pressure difference between both sides the membrane with the temperature and the Reynolds number variation of the hot water stream. It is worth to mention that the vapor pressure difference was calculated using average membrane temperature values.

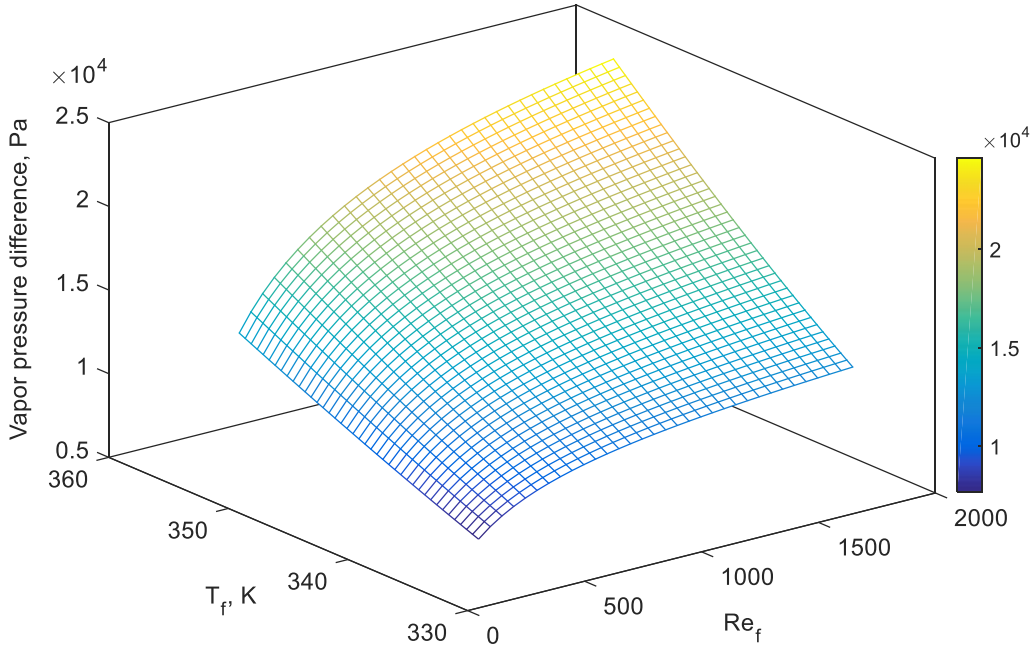

Figure 33. Vapor pressure difference variation with feed temperature and Reynolds number for $T_p = 293\ K$ and $Re_p = 1000$.

For the feed temperature, the permeate flux increment is exponential, due to the vapor pressure relation with the temperature. For feed Reynolds number, the increment in the driving force, and consequently in the permeate flux, is related to shorter residence times, allowing to maintain high temperatures inside the module, achieving higher vapor pressure differences. As can be seen in Figure 34, at higher feed Reynolds number, the feed outlet temperature is closer to the entry temperature.

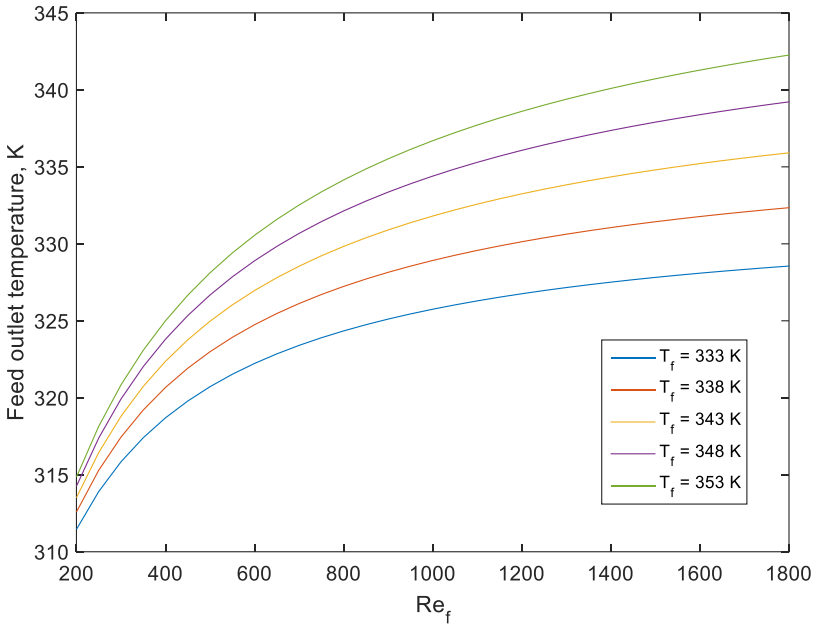

Figure 34. Feed outlet temperature variation with Reynolds number of hot water stream for different feed temperatures ($T_p = 293\ K$ and $Re_p = 1000$).

However, as previously mentioned, the increase in the driving force is limited to the reduction of the boundary layer to a thickness below which the feed Reynolds number increment has no effect. By the other hand, if it is no possible to operate at higher feed temperatures, the Reynolds number increment would allow to reach the same vapor pressure difference and therefore, the same permeate flux at a lower feed temperature. This can be seen in the Figure 35. For example, the same vapor pressure difference is achieved at 348 K and a Reynolds number of 1,000 as at 353 K and a Reynolds number of 500.

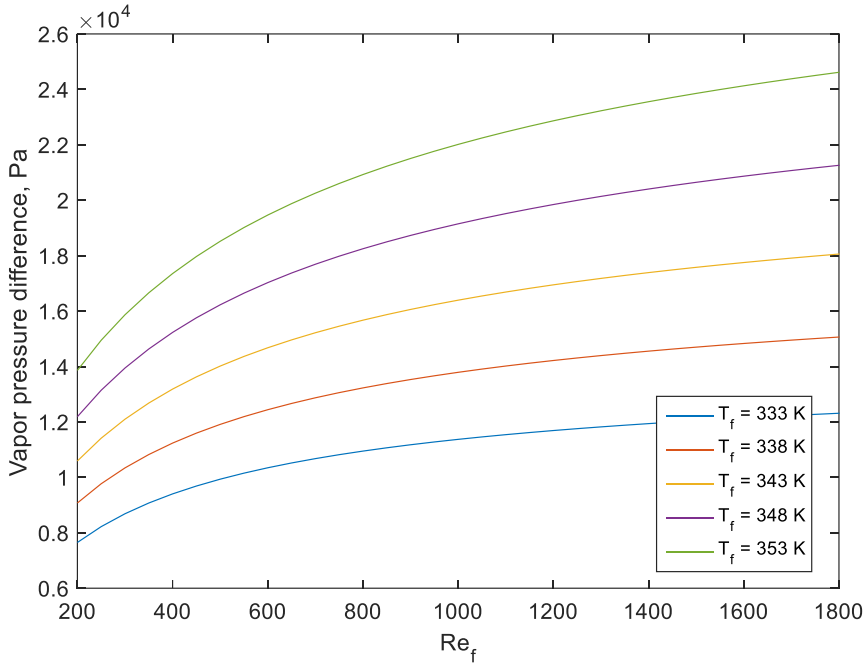

Figure 35. Vapor pressure difference variation with Reynolds number of hot water stream for different feed temperatures ($T_p = 293\ K$ and $Re_p = 1000$).

The temperature polarization coefficient (TPC) gives an idea of about how much the process moves away from an ideal process. The closer to 1 is the TPC, more efficient the process is. The temperature polarization is also related to the permeate flux, higher permeate flux causes higher temperature polarization, so, the TPC moves away from 1. Figure 36 shows the TPC for the case simulated in Figure 33. For all feed Reynolds numbers, when the feed temperature increases, the TPC decreases due to the higher permeate fluxes achieved. However, this decrease is not proportional for all cases. This indicates that there are some mechanisms intervening on the process. On one hand, low temperatures ($333\ K$) and low Reynolds number ($Re_f = 200$) are related to low permeate fluxes ($4.16\ kg/m^2h$), so the TPC is relatively high (0.8142). However, at low temperatures, the Reynolds number increment causes a TPC decrement because higher permeate fluxes are achieved. Then, above a certain Reynolds number, TPC increment is observed since the Reynolds number influence becomes more important, *i.e.*, due to the decrease of the boundary layer thickness.

It is worth to mention that the experimental tests of this work were performed at Reynolds numbers between 50 and 600 and, as shown in Figure 35, in this range the driving force of the process is highly affected by the Reynolds number.

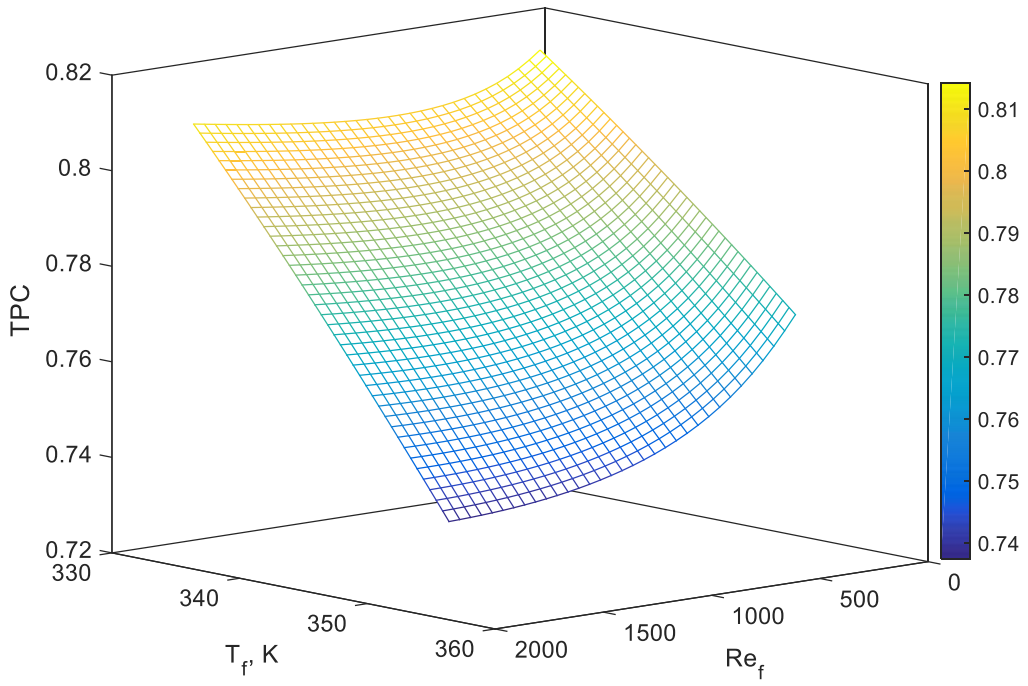

Figure 36. Temperature polarization coefficient variation with temperature and Reynolds number of hot water stream for $T_p = 293\ K$ and $Re_p = 1000$.

4.2.2.Model validation

First, the model developed was validated for water with the data obtained in this work. Secondly, the data from Al-Obaidani *et al*. (2008) were used to validate the model for a NaCl solution as feed stream. The physical properties and the water activity coefficient considered in this case are detailed in Section 3.2.2. Then, the synthetic stillage solution treatment by membrane distillation was validated with the experimental data obtained in this work. As it was mentioned above, for this model the volatile components (water, ethanol and acetic acid) were considered in the VRTherm plugin. Finally, the DCMD process for the industrial stillage concentration was validated.

The validation of the data required a parameter estimation. The membrane tortuosity was the parameter chosen for performing the fitting, which is frequently used in the literature [106]. Several values for the membrane tortuosity (τ) were found in the literature. Values of 1.28-1.37 were obtained for the case in which τ is considered to be the inverse of the membrane porosity (ϵ), which also varies between 73% and 78%

[153,157]. For these values of porosity, the correlation used by Srisurichan *et al*. (2006) gives values between 1.91 a 2.21. The parameter estimation was performed using EMSO. For this, the experimental data were used, and the tortuosity estimated was 1.61 (with a significance level of 0.95 and $R^2 = 0.98$). This tortuosity value was used in all the simulation results.

The simulation results for pure water are shown in Figure 37. For water, the simulation results presented a good agreement with the experimental data.

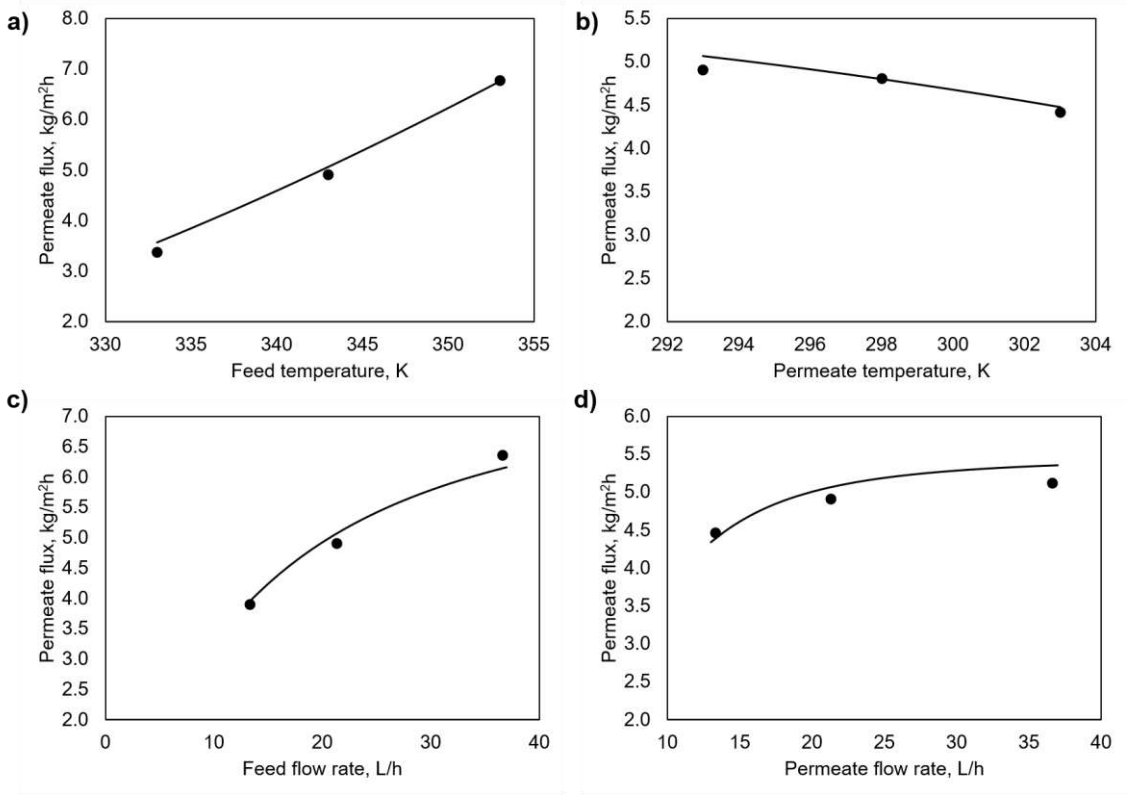

Figure 37. Experimental data (dots) and simulation results (solid line) for water in different conditions: a) $Q_f = Q_p = 21{,}3\ L/h$, $T_p = 293\ K$; b) $Q_f = Q_p = 21{,}3\ L/h$, $T_f = 343\ K$; *c*) $Q_p = 21{,}3\ L/h$, $T_f = 343K$, $T_p = 293\ K$; d) $Q_f = 21{,}3\ L/h$, $T_f = 343\ K, T_p = 293\ K$.

The simulation results for a NaCl solution are shown in Figure 38. In this case, the tortuosity was considered 1.61 as in the previous simulations. The experimental results are the ones reported by Al-Obaidani *et al.* (2008). The model showed a better agreement for low temperatures than higher temperatures.

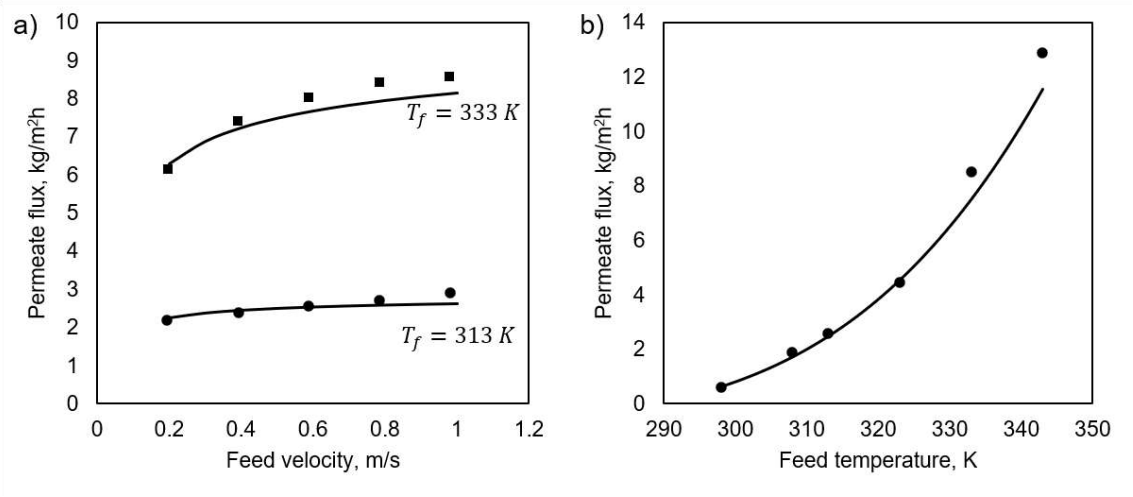

Figure 38. Experimental data (filled dots and squares) and simulation results (solid line) for a NaCl solution of $35\ g/L$ in different conditions: a) $v_p = 0.28\ m/s,\ T_p = 288\ K$; b) $\dot{m}_f = 0.055\ kg/s, \dot{m}_p = 0.027 kg/s,\ T_p = 288\ K$.

The validation of the model for a multicomponent solution was performed considering the transient dynamic of a stirred tank modelled as it was described in Section 3.2.4. This allowed to represent the batch process as it was carried out in the experiments.

The data of two experiments performed in this work using the synthetic stillage solution were used for validating the model developed. Synthetic stillage solution was simulated as an aqueous solution of sucrose, ethanol, acetic acid, and salts (expressed as NaCl). The calculation of the composition in the liquid phase was made considering the *IdealLiquid* model and the UNIFAC model. For the vapor phase, the *Ideal*, the SRK, and the PR models were considered. These models were compared in order to determine the ability to predict the concentration in the concentrated and the permeate (p) streams. Table 17 shows the experimental and the simulation results for two experimental conditions: 1) $T_f = 343\ K, T_p = 293\ K, Q_f = Q_p = 21.6\ L/h$ and 2) $T_f = 353\ K, T_p = 293\ K, Q_f = Q_p = 21.6\ L/h$. Bold values indicate the simulation results that are in agreement with the experimental data for the concentrate and the permeate streams.

Table 17. Model validation of the concentrate and permeate (p) streams for two experimental conditions using synthetic stillage solution. Ideal liquid and UNIFAC models were considered for the composition in the liquid phase and Ideal, SRK and PR models for the vapor phase.

Concentration	Experimental results (g/L)	Simulation results (g/L)				
		Ideal Liquid	Ideal Liquid	Ideal Liquid	UNIFAC	UNIFAC

		Feed	Concentrate	Ideal	SRK	PR	SRK	PR
1	Sucrose	2.440	2.912	**3.056**	3.061	3.061	3.066	3.066
	Acetic acid	1.583	1.469	1.754	1.750	1.750	**1.236**	**1.236**
	Ethanol	3.899	1.978	3.111	3.086	3.091	**1.700**	**1.700**
	Salt	3.310	-	4.146	4.152	4.152	4.159	4.159
	Acetic acid (p)	-	0.055	**0.206**	**0.211**	**0.211**	0.672	0.672
	Ethanol (p)	-	1.930	1.588	**1.612**	**1.609**	2.994	2.993
2	Sucrose	2.350	3.620	**3.744**	**3.756**	**3.753**	3.761	3.761
	Acetic acid	1.041	1.151	**1.343**	**1.339**	**1.339**	0.789	0.789
	Ethanol	4.230	1.442	3.276	3.246	3.253	**1.957**	**1.956**
	Salt	3.310	-	5.273	5.290	5.286	5.297	5.297
	Acetic acid (p)	-	0.183	**0.196**	**0.200**	**0.201**	0.538	0.539
	Ethanol (p)	-	2.231	**2.138**	**2.152**	**2.154**	3.372	3.370

1. $T_f = 333\ K, T_p = 293\ K, Q_f = Q_p = 21.6\ L/h$
2. $T_f = 353\ K, T_p = 293\ K, Q_f = Q_p = 21.6\ L/h$

(p): permeate stream

For a first approximation, considering the synthetic stillage solution as an ideal liquid mixture provides a good agreement mainly for the sucrose. The UNIFAC model presented a better agreement for the ethanol concentration in the concentrated stream. However, there was an overestimation of the concentration of volatile components in the permeate stream. In the second experimental condition, the concentrations of the acetic acid and the ethanol in the permeate stream were much higher (0.54 and 3.37 g/L, respectively) than the ones obtained using the *Ideal Liquid* model (0.20 and 2.15 g/L, respectively). These last are closer to the experimental data (0.18 and 2.23 g/L, respectively).

On the other hand, it could be considered that the ethanol concentration measured in the concentrate stream is lower than in an ideal situation because its boiling temperature is near to the temperatures used in the experiments and it could have been lost during the process. The models tested for the vapor phase do not show significantly difference for each case. The deviation of the simulated results from the experimental data is shown in Table 18 for both the concentrate and the permeate streams of the two experimental condition shown in Table 17. The simulations performed considering *Ideal Liquid* and SRK models showed the smaller sum of deviation from the experimental data. For this reason, these models were chosen for the following simulations.

Table 18. Deviation of the simulation results from the experimental data for the two experimental conditions shown in Table 17.

Concentration	Deviation from the experimental results

		Ideal Liquid Ideal	Ideal Liquid SRK	Ideal Liquid PR	UNIFAC SRK	UNIFAC PR
1	Sucrose	0.072	0.075	0.075	0.077	0.077
	Acetic acid	0.142	0.141	0.141	0.116	0.116
	Ethanol	0.567	0.554	0.557	0.139	0.139
	Salt	0.000	0.000	0.000	0.000	0.000
	Acetic acid (p)	0.075	0.078	0.078	0.309	0.309
	Ethanol (p)	0.171	0.159	0.161	0.532	0.532
	Sum of deviation	**1.028**	**1.007**	**1.011**	**1.173**	**1.173**
2	Sucrose	0.062	0.068	0.066	0.070	0.070
	Acetic acid	0.096	0.094	0.094	0.181	0.181
	Ethanol	0.917	0.902	0.905	0.257	0.257
	Salt	0.000	0.000	0.000	0.000	0.000
	Acetic acid (p)	0.006	0.008	0.009	0.177	0.178
	Ethanol (p)	0.046	0.039	0.038	0.570	0.569
	Sum of deviation	**1.128**	**1.112**	**1.114**	**1.257**	**1.256**

Regarding the permeate flux, for the experimental conditions 1 and 2 the values were 3.04 kg/m^2h and 6.16 kg/m^2h, respectively. For the simulation results, there was no difference between the total permeate flux values with the different simulated models for the liquid and the vapor phases. However, the simulation results were higher than the experimental data, being 3.56 and 6.69 kg/m^2h, for conditions 1 and 2, respectively.

It is worth to mention that the model does not consider the interactions that can take place between the different components in the stillage, which could be the cause of the difference found between the experimental data and the simulations results. For example, the sucrose in acid medium and at high temperatures tends to suffer an hydrolysis producing fructose and glucose [217] and Días *et al*. (2017) showed that VLE of the water + ethanol system is affected by the presence of fructose, which displaces the saturated liquid curve to lower temperatures [182]. Besides, it has been reported that the presence of salts in a mixture of water and ethanol increases the ethanol selectivity by the reduction in the water vapor pressure produced by the salt [181]. Galeotti *et al*. (2018) found that the acetic acid volatility increased in the presence of sugars [183]. Furthermore, the fact of encompassing the effect of salts in a single component (NaCl) simplifies the model even more.

Particularly for the synthetic stillage the *IdealLiquid* model showed better results because it is a diluted solution. By the other hand, it is important to mention that it is expected to obtain better results if the UNIFAC model is used with all the components

included into the VRTherm plugin. This will allow to consider the components interactions. In this work, this was not possible. However, despite the limitations, the model was useful for estimating the permeate flux under different operating conditions.

The model was adapted for the industrial sugarcane stillage and, even though its composition is very complex [7,52], it was decided to consider an aqueous solution of sucrose, glycerol, acetic acid, ethanol and salts (expressed as NaCl). The concentration of concentrate and permeate streams from the experiments were compared with the results obtained in the simulations for two conditions (1: $T_f = 333\ K, T_p = 293\ K, Q_f = 80\ L/h, Q_p = 36.6\ L/h$ and 2: $T_f = 353\ K, T_p = 293\ K, Q_f = 80\ L/h, Q_p = 36.6\ L/h$).

For these simulations, in the liquid phase, the *IdealLiquid* and UNIFAC models were compared and in the vapor phase, the Ideal and the SRK models. Besides these model comparisons, an adjustment of the water activity coefficient (γ_w) was carried out using the data obtained experimentally (Figure 25). These results are presented in the Table 19 and the adjustment of the water activity coefficient can be seen in the titled columns as γ_w.

Table 19. Model validation of the concentrate and permeate (p) streams for two experimental conditions using industrial stillage. Ideal liquid and UNIFAC models were considered for the liquid phase and Ideal and SRK models for the vapor phase. γ_w columns represent the water activity adjustment using the experimental data.

		Experimental results (g/L)		Simulation Results (g/L)					
				Ideal Liquid Ideal		Ideal Liquid SRK		UNIFAC SRK	
		Feed	Conc		γ_w		γ_w		γ_w
1	Glycerol	4.726	14.760	14.266	14.020	**14.484**	13.878	14.472	13.881
	Sucrose	2.788	7.003	8.416	8.271	8.545	**8.187**	8.538	**8.188**
	Acetic Ac.	0.412	-	0.761	0.748	0.759	0.731	0.236	0.230
	Ethanol	-	-	0.126	0.125	0.124	0.121	0.068	0.067
	Salt	-	111	105.655	103.836	**107.274**	102.784	107.186	102.803
	Acetic Ac. (p)	-	0.029	**0.110**	**0.111**	0.113	0.113	0.226	0.228
	Ethanol (p)	-	-	0.117	0.117	0.117	0.118	0.144	0.145
	ºBrix	-	11	12.143	11.929	12.332	**11.803**	12.266	**11.752**
2	Glycerol	4.523	11.585	12.803	12.658	12.923	**12.565**	12.929	**12.562**
	Sucrose	2.576	6.273	7.281	7.198	7.349	**7.145**	7.352	**7.143**
	Acetic Ac.	0.412	-	0.776	0.767	0.775	0.754	0.345	0.337
	Ethanol	-	-	0.180	0.178	0.179	0.175	0.137	0.135
	Salt	-	90	98.922	97.797	99.846	**97.079**	99.894	97.056
	Acetic Ac. (p)	-	0.048	**0.143**	**0.144**	**0.146**	**0.147**	0.300	0.303

Ethanol (p)	-	-	0.155	0.156	0.156	0.157	0.225	0.227
ºBrix	-	9	11.251	11.119	11.358	**11.035**	11.318	**10.988**

1. $T_f = 333\ K, T_p = 293\ K, Q_f = 80\ L/h, Q_p = 36.6\ L/h$ (120 min of test)
2. $T_f = 353\ K, T_p = 293\ K, Q_f = 80\ L/h, Q_p = 36.6\ L/h$ (90 min of test)

(p): permeate stream

Regarding the permeate flux, simulation results presented an average permeate flux of 4.70 kg/m^2h and 9.22 kg/m^2h for conditions 1 and 2, respectively, for which experimental data showed higher permeate fluxes (5.46 kg/m^2h and 13.37 kg/m^2h). This could be due to the consideration made in the model, in which only ethanol, acetic acid and water are the volatile components. This consideration was made based in the characterization of the industrial stillage sample (as it is shown in Table 11).

However, as aforementioned, the stillage is characterized for having a high content of volatiles, mainly organic matter. In this regard, it may be that due to the presence of other unidentified volatile components, the experimental permeate flux has been higher than the value found in the simulation. Besides, as it was mentioned, the VLE of the volatile components is affected by the presence of the sugars and other salts [181–183] and this effect was not considered in this work.

Clearly, this causes an underestimation in permeate flux values and could impact in the following considerations. Although the model does not represent exactly what is observed in the experimental data, it is useful as an estimative in order to predict the behavior of the permeate flux in different conditions and the concentration of the components, mainly the non-volatile ones. All the explanations given for synthetic stillage are valid for industrial stillage. Even more in this case, it is stated that if the data of all the stillage components can be included in the VRTherm, the UNIFAC model may present better results. Even the use of other models such as the NRTL may be suitable to represent which is experimentally observed.

The model was used to simulate the stillage concentration process showed in Section 4.1.3. At the beginning, the permeate flux was more stable than for the experimental test. This allowed to achieve higher concentrations in less time than the experimental data. In this regard, after 20 h of test for the experimental test 10 ºBrix was achieved while for the simulation a concentration twice higher was observed.

On the other hand, a decrement in the permeate flux was observed for the experimental and the simulated test from 20° Brix (Figure 18). As here no fouling or scaling phenomena were considered, the decrement in the permeate flux is attributed to the increment in the hydrodynamical properties (viscosity and density), confirming what is stated for the experimental test.

On this matter, the fast decrement in the permeate flux observed for the simulated test could be due to the lack of a higher content of volatiles components in the model. Despite the limitations of the model, it was used to simulate the stillage concentration by DCMD in an industrial scale as it will be seen in Section 4.2.4.

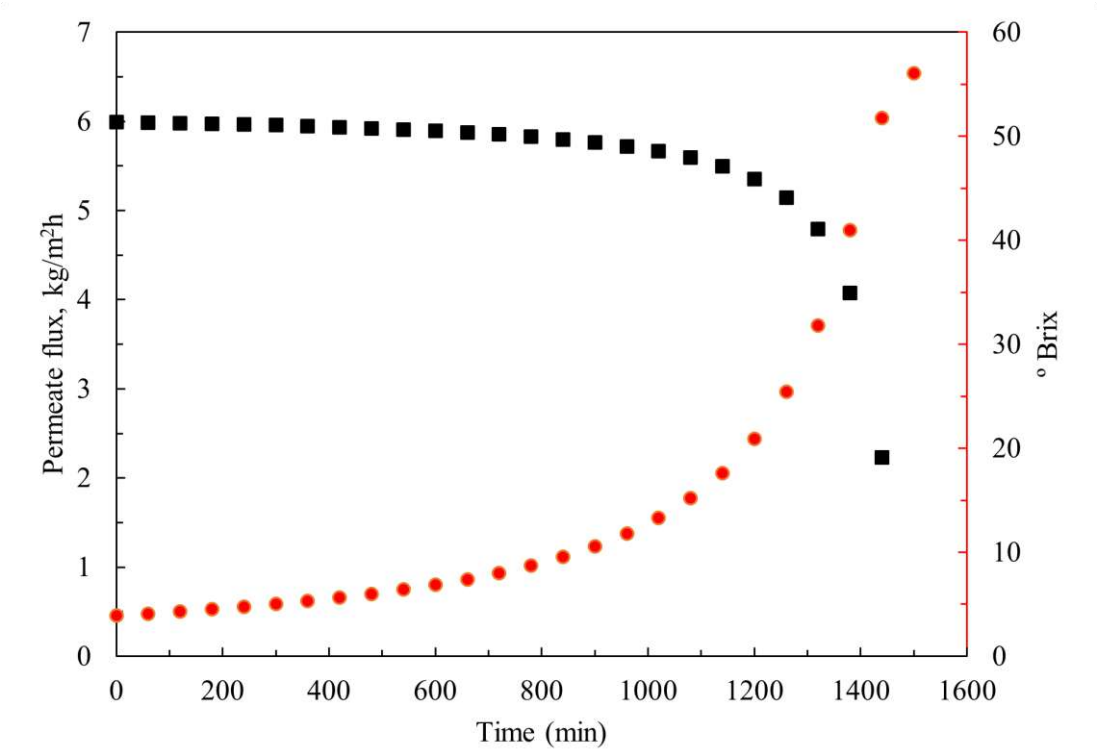

Figure 39. Simulation results for the permeate flux and ºBrix concentration along the industrial sugarcane stillage concentration by DCMD ($T_f = 65 \pm 5°C, T_p = 20 \pm 2°C$, feed and permeate flow rates: 40 L/h and 36.6 L/h, respectively)

4.2.3.Energy consumption

From this point onward, in all simulations the *IdealLiquid* and the SRK models were used for the liquid and the vapor phases, respectively. The water vapor pressure was

corrected by the water activity coefficient obtained experimentally as aforementioned. A greater membrane module was considered in this case and its characteristics are summarized in Table 20. These correspond to the commercial module MD070CP2L of Microdyn® and were taken from its data sheet.

Table 20. Membrane module (MD070CP2L) considered in the simulations of Section 4.2.3.

Symbol	Parameter	Value
r_s	Tube external radius (hollow fiber)	1.35 mm
r_l	Tube internal radius (hollow fiber)	0.9 mm
N_{fibers}	Number of tubes	350
d_{mod}	Shell internal diameter	7.2 cm
r_P	Nominal pore diameter	0.20 μm
ϵ	Porosity	73%

Regarding the module length, a reduction in the permeate flux is observed as the length of the module increases (Figure 39). This is due to the reduction of the driving force along the module (Figure 41). However, this effect may be compensated by the increasing in the effective permeation area, which allows to reach higher module productivities [220,221]. Nevertheless, this might not be a good strategy, especially considering that in long modules the permeate flux can decrease to values close to zero.

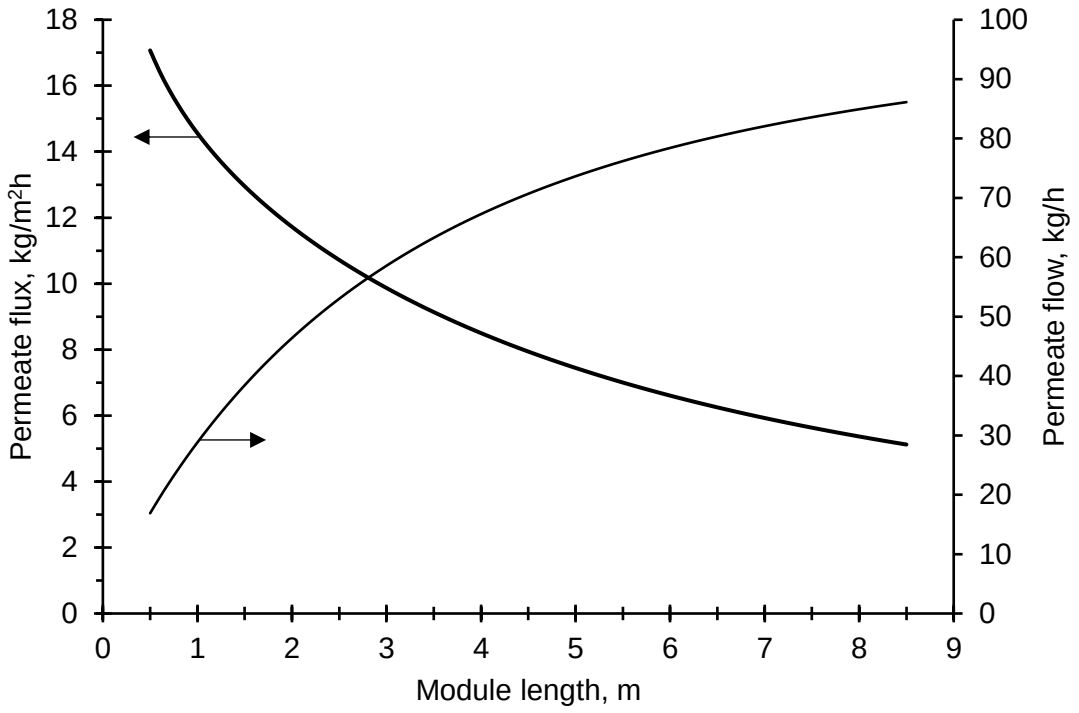

Figure 40. Effect of membrane length on the permeate flux and the permeate flow of industrial stillage. $T_f = 353\ K, T_p = 293\ K, Q_f = 3.2\ m^3/h, Q_p = 2.0\ m^3/h$ (considering as a unique module).

Besides, as it can be seen in Figure 41, when the length of the module increases, the feed outlet temperature decreases and the permeate outlet temperature increases which explains the decrement in the permeate flux, as it is shown in Figure 40. By the other hand, longer modules allow to achieve higher recoveries. Permeate recovery (REC) were defined by Eq. 92 [192]:

$$REC = \frac{MD\ Permeate\ flow}{Feed\ flow} \tag{92}$$

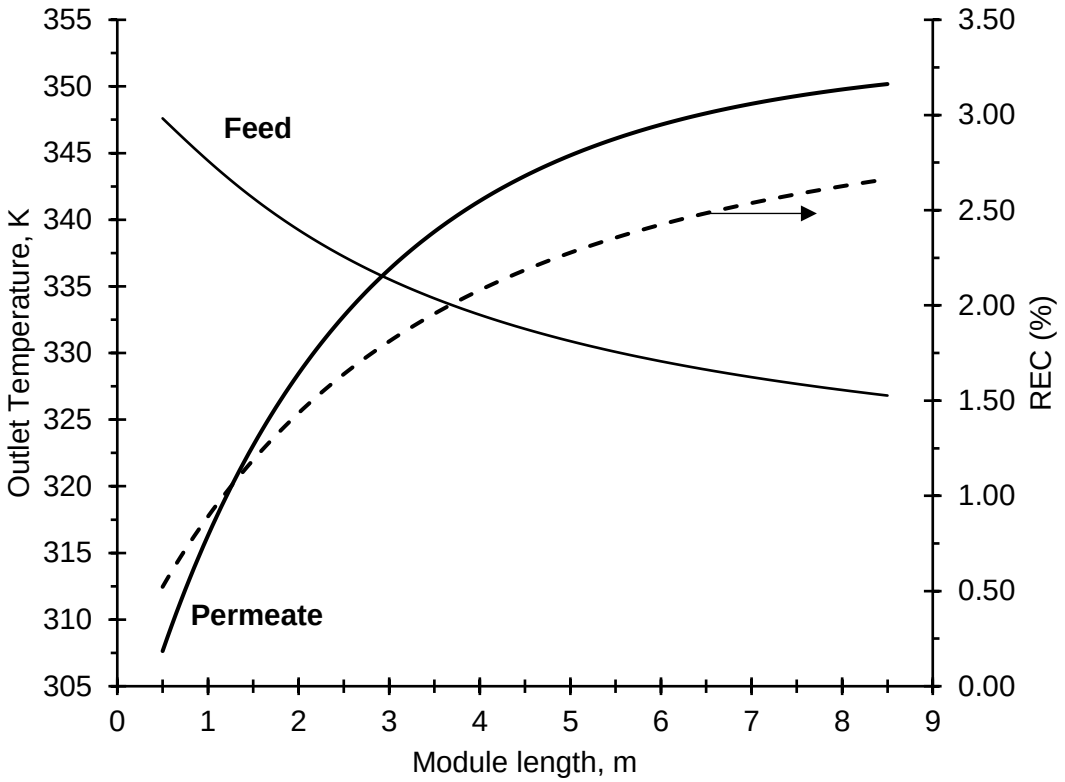

Figure 41. Effect of membrane length on the feed and permeate exit temperatures of industrial stillage and the permeate recovery achieved. $T_f = 353\ K, T_p = 293\ K, Q_f = 3.2\ m^3/h, Q_p = 2.0\ m^3/h$ (considering as a unique module).

Ali *et al*. (2016) evaluated the MD process consisting in modules connected in series and the module length was the main factor taken into account [153]. The authors also found low permeate flux and energy efficiency in long modules due to the temperature drop along the module. However, placing the modules in series allows to increase the recovery rate in a single pass as well as the energy contained in the concentrated stream to be reused.

As mentioned in Section 3.3 (Figure 10 and Figure 11), five cases were proposed and simulated. The performance of the system was compared as it can be seen in Table 21. For each case, the average permeate flux, the specific thermal energy consumption, the energy that has to be removed in the permeate side and the permeate recovery are shown in Table 21.

Specific thermal energy consumption in relation to the feed ($STEC_f$) and to the permeate ($STEC_p$) streams were defined in Section 3.3 and correspond to the energy

provided by the heater per the flow rates of the feed and the permeate, respectively. The energy that has to be removed from the permeate stream correspond to the energy taken in the coolers.

Despite the higher permeate recovery achieved in the first case (5.3 %), the energy demand is almost twice ($STEC_p$ =1,422 kWh/m^3) higher than in the Case 5 ($STEC_p$ =753.9 kWh/m^3), in which a REC of only 2.4 % was achieved. Comparing the two last cases, it is possible to see that the heat recovery from the permeate stream is determinant to decrease the energy consumption of the process [191,222–224]. For the first case, the feed stream maintains higher values along the modules due to the heaters, for this reason a higher energy has to be taken from the permeate stream (267 kW).

Table 21. Performance of 6 modules putted in series.

	Average permeate flux kg/m^2h	$STEC_f$ kWh/m^3	$STEC_p$ kWh/m^3	Energy to remove from the permeate stream kW	REC %
Case 1	14.65	75.2	1422	267	5.3
Case 2	11.84	58.4	1362	165	4.3
Case 3	9.99	47.5	1306	101	3.6
Case 4	6.68	28.4	1161	-	2.4
Case 5	6.68	18.5	753.9	-	2.4

Case 5 – HX: $A = 20\ m^2; U = 1000\ W/m \cdot K$

The water production obtained using more modules than six in series is not compensated by the effort of increasing the module length. This is important to evaluate due to the great impact of the membrane area in the investment cost of the process. It is estimated that 50% of total capital cost is related to the membrane cost [157]. On the other hand, the capital cost associated to use more heaters (Case 1) is also an important issue to take into account in order to choose between the first and the last cases [225]. On this matter, the use of six modules of 1.0 m of length in series without intercalating heaters (Case 5) could be adequate mainly because the low thermal energy requirement.

From this, for the following simulations, six modules were placed in series and in Figure 43, Figure 46 and Figure 49 the six modules are represented as a unique module. Figure 42 shows the permeate flux variation with the ºBrix concentration. The permeate flux decreases approximately linearly with the ºBrix concentration for the same temperature difference [201]. The reduction of the water vapor pressure due to the presence of dissolved salts is the main reason for the permeate flux behavior [120,226,227]. As it was mentioned, the increment in the hydrodynamic properties of stillage (both density and viscosity) causes a reduction in the permeate flux affecting mainly the thermal transfer. The permeate flux decreased 52% when the ºBrix concentration increased from 1 to 60. Although other membrane separation processes allow to reach higher fluxes, they do not achieve high concentration values [16,21,214]. Therefore, DCMD has a greater potential to treat solutions with high concentrations, proving to be more stable with time, which is the most significant advantages of this process [226].

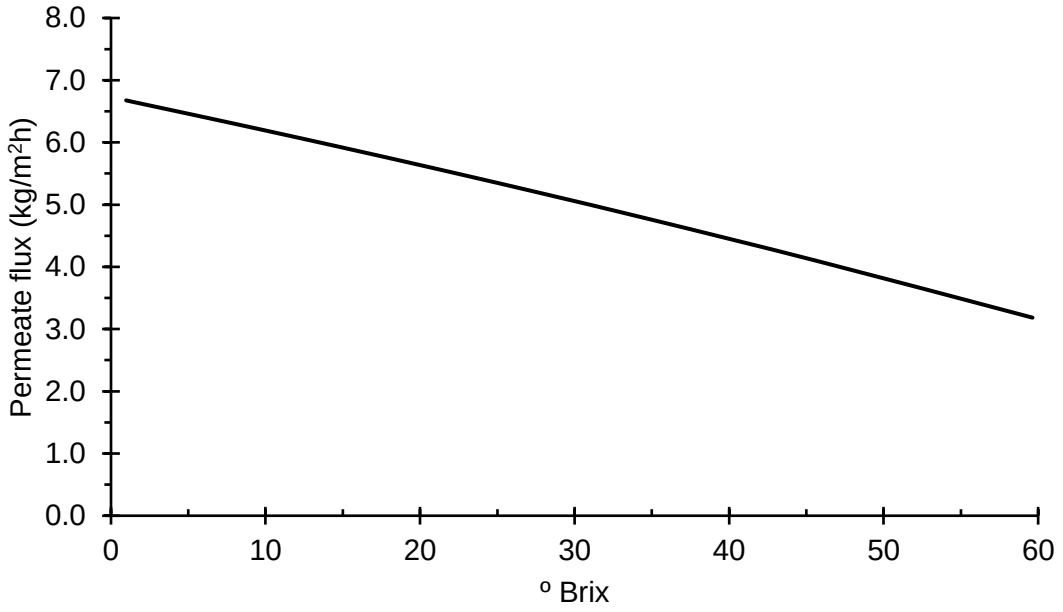

Figure 42. Effect of ºBrix concentration on the permeate flux of industrial stillage. $T_f = 353\ K, T_p = 293\ K, Q_f = 3.2\ m^3/h, Q_p = 2.0\ m^3/h$

As seen in Figure 41, the concentrate stream leaves the membrane module at temperatures that could be recovered by recycling this stream. First, it was considered a

system without a heater in which the industrial stillage (S01) entries the system at temperatures between 328 and 353 K, the permeate stream remains at 293 K and the concentrate stream is partially recycled (Figure 43).

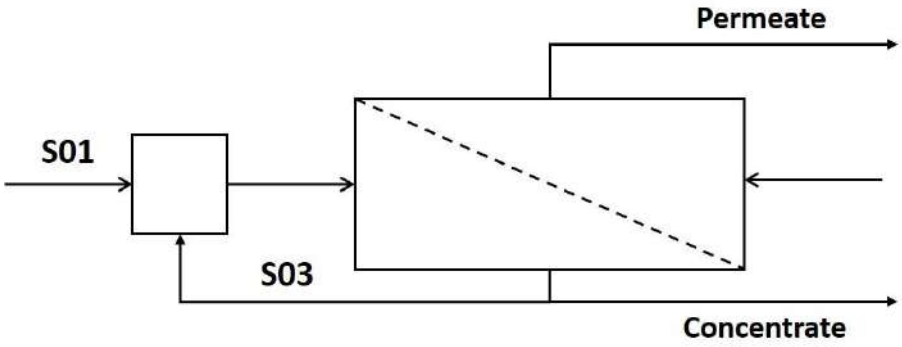

Figure 43. Direct contact membrane distillation system: concentrate recirculation without a heater for preheat the feed stream.

The recycle ratio (RR) is calculated by Eq. 93 [192].

$$RR = \frac{S03}{S01} \tag{93}$$

In Figure 44, the recovery (REC) as a function of the recycle ratio (RR) is shown for different fresh feed temperatures. For higher recycle ratio the recovery increases. Besides for higher feed inlet temperature, the permeate recovery is higher due to the greater permeate fluxes achieved. However, these values are relatively small. In this way, in order to have a better MD performance, it is necessary to put at least one heater to preheat the fresh stillage stream entering in the process and consequently, obtained higher recovery values.

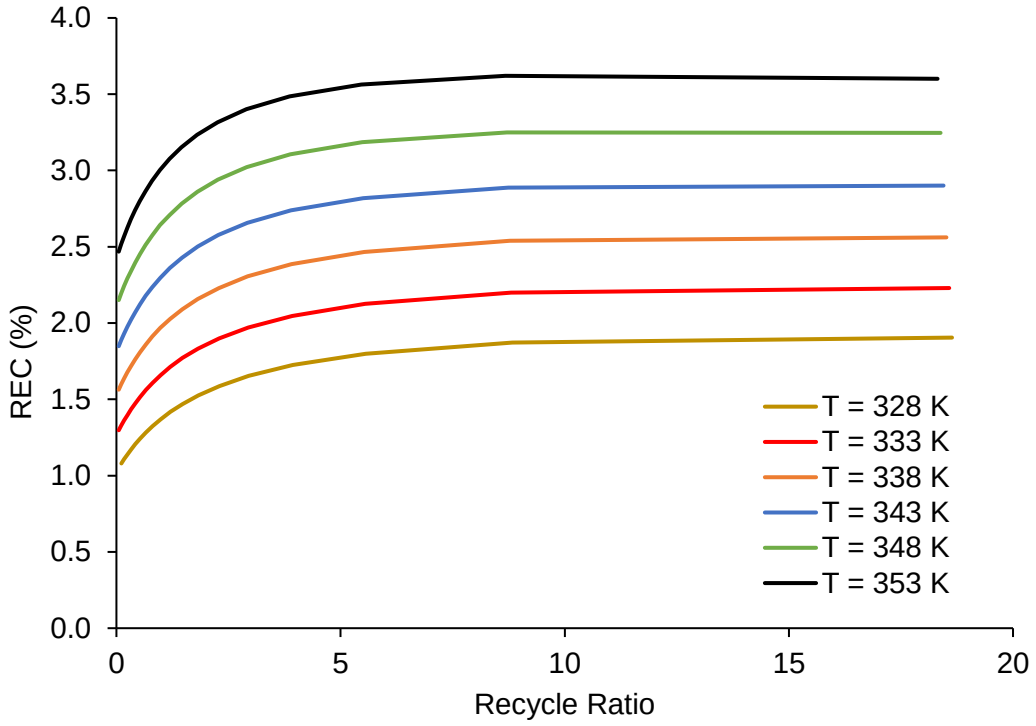

Figure 44. Effect of recycle ratio on in the permeate recovery for different inlet temperature of industrial stillage without heater. $T_p = 293\ K, Q_f = 3.2\ m^3/h, Q_p = 2.0\ m^3/h.$

Figure 45 shows the specific electrical energy consumption ($SEEC$) as a function of the recycle ratio in relation to the flow rates of the permeate ($SEEC_p$) and the feed ($SEEC_f$). The increment in the $SEEC$ with the recycle ratio is due to the increase in the flow rate of the S03 stream. For the $SEEC_p$, the same tendency is observed for the different feed temperatures. This behavior could be explained by the fact that for lower recycle ratio the flow rate of the industrial stillage is higher; thus, the MD feed stream is kept at a higher temperature and higher permeate fluxes are achieved in the DCMD process. This is more evident at higher fresh stillage inlet temperatures. The $SEEC_f$ independents of the fresh inlet temperature.

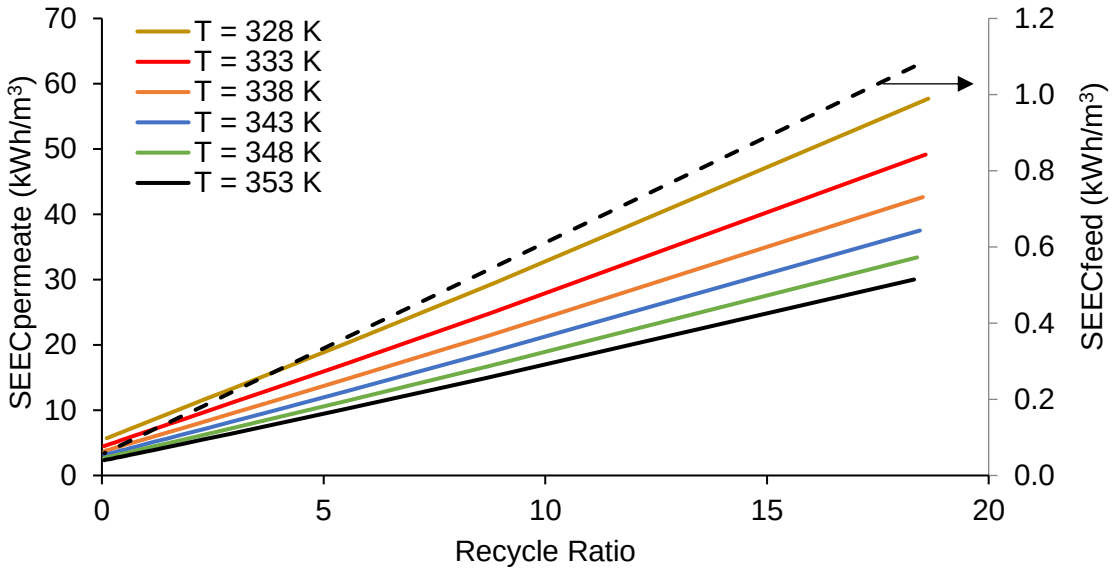

Figure 45. Effect of recycle ratio on the specific electrical energy consumption (SEEC) for different inlet temperature of industrial stillage without heater. $T_p = 293\ K, q_f = 3.2\ m^3/h, q_p = 2.0\ m^3/h$.

A better performance is reached in the DCMD process in terms of permeate recovery when a heater is included to heat the feed stream (Figure 46). In the simulations, the fresh stillage is heated to 353 K allowing to achieve higher permeate flux.

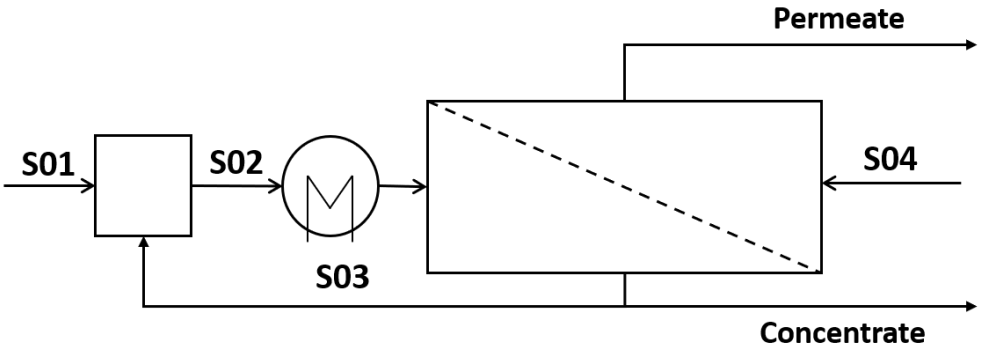

Figure 46. Direct contact membrane distillation system: concentrate recirculation with a heater for heating the feed stream.

As result, REC values up to 30% were achieved as it can be seen in Figure 47. Besides, the SEEC presented much less values. This is due to the higher permeate fluxes achieved in the process when a heater is used. However, this implies an energy consumption to keep on the process.

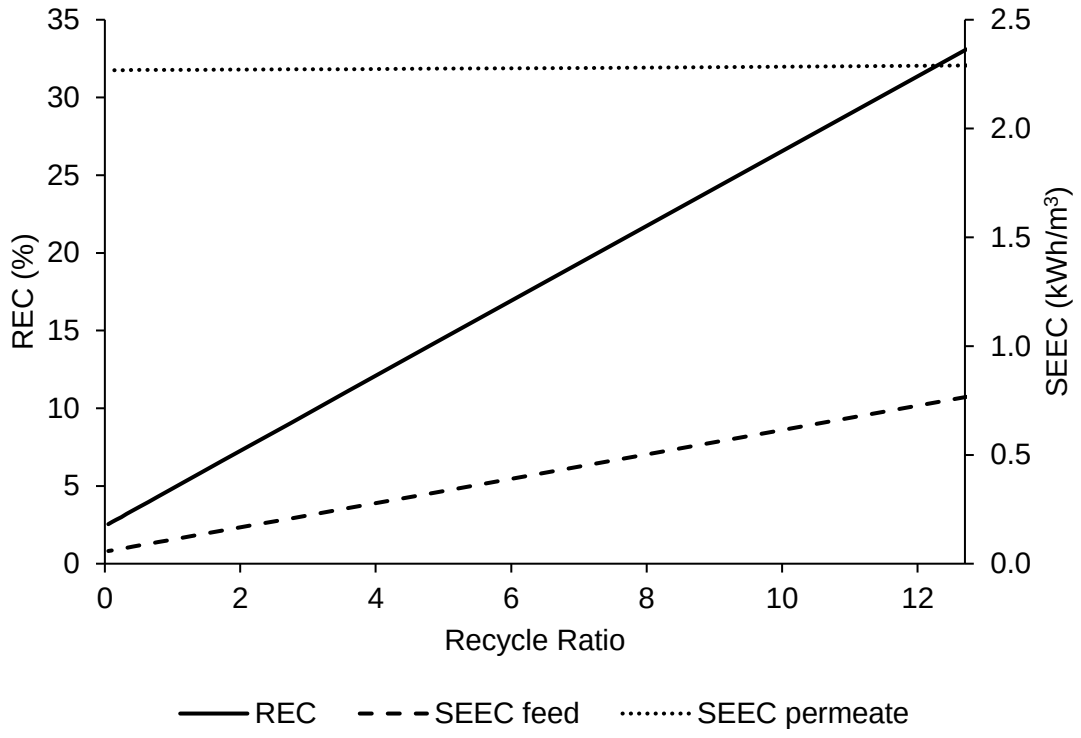

Figure 47. Effect of the recycle ratio on the permeate recovery and the specific electrical energy consumption (SEEC) for different fresh stillage temperatures. $T_p = 293\ K, Q_f = 3.3\ m^3/h, Q_p = 2.0\ m^3/h.$

The gain obtained in the permeate flow leads to high energy consumption as it can be seen in Figure 48. For higher fresh stillage temperature less is the energy consumption of the process. The increment in the recycle ratio increments the specific thermal consumption because it is necessary to heat a higher flow rate of recycle stream.

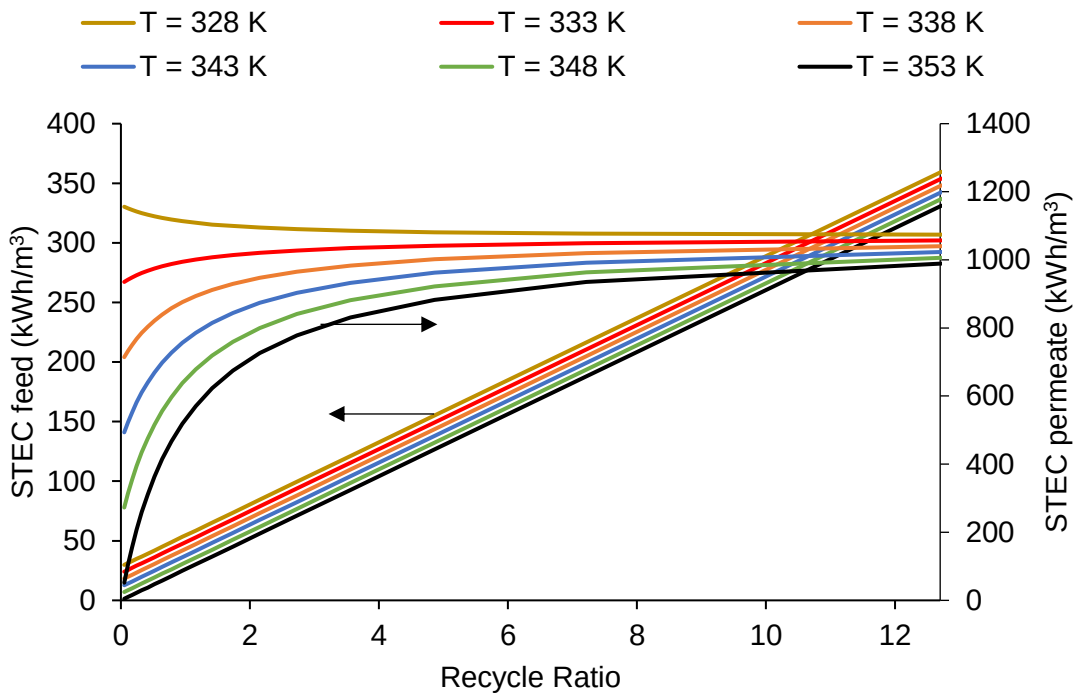

Figure 48. Effect of recycle ratio on the specific thermal energy consumption (STEC) related to the feed and permeate streams for different fresh stillage temperatures. $T_p = 293\,K, Q_f = 3.3\,m^3/h, Q_p = 2.0\,m^3/h$.

.

If a heat exchanger is placed before the mixer for recovery heat from the permeate stream as it shown in Figure 49, the specific thermal consumption decreases as it can be seen in Figure 50 [224].

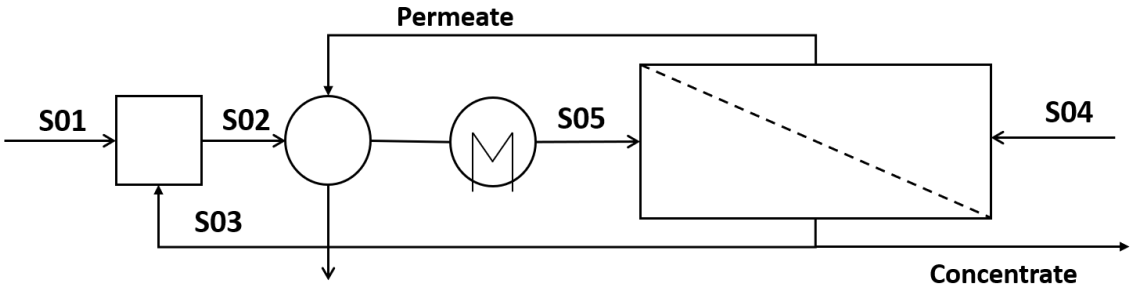

Figure 49. Direct contact membrane distillation system: concentrate recirculation with a heat exchanger for recovery the energy content in the permeate stream and a heater to heat the feed inlet stream of the DCMD process.

This configuration aims to recuperate the energy contained in the permeate stream, that leaves the DCMD system at temperatures around 348 K.

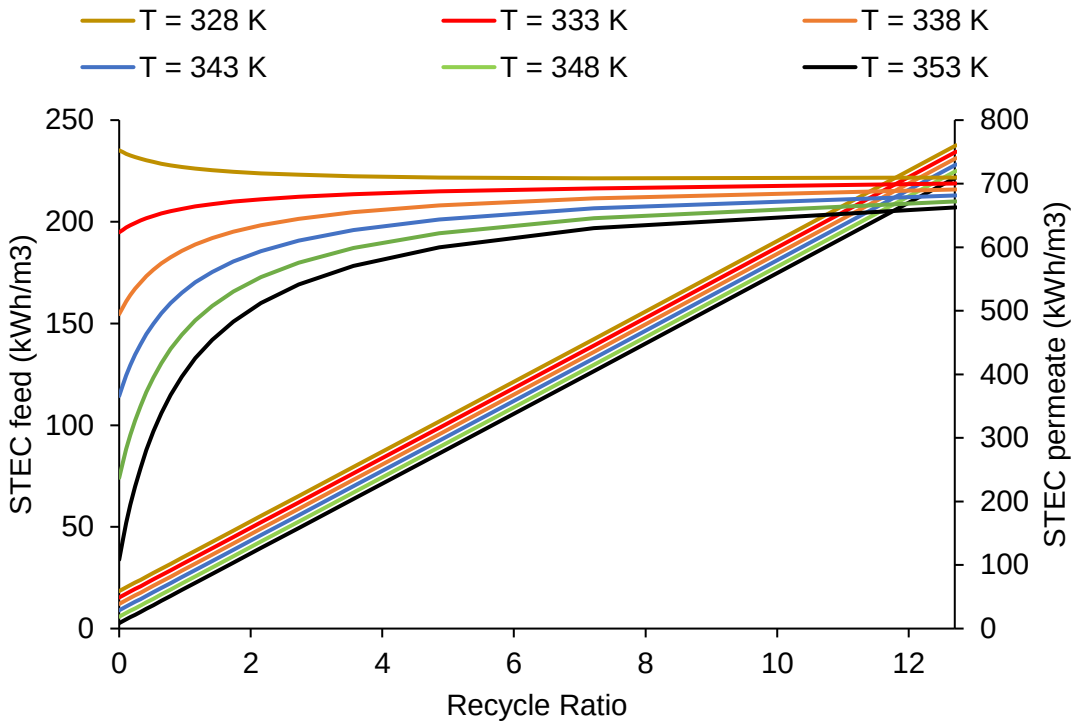

Figure 50. Effect of recycle ratio on the specific thermal energy consumption (STEC) related to the feed and permeate streams for different fresh stillage temperatures. $T_p = 293\ K, Q_f = 3.3\ m^3/h, Q_p = 2.0\ m^3/h$.

The energy consumption decreases almost 33% in all cases by means of the recovered energy from the permeate stream. Optimizations performed in the operational variables as well as in the module design would probably help to decrease the thermal energy consumption.

Thermal energy consumption in MD process is higher than in other processes like evaporation due mainly to the heat losses by conduction through the membrane material [18]. In membrane distillation, the thermal efficiency (η_{DCMD}) of the process is defined by Eq. 94. Ideally, a thermal efficiency of 100% could be achieved if all the energy provided to the MD process would have been used to evaporate the volatile components of the feed stream. However, due to the heat conduction through the membrane material and the energy carried by the concentrated stream, there are heat losses that are considered the main disadvantages of the process [222].

$$\eta_{DCMD} = \frac{\sum_{i=1}^{n}(\Delta H_i \cdot N_i)}{\sum_{i=1}^{n}(\Delta H_i \cdot N_i) + \frac{\kappa_m}{\delta_m}(T_{f,m} - T_{p,m})} \quad (94)$$

Because the MD process is commonly used for desalination, the performance criteria used in thermal desalination system are also applied for MD. The gain output ratio (GOR) is one of them and is defined as the ratio of the latent heat required for the evaporation of the produced permeate to the energy provided to the process from an external energy source (Eq. 95) [139,222,223]. In desalination processes as multi-effect distillation (MED) and multi-stage flash distillation (MSF), GOR takes values from 2 to 15 [139].

$$GOR = \frac{\sum_{i=1}^{n}(\Delta H_i \cdot N_i)}{q_{in}} \quad (95)$$

For a MD single pass operation, GOR values lesser than unity are found in the literature when it is necessary a great energy to heat the feed fresh stream, commonly from at room temperature [103]. GOR values higher than 25 were achieved using a MD series of cascades without interstage brine heating [223].

For the configuration presented in Figure 43, the thermal efficiency (η_{DCMD}) is lower and takes values between 0.43 and 0.78 depending on the permeate fluxes. In that case, no heat source is needed, so the $GOR \rightarrow \infty$, however due to the low permeate recuperation achieved a huge permeation area will be necessary to carry out the process at a large-scale [191,222]. When a heater (Figure 46) is used to increase the permeate recovery, the energy efficiency is around 0.79. For a same recycle ratio ($RR = 12.7$), GOR takes values of 0.60 and 0.64 for $T_f^{stillage} = 328\ K$ and $T_f^{stillage} = 353\ K$, respectively.

When a heat exchanger is added to the system for energy recovery, the GOR of DCMD is expressed as [103,222,223,228]:

$$GOR = \eta_{DCMD} H_R \quad (96)$$

where H_R is the maximum recoverable energy defined by Eq. 97:

$$H_R = \frac{\Delta T_{ax,MD}}{\Delta T_{MD} + \Delta T_{HX}} \quad (97)$$

where $\Delta T_{ax,MD}$ is the axial temperature difference (between inlet and outlet) of the feed stream. ΔT_{MD} is the terminal difference temperature (between feed inlet temperature and outlet permeate temperature) in the MD module. And ΔT_{HX} is the temperature difference in the heat exchanger, which is given by the inlet permeate temperature and the outlet feed temperature in the HX. In this case, for a same recycle ratio ($RR = 12.7$), GOR takes values of 1.18 and 1.26 for $T_f^{stillage} = 328\ K$ and $T_f^{stillage} = 353\ K$, respectively.

The specific energy consumption with respect to permeate is comparable with those obtained by Lokare *et al.* (2018) [192] for NaCl concentration and are in agreement with the values showed in Section 4.1.3 from the experimental data. Ullah *et al*. (2018) [103] highlighted that for an extensive and practical application of the DCMD the energy consumption has to be 1 kWh/m^3 or less, which is the minimum energy required to achieve a recovery ratio of 50% in a seawater desalination.

The use of solar energy (or other renewable energy) or low-grade waste heat were proposed as strategies to maximize the energy efficiency. Besides, improving the hydrodynamic conditions and the module design could help to reduce the polarization effects and, consequently, the energy efficiency. Also, the use of a heat exchanger as a recuperator is important to enhance the whole process efficiency [103]. As it was seen, recycling the concentrate stream is another way to reduce the thermal energy requirement. In this regard, values between 140 and 330 kWh/m^3 were reported for desalination processes using solar energy, brine recycling and internal heat recovery [229]. On the other hand, the use of multi-stage systems has been suggested as an appropriate approach to scale-up the membrane distillation process despite showing a slightly higher energy consumption [194,229].

As it has been seen, for large recycle ratios, high permeate recovery values are obtained at the expense of a higher energy consumption. Nonetheless, the concentrate recycle could be difficult to implement because just a low rate of fresh industrial stillage is treat at a time in the MD system [230].

Guillén-Burrieza *et al.* (2012) [231] compared two arrangements for AGMD, one of them consisted in six modules connected in parallel and the second one in two parallel system with three AGMD modules in series. The latter showed better performance than the first one, which is attributed to the fact that the increment in the number of modules in series is similar to the effect of increase the membrane area for a single module. Khalifa *et al.* (2017) also tested a multistage air gap membrane distillation arranged to operate in parallel or in series. The authors found a subtly higher permeate flow in the parallel arrangement compared with the one arranged in series [194]. Guan *et al*. (2018) [232] also found better performance for the parallel arrangement when comparing to the series one. Regarding to the energy consumption the authors only considered the pumping electricity cost considering that a low-grade waste heat was available. Still, the authors concluded that MD process has a great potential to show lower energy consumption as scale increases.

Finally, in order to treat greater flow rates of fresh industrial stillage solution, it is possible to consider a Christmas Tree arrangement (Figure 51), which will allow to reduce the membrane area needed and, consequently, the fixed costs.

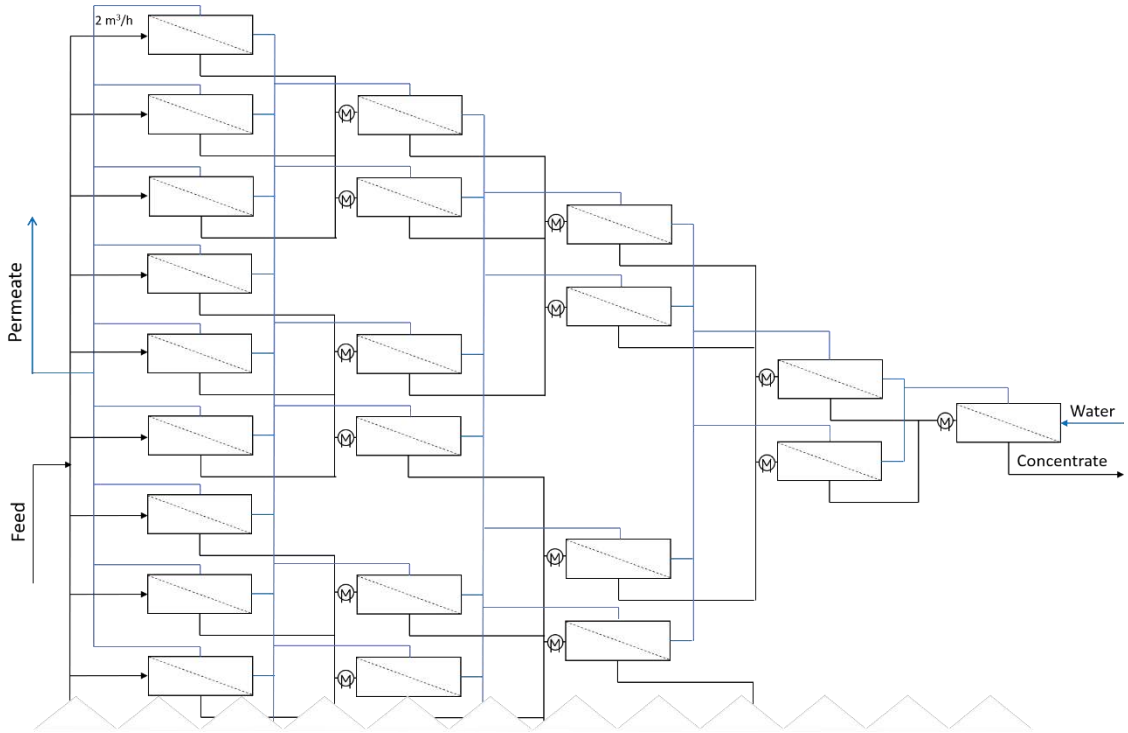

Figure 51. DCMD modules arrange as Christmas Tree.

4.2.4.Integrated process

Finally, to integrate the direct contact membrane distillation process to the ethanol production plant, different membrane module arrangements were studied. Modules connected in series (with and without recycling) and the Christmas Tree arrangement (as presented in Figure 51) were proposed. In all cases, every six modules a heat exchanger and a heater are placed to recover the energy of the permeate stream and to raise the temperature up to 353 K, respectively, in order to continue the concentration process.

Table 22 shows the average permeate flux, the water recovery, and the final $°Brix$ concentration achieved when 333 m^3/h of a fresh industrial stillage of 3.83 $°Brix$ are concentrated. Each membrane module has a membrane area of 1.978 m^2.

This allowed to maintain a high permeate flux. This arrangement allowed to achieve a final concentration of 65 °Brix.

Table 22. Different modules arrangement to treat 333.3 m^3/h of industrial stillage.

Configuration	Membrane area (m^2)	Water recovery (%)	$STEC_f$ (kWh/m^3)	$STEC_p$ (kWh/m^3)	Average permeate flux ($kg/m^2 \cdot h$)	Final concentration ($° Brix$)
1	49,851	78	550	705	5.1	17
2	49,138	94	762	807	6.2	21
3	49,138	94	772	814	6.3	22
4	49,138	94	802	846	6.3	23
5	48,712	93	734	762	6.5	65

Fukushima *et al*. (2019) performed the stillage concentration by evaporation and evaluated the stillage concentrated incineration. This allows to produce more vapor that it is used to achieve a final concentration of stillage of 65 $°Brix$. The authors estimated that in a conventional process without stillage concentration by evaporation it is possible to obtain 48.3 kg of steam at 65 bar/480 $°C$ per ton of processed cane (TC). By the other hand, to concentrate the stillage are necessary 91 kg of steam per TC. The stillage incineration generates 65.2 kg/TC of steam at 65 bar/480 $°C$. Thus, it is possible to perform the stillage concentration using the surplus steam available and the steam

obtained by concentrated stillage incineration. Besides, 78 kWh of electricity surplus per TC could be obtained (using extraction-condensing steam turbines) [18].

Considering the last case, if the concentration were performed by membrane distillation, the energy necessary to achieve a final concentration of 65 $°Brix$ would be 244,680 kW. Using steam as the energy source of the system, it would be necessary 574 kg of saturated steam at 1.4 bar for a plant that processes 687.64 TC/h and produces 30 m^3/h of ethanol[2]. However, as it was showed the vapor available is only 113.5 kg/TC. Thus, another source of energy would be needed. Still, the electricity surplus could be used to provide the energy required.

By the other hand, the membrane distillation process could be carried out using residual heat from low heat source that in the sugar and ethanol production processes are no longer possible to seize. In this way, an appropriate process integration could also allow to make an efficient use of the energy available. Besides, operating in optimized MD conditions would allow to increase the thermal efficiency of the process.

Clearly, the DCMD is not the most thermal efficient configuration due to the high heat loss by conduction, but because of its ease of operation it is the most widely used [222]. For DCMD, it has been reported that the membrane conductivity and thickness affect the thermal efficiency process since the smaller the thickness, higher is the mass flux. On the other hand, this causes an increment in the conductive heat loss which implies higher energy consumption [103,139,196,222]. On this matter, it is important to optimize the membrane properties to achieve higher thermal efficiencies and consequently, a decrement in the cost of the process. Finally, the performance of the other configurations or a combination of them for the stillage concentration could be also evaluated for this purpose.

4.2.5.Economic analysis

The economic study proposed in this work, considering a plant with 333 m^3/h of stillage to be disposed is described in the Section 3.4. The simulation data for the Christmas Tree arrangement (Configurations 5 of Table 22) were considered to perform

[2] F. Oliveira, personal communication, July 2018.

the preliminary economic analysis. Table 23 shows the values considered for the calculation. Bold values indicate the annual fixed charges, the O&M charges, and the total cost of stillage treatment, which is the sum of fixed and O&M charges, all expressed in $U\$D/m^3$ of water.

Table 23. Preliminary economical study for a stillage treatment plant by DCMD process

Data	Configuration 5		Reference
Plant capacity	333	$m^3\ stillage/h$	
Water recovered	309.7	$m^3\ water/h$	
Operating hours	4,000	h/y	[18]
Recovery	93.0	%	This work
DCMD Flux	6.50	kg/m^2h	This work
Membrane area required	48,712	m^2	
Capital Cost			
Cost of membrane	4,384,080	$U\$D$	[157]
Total Capital Cost	8,768,160	$U\$D$	[157]
Annual fixed charges	**0.57**	$U\$D/m^3\ water$	
O&M cost			
Membrane replacement	526,090	$U\$D/y$	[196]
Spares	40,879	$U\$D/y$	[157]
Labor	37,163	$U\$D/y$	[157]
Maintenance Cost	43,841	$U\$D/y$	[196]
Total O&M Cost	647,972	$U\$D$	
Annual O&M charges	**0.52**	$U\$D/m^3\ water$	
Total stillage treatment	**1.09**	$U\$D/m^3\ water$	

This gives a stillage treatment cost around of 1.10 $\$/m^3$ of water recovered without considering any optimization in the DCMD process and using the average permeate flux value in the stillage simulation results.

Considering a plant[3] that processes 687 ton of cane per hour with a specific water consumption of 1 m^3 per ton of cane [50], it is possible to decrease the water consumes almost in a 45% by reuse the permeate of the membrane distillation process. This implies

[3] F. Oliveira, personal communication, July 2018.

an economy of $ 2,372,550 for a water cost[4] of 1.91 $\$/m^3$ [233]. Besides, due to the volume reduction by the stillage concentration the transportation cost diminishes. These are determining factors that will have an important positive weight in the moment of choose this technology for the stillage treatment.

As it was already mentioned, the permeate fluxes obtained in the simulation approach are lower than those achieved experimentally. If the highest value achieved in this work is applied (13.3 $kg/m^2 \cdot h$, Table 14), it would be possible to reduce the water recovery cost to 0.55 $\$/m^3$. Besides, if the membrane cost reduces 50%, the treatment cost will be 0.31 $\$/m^3$.

Guerreiro *et al.* (2016) evaluated the stillage treatment costs by a Fenton's oxidation, a coagulation/flocculation or a combination of both. The first one has a very high cost (21.2 $€/m^3$) and the second one under optimized conditions could be cost 1.4 $€/m^3$. The cost of a combination of the coagulation/flocculation process followed by Fenton`s oxidation could be performed at 11.9 $€/m^3$. This last allows to obtain a high organic matter removal with a lesser chemical consumption [234].

Recently, S.C. d. Silva *et al.* (2020) performed a comparative analysis between an UF/NF process and a Coagulation followed by NF/UF (C/UF/NF) process for the stillage treatment. The authors found that for a stillage flow rate of 435 m^3/h the total costs are 1.96 $ and 2.92 $ per m^3 of water recovered for the UF/NF and the C/UF/NF treatments, respectively [235].

Finally, it could be said that the MD process is an innovative technology for the stillage treatment. Besides, it has been shown that this process is technically and economically suitable to be integrated to the ethanol production plant for this application.

[4] 1 R$ = $ 0.18 [236]

Chapter 5

Final considerations

5.1. Conclusions

In this work, a direct contact membrane distillation (DCMD) has been investigated to treat the sugarcane stillage and integrate it in an ethanol production plant. The main DCMD operational variables influencing the permeate flux are the feed temperature, concentration, and flow rates. Feed temperature and flow rates have a positive influence while the feed concentration a negative influence.

Regarding the removal efficiency of the DCMD process, as it was expected, non-volatile components were completely rejected while the volatile components were partially separated. However, COD removal was high and comparable to other stillage treatments. Despite the permeate stream presents low ionic conductivity, it also presents volatile components as acetic acid that must be separated or recovered to recycle it to the ethanol production process. During the stillage treatment no fouling or wettability phenomena were observed, which allows to perform the process until achieving high stillage concentration.

The physical properties of the stillage were determined as a function of its concentration. These values were used in the mathematical model developed to simulate the treatment process by membrane distillation. The Stefan-Maxwell approach was used for modeling the mass transfer process and the energy equation for the heat transfer process. In general, the mathematical model was able to describe the influence in the permeate flux of the main DCMD operational variables. However, it showed limitations to describe the concentration in the permeate and the concentrate streams due to the thermodynamical model considered.

The data obtained in this work suggest that DCMD process could be exploited in order to concentrate the sugarcane stillage and then, the concentrated stream (>60 °Brix) could be used as biofuel in the steam boiler to produce more energy. In this way, it can

be considered that the concentrated stillage incineration could be used to sustain the thermal requirements of the DCMD process, allowing to reach high concentrations due to the surplus steam obtained.

Finally, a preliminary economical study revealed that the stillage treatment cost by DCMD is around of 1.10 $\$/m^3$ of permeate without performing any DCMD process optimization. It is expected that higher permeate fluxes would allow reduce the unit cost of the process. Besides, the economy due to the water recovered as well as the concentrated stillage are determining factors for choosing this technology for the stillage treatment. In conclusion, results so far have been very promising to integrate the DCMD process to the ethanol production plant for the stillage management.

5.2. Suggestions for future research

Future studies should target to characterize extensively the sugarcane stillage sample as well as the DCMD process stream to have more data for the mathematical model. Besides, the design of a membrane distillation like vacuum membrane distillation for the recovery of the volatile components from the permeate stream is also an important topic for future research.

Other important issue to resolve for future studies is a more extensive study of the thermodynamical equilibrium in the interface liquid/vapor at the membrane surface in order to have a better description of the stream concentrations of the process.

It is suggested to carry out a pinch analysis in order to determine completely the energetic feasibility of the DCMD process integration to the ethanol plant.

Bibliography

[1] Moraes BS, Zaiat M, Bonomi A. Anaerobic digestion of vinasse from sugarcane ethanol production in Brazil: Challenges and perspectives. Renew Sustain Energy Rev 2015;44:888–903. doi:10.1016/j.rser.2015.01.023.

[2] UNICA (União da Indústria de Cana-de-açúcar). Produção: Histórico de produção e moagem: por safra 2018/19 2019. http://unicadata.com.br/historico-de-producao-e-moagem.php?idMn=31&tipoHistorico=2&acao=visualizar&idTabela=2333&produto=etanol_total&safraIni=2016%2F2017&safraFim=2018%2F2019&estado=RS%2CSC%2CPR%2CSP%2CRJ%2CMG%2CES%2CMS%2CMT%2CGO%2CDF%2CBA%2CSE%2CAL%2CPE (accessed July 2, 2019).

[3] MAPA. Sugarcane Industry , Sugar and Ethanol Production in Brazil. 2019.

[4] RFA (Renewable Fuels Association). Annual Ethanol Production – Renewable Fuels Association 2019. https://ethanolrfa.org/statistics/annual-ethanol-production/ (accessed July 2, 2019).

[5] Goldemberg J, Coelho ST, Guardabassi P. The sustainability of ethanol production from sugarcane. Energy Policy 2008;36:2086–97. doi:10.1016/j.enpol.2008.02.028.

[6] Nogueira CE, de Souza SN, Mircuanski VC, Azevedo RL. Exploring possibilities of energy insertion from vinasse biogas in the energy matrix of Paraná State , Brazil. Renew Sustain Energy Rev 2015;48:300–5. doi:10.1016/j.rser.2015.04.023.

[7] de Godoi LAG, Camiloti PR, Bernardes AN, Sanchez BLS, Torres APR, da Conceição Gomes A, et al. Seasonal variation of the organic and inorganic composition of sugarcane vinasse: main implications for its environmental uses. Environ Sci Pollut Res 2019. doi:10.1007/s11356-019-06019-8.

[8] Satyawali Y, Balakrishnan M. Wastewater treatment in molasses-based alcohol distilleries for COD and color removal : A review. J Environ Manage 2008;86:481–97. doi:10.1016/j.jenvman.2006.12.024.

[9] Gebreeyessus GD, Mekonen A, Alemayehu E. A review on progresses and performances in distillery stillage management. J Clean Prod 2019;232:295–307. doi:10.1016/j.jclepro.2019.05.383.

[10] Barrera EL, Rosa E, Spanjers H, Romero O, Meester S De, Dewulf J. A comparative assessment of anaerobic digestion power plants as alternative to lagoons for vinasse treatment : life cycle assessment and exergy analysis. J Clean Prod 2016;113:459–71. doi:10.1016/j.jclepro.2015.11.095.

[11] Hoarau J, Caro Y, Grondin I, Petit T. Sugarcane vinasse processing: Toward a status shift from waste to valuable resource. A review. J Water Process Eng 2018;24:11–25. doi:10.1016/j.jwpe.2018.05.003.

[12] Parnaudeau V, Condom N, Oliver R, Cazevieille P, Recous S. Vinasse organic matter quality and mineralization potential, as influenced by raw material, fermentation and concentration processes. Bioresour Technol 2008;99:1553–62. doi:10.1016/j.biortech.2007.04.012.

[13] Moraes BS, Junqueira TL, Pavanello LG, Cavalett O, Mantelatto PE, Bonomi A, et al. Anaerobic digestion of vinasse from sugarcane biorefineries in Brazil from energy , environmental , and economic perspectives : Profit or expense ? Appl Energy 2014;113:825–35. doi:10.1016/j.apenergy.2013.07.018.

[14] Christofoletti CA, Escher JP, Correia JE, Marinho JFU, Fontanetti CS. Sugarcane vinasse: Environmental implications of its use. Waste Manag 2013;33:2752–61. doi:10.1016/j.wasman.2013.09.005.

[15] Mohana S, Acharya BK, Madamwar D. Distillery spent wash: Treatment technologies and potential applications. J Hazard Mater 2009;163:12–25. doi:10.1016/j.jhazmat.2008.06.079.

[16] Elia Neto A. Estado da Arte da Vinhaça. Unica 2016:1–31. doi:10.1590/S0101-73302005000400018.

[17] Peiter FS, Hankins NP, Pires EC. Evaluation of concentration technologies in the design of biorefineries for the recovery of resources from vinasse. Water Res 2019;157:483–97. doi:10.1016/j.watres.2019.04.003.

[18] Fukushima NA, Palacios-Bereche MC, Palacios-Bereche R, Nebra SA. Energy analysis of the ethanol industry considering vinasse concentration and incineration. Renew Energy 2019;142:96–109. doi:10.1016/j.renene.2019.04.085.

[19] Rodrigues Reis CE, Hu B. Vinasse from Sugarcane Ethanol Production: Better Treatment or Better Utilization? Front Energy Res 2017;5:1–7. doi:10.3389/fenrg.2017.00007.

[20] Naspolini BF, De Oliveira Machado AC, Cravo WB, Freire DMG, Cammarota MC. Bioconversion of sugarcane vinasse into high-Added value products and energy. Biomed Res Int 2017;2017. doi:10.1155/2017/8986165.

[21] Nataraj SK, Hosamani KM, Aminabhavi TM. Distillery wastewater treatment by the membrane-based nanofiltration and reverse osmosis processes. Water Res 2006;40:2349–56. doi:10.1016/j.watres.2006.04.022.

[22] Wu Y V. Recovery of stillage soluble solids from hard and soft wheat by reverse osmosis and ultrafiltration. Cereal Chem 1987;64:260–4.

[23] Ryan D, Gadd A, Kavanagh J, Barton GW. Integrated biorefinery wastewater design. Chem Eng Res Des 2009;87:1261–8. doi:10.1016/j.cherd.2009.04.016.

[24] Vasić VM, Prodanović JM, Kukić D V., Šćiban MB, Antov MG, Ivetić DŽ. Application of membrane and natural coagulants for stillage purification. Desalin Water Treat 2013;51:437–41. doi:10.1080/19443994.2012.714525.

[25] Sousa SP, Lovato G, Albanez R, Ratusznei SM, Rodrigues JAD. Improvement of Sugarcane Stillage (Vinasse) Anaerobic Digestion with Cheese Whey as its Co-substrate: Achieving High Methane Productivity and Yield. Appl Biochem Biotechnol 2019. doi:10.1007/s12010-019-03056-4.

[26] Lovato G, Batista LPP, Preite MB, Yamashiro JN, Becker ALS, Vidal MFG, et al. Viability of Using Glycerin as a Co-substrate in Anaerobic Digestion of Sugarcane Stillage (Vinasse): Effect of Diversified Operational Strategies. Appl Biochem Biotechnol 2019;188:720–40. doi:10.1007/s12010-019-02950-1.

[27] Parsaee M, Kiani Deh Kiani M, Karimi K. A review of biogas production from sugarcane vinasse. Biomass and Bioenergy 2019;122:117–25. doi:10.1016/j.biombioe.2019.01.034.

[28] Alkhudhiri A, Darwish N, Hilal N. Membrane distillation: A comprehensive review. Desalination 2012;287:2–18. doi:10.1016/j.desal.2011.08.027.

[29] Kiss AA, Kattan Readi OM. An industrial perspective on membrane distillation processes. J Chem Technol Biotechnol 2018;93:2047–55. doi:10.1002/jctb.5674.

[30] Ashoor BB, Mansour S, Giwa A, Dufour V, Hasan SW. Principles and applications of direct contact membrane distillation (DCMD): A comprehensive review. Desalination 2016;398:222–46. doi:10.1016/j.desal.2016.07.043.

[31] Susanto H. Towards practical implementations of membrane distillation. Chem Eng Process Process Intensif 2011;50:139–50. doi:10.1016/j.cep.2010.12.008.

[32] Ding Z, Ma R, Fane AG. A new model for mass transfer in direct contact membrane distillation. Desalination 2002;151:217–27. doi:10.1016/S0011-9164(02)01014-7.

[33] Lawson KW, Lloyd DR. Membrane distillation. J Memb Sci 1997;124:1–25. doi:10.1016/S0376-7388(96)00236-0.

[34] Macedonio F, Drioli E. Membrane distillation development. Elsevier Inc.; 2019. doi:10.1016/b978-0-12-816170-8.00005-3.

[35] Elzahaby AM, Kabeel AE, Bassuoni MM, Elbar ARA. Direct contact membrane water distillation assisted with solar energy. Energy Convers Manag 2016;110:397–406. doi:10.1016/j.enconman.2015.12.046.

[36] Schwarzer K, Vieira da Silva E, Hoffschmidt B, Schwarzer T. A new solar desalination system with heat recovery for decentralised drinking water production. Desalination 2009;248:204–11. doi:10.1016/j.desal.2008.05.056.

[37] Zaragoza G, Ruiz-Aguirre A, Guillén-Burrieza E. Efficiency in the use of solar thermal energy of small membrane desalination systems for decentralized water production. Appl Energy 2014;130:491–9. doi:10.1016/j.apenergy.2014.02.024.

[38] CONAB. Acompanhamento da safra Brasileira. Cana de açúcar Safra 2018/19. Cia Nac Abast 2019;5:1–75.

[39] UNICA. Vinhaça: biofertilizante e energia sustentável - UNICA 2019. https://unica.com.br/nota/vinhaca-biofertilizante-e-energia-sustentavel/ (accessed March 17, 2020).

[40] de Oliveira S. Exergy Analysis and Parametric Improvement of the Combined Production of Sugar, Ethanol, and Electricity. Exergy, London: Springer London; 2013, p. 185–214. doi:10.1007/978-1-4471-4165-5_6.

[41] UNICA. Histórico de produção e moagem de cana de açúcar, etanol e açúcar. 2020.

[42] RFA. Renewable Fuels Association » Industry Statistics 2017. http://www.ethanolrfa.org/resources/industry/statistics/#1460745352774-cd978516-814c (accessed April 18, 2017).

[43] Cardona CA, Sánchez ÓJ. Fuel ethanol production: Process design trends and integration opportunities. Bioresour Technol 2007;98:2415–57. doi:10.1016/j.biortech.2007.01.002.

[44] CONAB CN de A-. Acompanhamento da Safra Brasileira - Cana de açúcar - V.7 - SAFRA 2020/21 - N.2 - Segundo levantamento - Agosto 2020. Acompan Da Safra Bras Grãos 2020;7:64.

[45] de Oliveira S. Exergy and Renewability Analysis of Liquid Biofuels Production Routes. Exergy, London: Springer London; 2013, p. 215–36. doi:10.1007/978-1-4471-4165-5_7.

[46] Lassmann T, Kravanja P, Friedl A. Simulation of the downstream processing in the ethanol production from lignocellulosic biomass with ASPEN Plus® and IPSEpro. Energy Sustain Soc 2014;4:7. doi:10.1186/s13705-014-0027-3.

[47] Gunkel G, Kosmol J, Sobral M, Rohn H, Montenegro S, Aureliano J. Sugar Cane Industry as a Source of Water Pollution – Case Study on the Situation in Ipojuca River, Pernambuco, Brazil. Water Air Soil Pollut 2007;180:261–9. doi:10.1007/s11270-006-9268-x.

[48] Fernandes A, Boczkaj G, Głazowska J, Tomczak-Wandzel R, Kamiński M. Comparison of Ozonation and Evaporation as Treatment Methods of Recycled Water for Bioethanol Fermentation Process. Waste and Biomass Valorization 2017:1–9. doi:10.1007/s12649-017-9888-y.

[49] Pant D, Adholeya A. Biological approaches for treatment of distillery wastewater : A review. Bioresour Technol 2007;98:2321–34. doi:10.1016/j.biortech.2006.09.027.

[50] Neto AE. Manual de Conservação e Reúso de água na Agroindústria Sucroenergética. Brasília: ANA; 2009. doi:978-85-89629-61-4.

[51] Wilkie AC, Riedesel KJ, Owens JM. Stillage characterization and anaerobic treatment of ethanol stillage from conventional and cellulosic feedstocks p. Biomass and Bioenergy 2000;19:63–102.

[52] Fuess LT, Garcia ML, Zaiat M. Seasonal characterization of sugarcane vinasse: Assessing environmental impacts from fertirrigation and the bioenergy recovery potential through biodigestion. Sci Total Environ 2018;634:29–40. doi:10.1016/j.scitotenv.2018.03.326.

[53] Bake JDVDW, Junginger M, Faaij A, Poot T, Walter A. Explaining the experience curve : Cost reductions of Brazilian ethanol from sugarcane. Biomass and Bioenergy

2009;33:644–58. doi:10.1016/j.biombioe.2008.10.006.

[54] Zi L, Liu C, Xin C, Bai F. Stillage backset and its impact on ethanol fermentation by the flocculating yeast. Process Biochem 2013;48:753–8. doi:10.1016/j.procbio.2013.03.014.

[55] Navarro AR, Sepúlveda MC, Rubio MC. Bio-concentration of vinasse from the alcoholic fermentation of sugar cane molasses. Waste Manag 2000;20:581–5.

[56] Prodanović JM, Vasić VM. Application of membrane processes for distillery wastewater purification—a review. Desalin Water Treat 2013;51:3325–34. doi:10.1080/19443994.2012.749178.

[57] Mota VT, Santos FS, Amaral MCS. Two-stage anaerobic membrane bioreactor for the treatment of sugarcane vinasse: Assessment on biological activity and filtration performance. Bioresour Technol 2013;146:494–503. doi:10.1016/j.biortech.2013.07.110.

[58] Chang IS, Choo KH, Lee CH, Pek UH, Koh UC, Kim SW, et al. Application of ceramic membrane as a pretreatment in anaerobic digestion of alcohol-distillery wastes. J Memb Sci 1994;90:131–9. doi:10.1016/0376-7388(94)80040-5.

[59] Rais M, Sheoran A. Treatment of Sugarcane Industry Effluents: Science & Technology issues. Int J Eng Res Appl 2015;5:11–9.

[60] Pazuch FA, Eduardo C, Nogueira C, Nelson S, Souza M, Micuanski VC, et al. Economic evaluation of the replacement of sugar cane bagasse by vinasse , as a source of energy in a power plant in the state of Paraná , Brazil. Renew Sustain Energy Rev 2017;76:34–42. doi:10.1016/j.rser.2017.03.047.

[61] Souza RP De, Girardi F, Santana VS, Fernandes-Machado NR, Gimenes M. Vinasse treatment using a vegetable-tannin coagulant and photocatalysis. Acta Sci Technol 2013;35:89–95. doi:10.4025/actascitechnol.v35i1.11011.

[62] Santana VS, Fernandes Machado NRC. Photocatalytic degradation of the vinasse under solar radiation. Catal Today 2008;133–135:606–10. doi:10.1016/j.cattod.2007.12.131.

[63] Martín MA, Raposo F, Borja R, Martín A. Kinetic study of the anaerobic digestion of vinasse pretreated with ozone, ozone plus ultraviolet light, and ozone plus ultraviolet light in the presence of titanium dioxide. Process Biochem 2002;37:699–706.

[64] Sangave PC, Gogate PR, Pandit AB. Combination of ozonation with conventional aerobic oxidation for distillery wastewater treatment. Chemosphere 2007;68:32–41.

doi:10.1016/j.chemosphere.2006.12.053.

[65] GEA Wiegand GmbH. Evaporators for Stillage Concentration Evaporation for Stillage Concentration 2007:1–8. www.gea-wiegand.com.

[66] Nandy T, Shastry S, Kaul SN. Wastewater management in a cane molasses distillery involving bioresource recovery. vol. 65. 2002. doi:10.1006/jema.2001.0505.

[67] CITROTEC. Soluções Tecnológicas para Sucroenergia 2016:1–28. www.citrotec.com.br.

[68] Cortes-Rodríguez EF, Fukushima NA, Palacios-Bereche R, Ensinas A V., Nebra SA. Vinasse concentration and juice evaporation system integrated to the conventional ethanol production process from sugarcane – Heat integration and impacts in cogeneration system. Renew Energy 2018;115:474–88. doi:10.1016/j.renene.2017.08.036.

[69] Decloux M, Bories A. Sugar Cane Stillage : A Potential Source of Natural Antioxidants. Int Sugar J 2002;104:509–17. doi:10.1021/jf4039474.

[70] Drosg B, Wirthensohn T, Konrad G, Hornbachner D, Resch C, Wäger F, et al. Comparing centralised and decentralised anaerobic digestion of stillage from a large-scale bioethanol plant to animal feed production. Water Sci Technol 2008;58:1483–90. doi:10.2166/wst.2008.515.

[71] Rochem. Low energy spent wash concentration for grain based distillery n.d.:1–23. https://www.aidaindia.org/pdf/hyderabad-seminar/16.pdf.

[72] CETESB. Vinhaça – Critérios e procedimentos para aplicação no solo agrícola 2015:1–15.

[73] Ortegón GP, Arboleda FM, Candela L, Tamoh K, Valdes-Abellan J. Vinasse application to sugar cane fields. Effect on the unsaturated zone and groundwater at Valle del Cauca (Colombia). Sci Total Environ 2016;539:410–9. doi:10.1016/j.scitotenv.2015.08.153.

[74] Chang H, Lyu S-G, Tsai C-M, Chen Y-H, Cheng T-W, Chou Y-H. Experimental and simulation study of a solar thermal driven membrane distillation desalination process. Desalination 2012;286:400–11. doi:10.1016/j.desal.2011.11.057.

[75] Sarbatly R, Chiam CK. Evaluation of geothermal energy in desalination by vacuum membrane distillation. Appl Energy 2013;112:737–46. doi:10.1016/j.apenergy.2012.12.028.

[76] Schwantes R, Cipollina A, Gross F, Koschikowski J, Pfeifle D, Rolletschek M, et al. Membrane distillation: Solar and waste heat driven demonstration plants for desalination. Desalination 2013;323:93–106. doi:10.1016/j.desal.2013.04.011.

[77] Chiam C-K, Sarbatly R. Vacuum membrane distillation processes for aqueous solution treatment-A review. Chem Eng Process Process Intensif 2014;74:27–54. doi:10.1016/j.cep.2013.10.002.

[78] Wirth D, Cabassud C. Water desalination using membrane distillation : comparison between inside / out and outside / in permeation. Desalination 2002;147:139–45.

[79] Chen G, Lu Y, Krantz WB, Wang R, Fane AG. Optimization of operating conditions for a continuous membrane distillation crystallization process with zero salty water discharge. J Memb Sci 2014;450:1–11. doi:10.1016/j.memsci.2013.08.034.

[80] Guan G, Wang R, Wicaksana F, Yang X, Fane AG. Analysis of membrane distillation crystallization system for high salinity brine treatment with zero discharge using Aspen flowsheet simulation. Ind Eng Chem Res 2012;51:13405–13. doi:10.1021/ie3002183.

[81] Pantoja CE, Nariyoshi YN, Seckler MM. Membrane Distillation Crystallization Applied to Brine Desalination: A Hierarchical Design Procedure. Ind Eng Chem Res 2015;54:2776–93. doi:10.1021/ie504695p.

[82] Tun CM, Fane AG, Matheickal JT, Sheikholeslami R. Membrane distillation crystallization of concentrated salts - Flux and crystal formation. J Memb Sci 2005;257:144–55. doi:10.1016/j.memsci.2004.09.051.

[83] El-Bourawi MS, Ding Z, Ma R, Khayet M. A framework for better understanding membrane distillation separation process. J Memb Sci 2006;285:4–29. doi:10.1016/j.memsci.2006.08.002.

[84] Abu-Zeid MAE-R, Zhang Y, Dong H, Zhang L, Chen H-L, Hou L. A comprehensive review of vacuum membrane distillation technique. Desalination 2015;356:1–14. doi:10.1016/j.desal.2014.10.033.

[85] Charfi K, Khayet M, Safi MJ. Numerical simulation and experimental studies on heat and mass transfer using sweeping gas membrane distillation. Desalination 2010;259:84–96. doi:10.1016/j.desal.2010.04.028.

[86] Karanikola V, Corral AF, Jiang H, Eduardo Sáez A, Ela WP, Arnold RG. Sweeping gas

membrane distillation: Numerical simulation of mass and heat transfer in a hollow fiber membrane module. J Memb Sci 2015;483:15–24. doi:10.1016/j.memsci.2015.02.010.

[87] Khayet M, Cojocaru C, Baroudi A. Modeling and optimization of sweeping gas membrane distillation. Desalination 2012;287:159–66. doi:10.1016/j.desal.2011.04.070.

[88] Gao L, Zhang J, Gray S, Li J. Modelling mass and heat transfers of Permeate Gap Membrane Distillation using hollow fi bre membrane. Desalination 2019;467:196–209. doi:10.1016/j.desal.2019.06.014.

[89] Cheng L, Zhao Y, Li P, Li W, Wang F. Comparative study of air gap and permeate gap membrane distillation using internal heat recovery hollow fi ber membrane module. Desalination 2018;426:42–9. doi:10.1016/j.desal.2017.10.039.

[90] Khalifa AE. Water and air gap membrane distillation for water desalination – An experimental comparative study. Sep Purif Technol 2015;141:276–84. doi:10.1016/j.seppur.2014.12.007.

[91] Francis L, Ghaffour N, Alsaadi AA, Amy GL. Material gap membrane distillation: A new design for water vapor flux enhancement. J Memb Sci 2013;448:240–7. doi:10.1016/j.memsci.2013.08.013.

[92] Swaminathan J, Chung HW, Warsinger DM, V JHL. Energy efficiency of membrane distillation up to high salinity: Evaluating critical system size and optimal membrane thickness. Appl Energy 2018;211:715–34. doi:10.1016/j.apenergy.2017.11.043.

[93] Alkhudhiri A, Darwish N, Hilal N. Produced water treatment: Application of Air Gap Membrane Distillation. Desalination 2013;309:46–51. doi:10.1016/j.desal.2012.09.017.

[94] ALKLAIBI A, LIOR N. Transport analysis of air-gap membrane distillation. J Memb Sci 2005;255:239–53. doi:10.1016/j.memsci.2005.01.038.

[95] Chiam C-K, Sarbatly R. Heat transfer in the rectangular cross-flow flat-sheet membrane module for vacuum membrane distillation. Chem Eng Process Process Intensif 2014;79:23–33. doi:10.1016/j.cep.2014.03.005.

[96] Andrjesdóttir Ó, Ong CL, Nabavi M, Paredes S, Khalil ASG, Michel B, et al. An experimentally optimized model for heat and mass transfer in direct contact membrane distillation. Int J Heat Mass Transf 2013;66:855–67. doi:10.1016/j.ijheatmasstransfer.2013.07.051.

[97] Naidu G, Jeong S, Vigneswaran S. Influence of feed/permeate velocity on scaling development in a direct contact membrane distillation. Sep Purif Technol 2014;125:291–300. doi:10.1016/j.seppur.2014.01.049.

[98] Termpiyakul P, Jiraratananon R, Srisurichan S. Heat and mass transfer characteristics of a direct contact membrane distillation process for desalination. Desalination 2005;177:133–41. doi:10.1016/j.desal.2004.11.019.

[99] Martínez-Díez L, Vázquez-González M. Temperature and concentration polarization in membrane distillation of aqueous salt solutions. J Memb Sci 1999;156:265–73. doi:10.1016/S0376-7388(98)00349-4.

[100] Schofield RW, Fane AG, Fell CJD, Macoun R. Factors affecting flux in membrane distillation. Desalination 1990;77:279–94. doi:10.1016/0011-9164(90)85030-E.

[101] Deshmukh SK, Sapkal VS, Sapkal RS. Evaluation of Direct Contact Membrane Distillation for Concentration of Orange Juice 2011;01:39–48.

[102] Schneider K, Hölz W, Wollbeck R, Ripperger S. Membranes and modules for transmembrane distillation. J Memb Sci 1988;39:25–42. doi:10.1016/S0376-7388(00)80992-8.

[103] Ullah R, Khraisheh M, Esteves RJ, McLeskey JT, AlGhouti M, Gad-el-Hak M, et al. Energy efficiency of direct contact membrane distillation. Desalination 2018;433:56–67. doi:10.1016/j.desal.2018.01.025.

[104] Tijing LD, Choi JS, Lee S, Kim SH, Shon HK. Recent progress of membrane distillation using electrospun nanofibrous membrane. J Memb Sci 2014;453:435–62. doi:10.1016/j.memsci.2013.11.022.

[105] Laganà F, Barbieri G, Drioli E. Direct contact membrane distillation: modelling and concentration experiments. J Memb Sci 2000;166:1–11. doi:10.1016/S0376-7388(99)00234-3.

[106] Khayet M. Membranes and theoretical modeling of membrane distillation: A review. Adv Colloid Interface Sci 2011;164:56–88. doi:10.1016/j.cis.2010.09.005.

[107] Figoli A, Simone S, Criscuoli A, Al-Jlil SA, Al Shabouna FS, Al-Romaih HS, et al. Hollow fibers for seawater desalination from blends of PVDF with different molecular weights: Morphology, properties and VMD performance. Polym (United Kingdom)

2014;55:1296–306. doi:10.1016/j.polymer.2014.01.035.

[108] Srisurichan S, Jiraratananon R, Fane AG. Mass transfer mechanisms and transport resistances in direct contact membrane distillation process 2006;277:186–94. doi:10.1016/j.memsci.2005.10.028.

[109] Phattaranawik J, Jiraratananon R, Fane AG. Heat transport and membrane distillation coefficients in direct contact membrane distillation. J Memb Sci 2003;212:177–93. doi:10.1016/S0376-7388(02)00498-2.

[110] Drioli E, Ali A, Macedonio F. Membrane distillation: Recent developments and perspectives. Desalination 2015;356:56–84. doi:10.1016/j.desal.2014.10.028.

[111] Tijing LD, Woo YC, Choi J-S, Lee S, Kim S-H, Shon HK. Fouling and its control in membrane distillation—A review. J Memb Sci 2015;475:215–44. doi:10.1016/j.memsci.2014.09.042.

[112] Gryta M. Fouling in direct contact membrane distillation process. J Memb Sci 2008;325:383–94. doi:10.1016/j.memsci.2008.08.001.

[113] Warsinger DM, Swaminathan J, Guillen-Burrieza E, Arafat HA, Lienhard V JH. Scaling and fouling in membrane distillation for desalination applications: A review. Desalination 2015;356:294–313. doi:10.1016/j.desal.2014.06.031.

[114] Kayvani Fard A, Rhadfi T, Khraisheh M, Atieh MA, Khraisheh M, Hilal N. Reducing flux decline and fouling of direct contact membrane distillation by utilizing thermal brine from MSF desalination plant. Desalination 2016;379:172–81. doi:10.1016/j.desal.2015.11.004.

[115] Edwie F, Chung TS. Development of simultaneous membrane distillation-crystallization (SMDC) technology for treatment of saturated brine. Chem Eng Sci 2013;98:160–72. doi:10.1016/j.ces.2013.05.008.

[116] Yao M, Tijing LD, Naidu G, Kim SH, Matsuyama H, Fane AG, et al. A review of membrane wettability for the treatment of saline water deploying membrane distillation. Desalination 2020;479:114312. doi:10.1016/j.desal.2020.114312.

[117] Rahimpour MR, Esmaeilbeig MA. Membrane wetting in membrane distillation. Elsevier Inc.; 2018. doi:10.1016/B978-0-12-813551-8.00006-1.

[118] Rezaei M, Warsinger DM, Lienhard V JH, Duke MC, Matsuura T, Samhaber WM.

Wetting phenomena in membrane distillation: Mechanisms, reversal, and prevention. vol. 139. Elsevier B.V.; 2018. doi:10.1016/j.watres.2018.03.058.

[119] Singh D, Sirkar KK. Desalination of brine and produced water by direct contact membrane distillation at high temperatures and pressures. J Memb Sci 2012;389:380–8. doi:10.1016/j.memsci.2011.11.003.

[120] Fan H, Peng Y. Application of PVDF membranes in desalination and comparison of the VMD and DCMD processes. Chem Eng Sci 2012;79:94–102. doi:10.1016/j.ces.2012.05.052.

[121] Rao G, Hiibel SR, Achilli A, Childress AE. Factors contributing to flux improvement in vacuum-enhanced direct contact membrane distillation. Desalination 2015;367:197–205. doi:10.1016/j.desal.2015.04.002.

[122] Singh D, Sirkar KK. High temperature direct contact membrane distillation based desalination using PTFE hollow fibers. Chem Eng Sci 2014;116:824–33. doi:10.1016/j.ces.2014.05.042.

[123] He K, Hwang HJ, Woo MW, Moon IS. Production of drinking water from saline water by direct contact membrane distillation (DCMD). J Ind Eng Chem 2011;17:41–8. doi:10.1016/j.jiec.2010.10.007.

[124] Boubakri A, Hafiane A, Bouguecha SAT. Direct contact membrane distillation: Capability to desalt raw water. Arab J Chem 2014;4:557–63. doi:http://dx.doi.org/10.1016/j.arabjc.2014.02.010.

[125] Boubakri A, Bouguecha SA-T, Dhaouadi I, Hafiane A. Effect of operating parameters on boron removal from seawater using membrane distillation process. Desalination 2015;373:86–93. doi:10.1016/j.desal.2015.06.025.

[126] Chen T-C, Ho C-D, Yeh H-M. Theoretical modeling and experimental analysis of direct contact membrane distillation. J Memb Sci 2009;330:279–87. doi:10.1016/j.memsci.2008.12.063.

[127] Yang X, Duke M, Zhang J, Li J De. Modeling of heat and mass transfer in vacuum membrane distillation for ammonia separation. Sep Purif Technol 2019;224:121–31. doi:10.1016/j.seppur.2019.05.004.

[128] Dao TD, Laborie S, Cabassud C. Direct As(III) removal from brackish groundwater by

vacuum membrane distillation: Effect of organic matter and salts on membrane fouling. Sep Purif Technol 2016;157:35–44. doi:10.1016/j.seppur.2015.11.018.

[129] Chiam C-K, Sarbatly R. Study of the rectangular cross-flow flat-sheet membrane module for desalination by vacuum membrane distillation. Chem Eng Process Process Intensif 2016;102:169–85. doi:10.1016/j.cep.2016.01.014.

[130] Xie Z, Duong T, Hoang M, Nguyen C, Bolto B. Ammonia removal by sweep gas membrane distillation. Water Res 2009;43:1693–9. doi:10.1016/j.watres.2008.12.052.

[131] Shirazi MMA, Kargari A, Tabatabaei M. Sweeping Gas Membrane Distillation (SGMD) as an Alternative for Integration of Bioethanol Processing: Study on a Commercial Membrane and Operating Parameters. Chem Eng Commun 2015;202:457–66. doi:10.1080/00986445.2013.848805.

[132] He Q, Li P, Geng H, Zhang C, Wang J, Chang H. Modeling and optimization of air gap membrane distillation system for desalination. Desalination 2014;354:68–75. doi:10.1016/j.desal.2014.09.022.

[133] EL-Bourawi MS, Khayet M, Ma R, Ding Z, Li Z, Zhang X. Application of vacuum membrane distillation for ammonia removal. J Memb Sci 2007;301:200–9. doi:10.1016/j.memsci.2007.06.021.

[134] Gao L, Zhang J, Gray S, Li J. Influence of PGMD module design on the water productivity and energy efficiency in desalination. Desalination 2019;452:29–39. doi:10.1016/j.desal.2018.10.005.

[135] Madalosso HB, Silva DS, Merlini A, Battisti R. Modeling and experimental validation of direct contact membrane distillation applied to synthetic dye solutions. J Chem Technol Biotechnol 2021. doi:10.1002/jctb.6599.

[136] Ruiz-Aguirre A, Andrés-Mañas JA, Zaragoza G. Evaluation of permeate quality in pilot scale membrane distillation systems. Membranes (Basel) 2019;9:1–14. doi:10.3390/membranes9060069.

[137] Qtaishat M, Matsuura T, Kruczek B, Khayet M. Heat and mass transfer analysis in direct contact membrane distillation. Desalination 2008;219:272–92. doi:10.1016/j.desal.2007.05.019.

[138] Sarti GC, Gostoli C, Matulli S. Low energy cost desalination processes using hydrophobic

membranes. Desalination 1985;56:277–86. doi:10.1016/0011-9164(85)85031-1.

[139] Zhang Y, Peng Y, Ji S, Li Z, Chen P. Review of thermal efficiency and heat recycling in membrane distillation processes. Desalination 2015;367:223–39. doi:10.1016/j.desal.2015.04.013.

[140] Hitsov I, Maere T, De Sitter K, Dotremont C, Nopens I. Modelling approaches in membrane distillation: A critical review. Sep Purif Technol 2015;142:48–64. doi:10.1016/j.seppur.2014.12.026.

[141] Gryta M, Tomaszewska M. Heat transport in the membrane distillation process. J Memb Sci 1998;144:211–22. doi:10.1016/S0376-7388(98)00050-7.

[142] Mengual JI, Khayet M, Godino MP. Heat and mass transfer in vacuum membrane distillation. Int J Heat Mass Transf 2004;47:865–75. doi:10.1016/j.ijheatmasstransfer.2002.09.001.

[143] Bandini S, Gostoli C, Sarti GC. Separation efficiency in vacuum membrane distillation. J Memb Sci 1992;73:217–29. doi:10.1016/0376-7388(92)80131-3.

[144] Curcio E, Drioli E. Membrane Distillation and Related Operations - A Review. Sep Purif Rev 2005;34:35–86. doi:10.1081/SPM-200054951.

[145] Schofield RW, Fane AG, Fell CJD. Heat and mass transfer in membrane distillation. J Memb Sci 1987;33:299–313. doi:10.1016/S0376-7388(00)80287-2.

[146] Taylor R, Krishna R. Multicomponent Mass Transfer. Wiley series in chemical engineering; 1993.

[147] Banat FA, Abu Al-Rub F, Jumah R, Al-Shannag M. Application of Stefan-Maxwell approach to azeotropic separation by membrane distillation. Chem Eng J 1999;73:71–5. doi:10.1016/S1385-8947(99)00016-9.

[148] Shirazi MMA, Kargari A, Ismail AF, Matsuura T. Computational Fluid Dynamic (CFD) opportunities applied to the membrane distillation process: State-of-the-art and perspectives. Desalination 2016;377:73–90. doi:10.1016/j.desal.2015.09.010.

[149] Khayet M, Cojocaru C. Artificial neural network model for desalination by sweeping gas membrane distillation. Desalination 2013;308:102–10. doi:10.1016/j.desal.2012.06.023.

[150] Khayet M, Cojocaru C. Artificial neural network modeling and optimization of

desalination by air gap membrane distillation. Sep Purif Technol 2012;86:171–82. doi:10.1016/j.seppur.2011.11.001.

[151] Boubakri A, Hafiane A, Bouguecha SAT. Application of response surface methodology for modeling and optimization of membrane distillation desalination process. J Ind Eng Chem 2014;20:3163–9. doi:10.1016/j.jiec.2013.11.060.

[152] Khalifa A, Lawal D, Antar M, Khayet M. Experimental and theoretical investigation on water desalination using air gap membrane distillation. Desalination 2015;376:94–108. doi:10.1016/j.desal.2015.08.016.

[153] Ali A, Quist-Jensen CA, Macedonio F, Drioli E. Optimization of module length for continuous direct contact membrane distillation process. Chem Eng Process Process Intensif 2016;110:188–200. doi:10.1016/j.cep.2016.10.014.

[154] Olatunji SO, Camacho LM. Heat and Mass Transport in Modeling Membrane Distillation Configurations: A Review. Front Energy Res 2018;6:1–18. doi:10.3389/fenrg.2018.00130.

[155] Lou J, Vanneste J, DeCaluwe SC, Cath TY, Tilton N. Computational fluid dynamics simulations of polarization phenomena in direct contact membrane distillation. J Memb Sci 2019;591:117150. doi:10.1016/j.memsci.2019.05.074.

[156] Ali A, Criscuoli A, Macedonio F, Drioli E. A comparative analysis of flat sheet and capillary membranes for membrane distillation applications. Desalination 2019;456:1–12. doi:10.1016/j.desal.2019.01.006.

[157] Al-Obaidani S, Curcio E, Macedonio F, Di Profio G, Al-Hinai H, Drioli E. Potential of membrane distillation in seawater desalination: Thermal efficiency, sensitivity study and cost estimation. J Memb Sci 2008;323:85–98. doi:10.1016/j.memsci.2008.06.006.

[158] Lawson KW, Lloyd DR. Membrane distillation. II. Direct contact MD. J Memb Sci 1996;120:123–33. doi:10.1016/0376-7388(96)00141-X.

[159] Banat FA, Abu Al-Rub F, Shannag M. Modeling of dilute ethanol-water mixture separation by membrane distillation. Sep Purif Technol 1999;16:119–31. doi:10.1016/S1383-5866(98)00117-8.

[160] Hayer H, Bakhtiari O, Mohammadi T. Simulation of momentum, heat and mass transfer in direct contact membrane distillation: A computational fluid dynamics approach. J Ind

Eng Chem 2015;21:1379–82. doi:10.1016/j.jiec.2014.06.009.

[161] Salem MS, El-Shazly AH, Nady N, Elmarghany MR, Shouman MA, Sabry MN. 3-D numerical investigation on commercial PTFE membranes for membrane distillation: Effect of inlet conditions on heat and mass transfer. Case Stud Therm Eng 2019;13:100396. doi:10.1016/j.csite.2019.100396.

[162] Park D, Norouzi E, Park C. Experimental and Numerical Study of Water Distillation Performance of Small-Scale Direct Contact Membrane Distillation System. Proc ASME 2017 Int Mech Eng Congr Expo (Vol IMECE2017-72175) 2017:1–9. doi:10.1115/IMECE2017-72125.

[163] Banat FA, Al-Rub FA, Shannag M. Simultaneous removal of acetone and ethanol from aqueous solutions by membrane distillation: Prediction using the Fick's and the exact and approximate Stefan-Maxwell relations. Warme- Und Stoffubertragung Zeitschrift 1999;35:423–31. doi:10.1007/s002310050344.

[164] Guiot SR, van den Berg L. Performance of an upflow anaerobic reactor combining a sludge blanket and a filter treating sugar waste. Biotechnol Bioeng 1985;27:800–6. doi:10.1002/bit.260270608.

[165] Song KH, Young JC. Media Design Factors for Fixed-Bed Filters. J WPCF, 58,(2), 1986 1986;58:115–21. doi:10.2307/25042862.

[166] Kuusisto LM. Development of a mathematical model, VUMP (Vinasse utilization for methane production). University of Texas at Arlington, 2013.

[167] Cho JK, Kim BS, Park SC, Choi YS, Chang HN. Effect of stepwise seeding on the performance of four anaerobic biofilters treating a synthetic stillage waste. Biomass and Bioenergy 1996;10:25–35. doi:10.1016/0961-9534(95)00033-X.

[168] Ongaratto RS, Submetida T, Corpo AO, Do D, Alberto I. No Title 2014.

[169] APHA. Standard Methods for the Examination of Water and Wastewater - Inorganic Metals, Organics, Oxygen, Carbon, Humics, DBPs 1999:733.

[170] Noukeu NA, Gouado I, Priso RJ, Ndongo D, Taffouo VD, Dibong SD, et al. Characterization of effluent from food processing industries and stillage treatment trial with Eichhornia crassipes (Mart .) and Panicum maximum (Jacq .). Water Resour Ind 2016;16:1–18. doi:10.1016/j.wri.2016.07.001.

[171] Larsson E, Tengberg T. Evaporation of Vinasse - Pilot Plant Investigation and Preliminary Process Design. Chalmers University of Technology, 2014.

[172] Gill WN, Bansal B. Hollow fiber reverse osmosis systems analysis and design. AIChE J 1973;19:823–31. doi:10.1002/aic.690190422.

[173] Zhang L-Z, Huang S-M, Chi J-H, Pei L-X. Conjugate heat and mass transfer in a hollow fiber membrane module for liquid desiccant air dehumidification: A free surface model approach. Int J Heat Mass Transf 2012;55:3789–99. doi:10.1016/j.ijheatmasstransfer.2012.03.034.

[174] Ho C-D, Chang H, Yang T-J, Wu K-Y, Chen L. Theoretical and experimental studies of laminar flow hollow fiber direct contact membrane distillation modules. Desalination 2016;378:108–16. doi:10.1016/j.desal.2015.10.003.

[175] Hayer H, Bakhtiari O, Mohammadi T. Simulation of momentum, heat and mass transfer in direct contact membrane distillation: A computational fluid dynamics approach. J Ind Eng Chem 2015;21:1379–82. doi:10.1016/j.jiec.2014.06.009.

[176] Soares R de P, Secchi AR. EMSO: A new environment for modelling, simulation and optimisation. Comput. Aided Chem. Eng., vol. 14, 2003, p. 947–52. doi:10.1016/S1570-7946(03)80239-0.

[177] Secchi AR, Wada K, Tessaro IC. Simulation of an ultrafiltration process of bovine serum albumin in hollow-fiber membranes. J Memb Sci 1999;160:255–65. doi:10.1016/S0376-7388(99)00091-5.

[178] Bird RB, Stewart WE, Lightfoot EN. Transport Phenomena 2006:1045. doi:10.3139/9781569905234.004.

[179] Kozinski a. a., Schmidt FP, Lightfoot EN. Velocity Profiles in Porous-Walled Ducts. Ind Eng Chem Fundam 1970;9:502–5. doi:10.1021/i160035a033.

[180] Smith JM, Van Ness HC, Abbott M. Introduction to Chemical Engineering Thermodynamics. McGraw-Hill Education; 2005.

[181] Banat FA, Simandl J. Membrane distillation for dilute ethanol Separation from aqueous streams. J Memb Sci 1999;163:333–48.

[182] Dias RM, Chiavone-Filho O, Bernardo A, Giulietti M. Vapour-liquid equilibria for (water + ethanol + fructose): Experimental data and thermodynamic modelling. J Chem

Thermodyn 2017;115:27–33. doi:10.1016/j.jct.2017.07.021.

[183] Galeotti N, Burger J, Hasse H. Fluid Phase Equilibria Vapor-liquid equilibrium in the ternary systems acetic acid þ water þ (xylose or glucose). Fluid Phase Equilib 2018;473:323–9. doi:10.1016/j.fluid.2018.06.011.

[184] Air - Diffusion Coefficients of Gases in Excess of Air n.d. https://www.engineeringtoolbox.com/air-diffusion-coefficient-gas-mixture-temperature-d_2010.html (accessed November 1, 2020).

[185] Perry RH, Green DW. Perry´s Chemical Engineers´ Handbook. Seventh ed. New York: McGraw-Hill; 1997.

[186] Hines & Maddox_Mass Transfer Fundamentals and applications.pdf n.d.

[187] Poling BE, Prausnitz JM. THE PROPERTIES OF GASES AND LIQUIDS. n.d.

[188] Wesselingh J, Krishna R. Mass transfer in multicomponent mixtures 2000.

[189] Guillén-Burrieza E, Blanco J, Zaragoza G, Alarcón DC, Palenzuela P, Ibarra M, et al. Experimental analysis of an air gap membrane distillation solar desalination pilot system. J Memb Sci 2011;379:386–96. doi:10.1016/j.memsci.2011.06.009.

[190] Jantaporn W, Ali A, Aimar P. Specific energy requirement of direct contact membrane distillation. Chem Eng Res Des 2017. doi:10.1016/j.cherd.2017.09.031.

[191] Luo A, Lior N. Critical review of membrane distillation performance criteria. Desalin Water Treat 2016;57:20093–140. doi:10.1080/19443994.2016.1152637.

[192] Lokare OR, Tavakkoli S, Khanna V, Vidic RD. Importance of feed recirculation for the overall energy consumption in membrane distillation systems. Desalination 2018;428:250–4. doi:10.1016/j.desal.2017.11.037.

[193] Sirkar K, Song L. Pilot-Scale Studies for Direct Contact Membrane Desalination Process. Reclamation 2009:1–122.

[194] Khalifa AE, Alawad SM, Antar MA. Parallel and series multistage air gap membrane distillation. Desalination 2017;417:69–76. doi:10.1016/j.desal.2017.05.003.

[195] Baker RW. Membrane technology and applications. Second. John Wiley & Sons; 2004. doi:10.1016/0166-6622(87)80171-3.

[196] Ali MI, Summers EK, Arafat HA, Lienhard V JH. Effects of membrane properties on water production cost in small scale membrane distillation systems. Desalination 2012;306:60–71. doi:10.1016/j.desal.2012.07.043.

[197] Kesieme UK, Milne N, Aral H, Cheng CY, Duke M. Economic analysis of desalination technologies in the context of carbon pricing, and opportunities for membrane distillation. Desalination 2013;323:66–74. doi:10.1016/j.desal.2013.03.033.

[198] Gryta M. Effectiveness of Water Desalination by Membrane Distillation Process. Membranes (Basel) 2012;2:415–29. doi:10.3390/membranes2030415.

[199] Kayvani Fard A, Manawi YM, Rhadfi T, Mahmoud KA, Khraisheh M, Benyahia F. Synoptic analysis of direct contact membrane distillation performance in Qatar: A case study. Desalination 2015;360:97–107. doi:10.1016/j.desal.2015.01.016.

[200] Khayet M, Matsuura T. Membrane Distillation Principles and Applications. Elsevier; 2011.

[201] Abdel-Rahman A. Modeling Temperature and Salt Concentration Distribution in Direct Contact Membrane Distillation. J Eng Sci Assiut Univ 2008;36:1167–88.

[202] Perfilov V, Ali A, Fila V. A general predictive model for direct contact membrane distillation. Desalination 2018;445:181–96. doi:10.1016/j.desal.2018.08.002.

[203] Soomro MI, Kim WS. Performance and economic investigations of solar power tower plant integrated with direct contact membrane distillation system. Energy Convers Manag 2018;174:626–38. doi:10.1016/j.enconman.2018.08.056.

[204] Ions in Water, and Conductivity - LAQUA [Water Quality Analyzer Website] - HORIBA n.d. https://www.horiba.com/uk/application/material-property-characterization/water-analysis/water-quality-electrochemistry-instrumentation/the-story-of-ph-and-water-quality/the-basis-of-conductivity/ions-in-water-and-conductivity/ (accessed January 28, 2021).

[205] Gryta M, Markowska-Szczupak A, Bastrzyk J, Tomczak W. The study of membrane distillation used for separation of fermenting glycerol solutions. J Memb Sci 2013;431:1–8. doi:10.1016/j.memsci.2012.12.032.

[206] Berenjian A, Chan N, Malmiri HJ. Volatile Organic Compounds removal methods: A review. Am J Biochem Biotechnol 2012;8:220–9. doi:10.3844/ajbbsp.2012.220.229.

[207] Sarti GC, Gostoli C, Bandini S. Extraction of organic components from aqueous streams by vacuum membrane distillation. J Memb Sci 1993;80:21–33. doi:10.1016/0376-7388(93)85129-K.

[208] Yang X, Wang K, Wang H, Zhang J, Mao Z. Novel process combining anaerobic-aerobic digestion and ion exchange resin for full recycling of cassava stillage in ethanol fermentation. Waste Manag 2017;62:241–6. doi:10.1016/j.wasman.2017.01.040.

[209] Zhang Q, Lu X, Tang L, Mao Z, Zhang J, Zhang H, et al. A novel full recycling process through two-stage anaerobic treatment of distillery wastewater for bioethanol production from cassava. J Hazard Mater 2010;179:635–41. doi:10.1016/j.jhazmat.2010.03.050.

[210] Alkasrawi M, Abu A, Al-muhtaseb AH. Simultaneous saccharification and fermentation process for ethanol production from steam-pretreated softwood : Recirculation of condensate streams. Chem Eng J 2013;225:574–9. doi:10.1016/j.cej.2013.04.014.

[211] Ma H, Yang J, Jia Y, Wang Q, Tashiro Y, Sonomoto K. Bioresource Technology Stillage reflux in food waste ethanol fermentation and its by-product accumulation. Bioresour Technol 2016;209:254–8. doi:10.1016/j.biortech.2016.02.127.

[212] Rai UK, Muthukrishnan M, Guha BK. Tertiary treatment of distillery wastewater by nanofiltration 2008;230:70–8. doi:10.1016/j.desal.2007.11.017.

[213] Murthy ZVP, Chaudhari LB. Treatment of distillery spent wash by combined UF and RO processes. Glob NEST JournalGlobal NEST Int J 2009;11:235–40. doi:10.30955/gnj.000581.

[214] Arora A, Seth A, Dien BS, Belyea RL, Singh V, Tumbleson ME, et al. Microfiltration of thin stillage : Process simulation and economic analyses. Biomass and Bioenergy 2011;35:113–20. doi:10.1016/j.biombioe.2010.08.024.

[215] Ali MT, Fath HES, Armstrong PR. A comprehensive techno-economical review of indirect solar desalination. Renew Sustain Energy Rev 2011;15:4187–99. doi:10.1016/j.rser.2011.05.012.

[216] Bio-Rad. Aminex HPLC Columns ®. Bull 6333 Rev A US/EG 2012:7–10.

[217] Clarke MA, Edye LA, Eggleston G. Sucrose decomposition in aqueous solution, and losses in sugar manufacture and refining. Adv Carbohydr Chem Biochem 1997;52:441–70. doi:10.1016/s0065-2318(08)60095-5.

[218] Nair RB, Taherzadeh MJ. Valorization of sugar-to-ethanol process waste vinasse: A novel biorefinery approach using edible ascomycetes filamentous fungi. Bioresour Technol 2016;221:469–76. doi:10.1016/j.biortech.2016.09.074.

[219] Choudhury MR, Anwar N, Jassby D, Rahaman MS. Fouling and wetting in the membrane distillation driven wastewater reclamation process – A review. Adv Colloid Interface Sci 2019;269:370–99. doi:10.1016/j.cis.2019.04.008.

[220] Lee J-G, Kim W-S. Numerical modeling of the vacuum membrane distillation process. Desalination 2013;331:46–55. doi:10.1016/j.desal.2013.10.022.

[221] Dong G, Cha-Umpong W, Hou J, Ji C, Chen V. Open-source industrial-scale module simulation: Paving the way towards the right configuration choice for membrane distillation. Desalination 2019;464:48–62. doi:10.1016/j.desal.2019.04.018.

[222] Swaminathan J, Chung HW, Warsinger DM, Lienhard V JH. Membrane distillation model based on heat exchanger theory and configuration comparison. Appl Energy 2016;184:491–505. doi:10.1016/j.apenergy.2016.09.090.

[223] He F, Gilron J, Sirkar KK. High water recovery in direct contact membrane distillation using a series of cascades. Desalination 2013;323:48–54. doi:10.1016/j.desal.2012.08.006.

[224] Christie KSS, Horseman T, Lin S. Energy efficiency of membrane distillation: Simplified analysis, heat recovery, and the use of waste-heat. Environ Int 2020;138:105588. doi:10.1016/j.envint.2020.105588.

[225] Ali E. Optimization of module length and number of stages in a multistage membrane distillation configuration. Exp Heat Transf 2019;33:526–46. doi:10.1080/08916152.2019.1667927.

[226] Cath TY, Adams VD, Childress AE. Experimental study of desalination using direct contact membrane distillation: a new approach to flux enhancement. J Memb Sci 2004;228:5–16. doi:10.1016/j.memsci.2003.09.006.

[227] Boubakri A, Hafiane A, Bouguecha SAT. Direct contact membrane distillation: Capability to desalt raw water. Arab J Chem 2014;4:557–63. doi:10.1016/j.arabjc.2014.02.010.

[228] Khayet M. Solar desalination by membrane distillation: Dispersion in energy

consumption analysis and water production costs (a review). Desalination 2013;308:89–101. doi:10.1016/j.desal.2012.07.010.

[229] Gopi G, Arthanareeswaran G, AF I. Perspective of renewable desalination by using membrane distillation. Chem Eng Res Des 2019;144:520–37. doi:10.1016/j.cherd.2019.02.036.

[230] Duong HC, Cooper P, Nelemans B, Cath TY, Nghiem LD. Evaluating energy consumption of air gap membrane distillation for seawater desalination at pilot scale level. Sep Purif Technol 2016;166:55–62. doi:10.1016/j.seppur.2016.04.014.

[231] Guillén-Burrieza E, Zaragoza G, Miralles-Cuevas S, Blanco J. Experimental evaluation of two pilot-scale membrane distillation modules used for solar desalination. J Memb Sci 2012;409–410:264–75. doi:10.1016/j.memsci.2012.03.063.

[232] Guan G, Yang X, Wang R, Fane AG. Modular matrix design for large-scale membrane distillation system via Aspen simulations. Desalination 2018;428:207–17. doi:10.1016/j.desal.2017.11.033.

[233] SABESP. Comunicado - 9/20. São Paulo: 2020.

[234] Guerreiro LF, Rodrigues CSD, Duda RM, Oliveira RA De, Boaventura RAR, Madeira LM. Treatment of sugarcane vinasse by combination of coagulation / fl occulation and Fenton ' s oxidation 2016;181:237–48. doi:10.1016/j.jenvman.2016.06.027.

[235] da Silva CS, Amaral MCS, Couto CF. COMBINED PROCESS OF ULTRAFILTRATION AND NANOFILTRATION FOR VINASSE TREATMENT WITH AND WITHOUT PRE-COAGULATION. J Water Process Eng 2020;36:101326. doi:10.1016/j.jwpe.2020.101326.

[236] BCB. Conversor de Moedas n.d. https://www.bcb.gov.br/conversao (accessed February 4, 2021).